

HYPHAL MORPHOGENESIS OF THE HUMAN FUNGAL PATHOGEN *CRYPTOCOCCUS*  
*NEOFORMANS*

by

JIANFENG LIN

(Under the Direction of XIAORONG LIN)

ABSTRACT

Morphotype switch is a cellular response to external and internal cues. The *Cryptococcus neoformans* species complex can undergo morphological transitions between the yeast and the filament form, and such morphological changes profoundly affect cryptococcal interaction with various hosts as shown in this research. Filamentation in *Cryptococcus* was historically considered a mating response activated by pheromone. Recent studies indicate the existence of pheromone-independent signaling pathways but their identity or the effectors remain unknown. Here, we demonstrated that glucosamine stimulated the *C. neoformans* species complex to undergo self-filamentation independent of the key components of the pheromone pathway. Through a genetic screen we found that Crz1, a transcription factor downstream of the highly conserved phosphatase complex calcineurin, was essential for glucosamine-stimulated filamentation. Glucosamine promoted Crz1 translocation from the cytoplasm to the nucleus. Interestingly, multiple components of the high osmolality glycerol response (HOG) pathway acted as repressors of glucosamine-elicited filamentation through their calcineurin-opposing effect on Crz1's nuclear translocation. The results demonstrate that *Cryptococcus* can resort to multiple genetic pathways for morphological transition in response to different stimuli. The

genetic pathways converge on the transcription factor Znf2 that regulates hyphal differentiation. How Znf2 orchestrates its functions in filamentation remains elusive. In this research, we identified two factors, Brf1 and Snf5, that are essential for Znf2 to fulfill its genetic regulation by a forward genetics screen. As a basidiomycete-specific factor, Brf1 functions in the same genetic pathway as Snf5. Later we found that Brf1 and Sn5 work together in the conserved chromatin remodeling complex called SWI/SNF. The SWI/SNF complex is required to open up the chromatin of promoter regions of Znf2 and its targets. Meanwhile, as a subunit in the SWI/SNF complex, Brf1 is required for transcription factor Znf2's full association to DNA. This molecular and genetic study has advanced our understanding in the regulations of hyphal cellular differentiation in *Cryptococcus*, yielded novel insights on the conserved and species-specific regulation mechanisms in other fungi, and raised possibilities for diminishing *Cryptococcus* virulence by inducing hyphal growth in the host.

INDEX WORDS: *Cryptococcus neoformans*, pathogenicity, dimorphism, filamentation, mating, unisexual, bisexual, differentiation

HYPHAL MORPHOGENESIS OF THE HUMAN FUNGAL PATHOGEN *CRYPTOCOCCUS*  
*NEOFORMANS*

by

JIANFENG LIN

BS, Shandong University, CHINA, 2013

A Dissertation Submitted to the Graduate Faculty of The University of Georgia in Partial  
Fulfillment of the Requirements for the Degree

DOCTOR OF PHILOSOPHY

ATHENS, GEORGIA

2019

© 2019

Jianfeng Lin

All Rights Reserved

HYPHAL MORPHOGENESIS OF THE HUMAN FUNGAL PATHOGEN *CRYPTOCOCCUS*  
*NEOFORMANS*

by

JIANFENG LIN

Major Professor:	Xiaorong Lin
Committee:	Lukasz Kozubowski
	Zachary Lewis
	Vincent Starai

Electronic Version Approved:

Suzanne Barbour  
Dean of the Graduate School  
The University of Georgia  
August 2019

## TABLE OF CONTENTS

	Page
LIST OF TABLES .....	vi
LIST OF FIGURES .....	vii
CHAPTER	
1 INTRODUCTION AND LITERATURE REVIEW .....	1
Fungi and fungal infections .....	1
<i>Cryptococcus neoformans</i> and cryptococcosis .....	2
Morphogenesis and virulence in <i>Cryptococcus neoformans</i> .....	3
The regulation of morphogenesis by transcription factor Znf2 and RAM pathway .....	4
The regulation of virulence by transcription factor Znf2.....	6
References.....	7
2 MORPHOLOGY AND ITS UNDERLYING GENETIC REGULATION IMPACT	
THE INTERACTION BETWEEN <i>CRYPTOCOCCUS NEOFORMANS</i> AND ITS	
HOSTS .....	14
Abstract .....	15
Introduction.....	16
Methods and Materials.....	19
Results.....	22
Discussion.....	29
References.....	33

3	GLUCOSAMINE STIMULATES PHEROMONE-INDEPENDENT DIMORPHIC TRANSITION IN <i>CRYPTOCOCCUS NEOFORMANS</i> BY PROMOTING CRZ1 NUCLEAR TRANSLOCATION .....	54
	Abstract .....	55
	Author Summary .....	56
	Introduction .....	57
	Results .....	60
	Discussion .....	70
	Materials and Methods .....	75
	References .....	82
4	TRANSCRIPTION FACTOR ZNF2 COORDINATES WITH THE CHROMATIN REMODELING SNF/SWI COMPLEX TO REGULATE CELLULAR DIFFERENTIATION IN THE HUMAN FUNGAL PATHOGEN <i>CRYPTOCOCCUS NEOFORMANS</i> .....	130
	Abstract .....	131
	Introduction .....	131
	Results .....	135
	Discussion .....	147
	Materials and Methods .....	151
	References .....	161
5	CONCLUSIONS.....	187

## LIST OF TABLES

	Page
Table 2.1: Morphotype affects the interaction between <i>C. neoformans</i> and its hosts .....	42
Table S2.1: Strains used in this study .....	50
Table S3.1: The screening results from forward genetic screening.....	129
Table S3.2: The strains used in this research.....	129
Table S3.3: The primers used in this research .....	129
Table 4.1: The list of proteins identified from Co-IP/MS by Brf1-CBP-2xFLAG as bait .....	176
Table 4.2: The BLAST analysis of the SWI/SNF and RSC subunits in <i>C. neoformans</i> , <i>S. cerevisiae</i> (selected subunits) and <i>S. pombe</i> (selected subunits) .....	177
Table S4.1: The list of eight-four filament-defective <i>Agrobacterium</i> -mediated transformants ..	185
Table S4.2: The list of insertion sites from the eight linked insertional mutants .....	185
Table S4.3: The list of proteins identified from Co-IP/MS by Sfh1-mNeonGreen as bait .....	185
Table S4.4: The Snf5 domain search in fungi.....	186
Table S4.5: The list of Snf2 proteins in fungi by RBOMO and BSA domains search.....	186
Table S4.6: The strains used in this study.....	186
Table S4.7: The vectors used in this study .....	186
Table S4.8: The primers used in this study.....	186

## LIST OF FIGURES

	Page
Figure 2.1: .....	43
Figure 2.2: .....	45
Figure 2.3: .....	46
Figure 2.4: .....	47
Figure 2.5: .....	49
Figure S2.1: .....	52
Figure S2.2: .....	53
Figure 3.1: Glucosamine stimulates self-filamentation in H99 and other cryptococcal isolates.	106
Figure 3.2: Glucosamine-stimulated filamentation is independent of the Mat2-controlled pheromone pathway but requires the morphogenesis regulator Znf2.....	108
Figure 3.3: Multiple components of the HOG pathway suppress filamentation on glucosamine medium .....	110
Figure 3.4: The calcineurin pathway is required for glucosamine-induced self-filamentation ...	111
Figure 3.5: Crz1 acts upstream of Znf2 in regulating filamentation induced by glucosamine....	113
Figure 3.6: Glucosamine stimulates Crz1 translocation to the nucleus .....	114
Figure 3.7: Crz1 depends on calcineurin for its nuclear localization and its regulation of filamentation on glucosamine medium.....	117
Figure 3.8: The HOG components function upstream of Crz1 and suppress Crz1's nuclear localization.....	118

Figure 3.9: Proposed model of genetic regulation of glucosamine-stimulated filamentation in <i>Cryptococcus neoformans</i> .....	120
Figure S3.1: Phenotypes of <i>Candida albicans</i> strains on YPD, YP+GlcNAc, YP+GlcN, and YP+Deoxyl-Glc .....	121
Figure S3.2: Znf2, but not Mat2, is required for filamentation of the serotype D strain XL280 on glucosamine medium .....	122
Figure S3.3: Phenotypes of the hexamine metabolism mutants <i>gnd1Δ</i> and <i>gnat1Δ</i> .....	124
Figure S3.4: Colony images of represented strains of the four classified groups based on the robustness of filamentation on glucosamine medium compared to the control.....	125
Figure S3.5: Mutants in the calcineurin pathway showed different susceptibility towards various stresses .....	125
Figure S3.6: Crz1 does not regulate pheromone-induced filamentation .....	126
Figure S3.7: Calcium, high temperature, and glucosamine induce the nuclear translocation of Crz1-mCherry expressed under its native promoter .....	127
Figure S3.8: Crz1 is not important for osmotic stress response .....	128
Figure 4.1: <i>BRF1</i> and <i>SNF5</i> are essential factors for filamentation .....	169
Figure 4.2: The <i>brf1Δ</i> , <i>snf5Δ</i> , and <i>brf1Δsnf5Δ</i> mutants are phenotypically identical.....	170
Figure 4.3: Brf1 and Snf5 are both subunits specific to the SWI/SNF complex .....	171
Figure 4.4: <i>BRF1</i> is required for <i>ZNF2</i> transcription induction during hyphal differentiation ...	173
Figure 4.5: Znf2 and the SWI/SNF complex coordinate in transcription activation of filamentation genes .....	174
Figure S4.1: A <i>BRF1</i> gene tree .....	178
Figure S4.2: The <i>brf1Δ</i> and <i>snf5Δ</i> strains are defective in cell fusion .....	179

Figure S4.3: BRF1 is the only ARID containing gene involved in growth on raffinose medium 180

Figure S4.4: The *BRF1* overexpression restored the defects in *brf1*Δ.....181

Figure S4.5: Diagrams of domain layout of the subunits in the SWI/SNF and RSC complex in *C. neoformans*.....182

Figure S4.6: Znf2 binds to the promoter of *ZNF2* and *CFL1* .....184

## CHAPTER 1

### INTRODUCTION AND LITERATURE REVIEW

#### **Fungi and fungal infections**

The fungal kingdom is one of the six kingdoms of life. The fungi, animals, and plants are the three eukaryotic kingdoms that developed multicellularity in terrestrial environments. The immobility of fungi, the presence of cell wall, and the manifest morphological features of mushrooms likely contributed to the misclassification of fungi within botany. We now acknowledge that fungi are much more closely related to animals than to plants, with the help of molecular phylogenetic analysis [1].

Fungi are ubiquitous in the natural environment. They are found deep in the oceans, up in the earth's upper atmosphere, and in all of the habitats in between. It is estimated that the Kingdom Fungi include as many as 2.2 to 3.8 million or more distinct species, with only about 3-8% of fungi have been described by taxonomists [2]. Most fungal species are decomposers. They degrade biological matter, such as fallen leaves, wood, shed skin, and animal droppings. Some fungi make an enormous contribution to human life. The role of the baker/wine yeast in the production of alcohol and bread is well characterized. We consume some fungi directly in the form of edible mushrooms such as such as porcini and truffles as well as shiitake, enoki, oyster, and more. Additionally, fungi are also used for the production of antibiotics, such as penicillin, which revolutionized medicine and health care. Since the 1990s, fungi have been utilized for the production of recombinant proteins, some of which have great therapeutic potential. On the dark side, fungi can be serious pathogens to plants, animals and humans. Some fungi (species of the

genus *Aspergillus*, *Candida* and *Cryptococcus*) are capable of causing life-threatening infections in immunocompromised patients.

The last several decades have seen unprecedented increase in fungal infections in humans due to dramatic increases in populations with impaired immunity caused by the acquired immunodeficiency syndrome (AIDS), organ transplant, and other disorders or medical interventions. Despite the fact that fungal pathogens affect more than a billion people, resulting in approximately 11.5 million life-threatening infections and more than 1.5 million deaths annually [3], fungal infections have been largely neglected by social and political communities. This prompted an editorial paper titled ‘Stop neglecting fungi’ published by *Nature Microbiology* in 2017. Invasive fungal infections are devastating. The mortality rates for invasive fungal infections are generally exceptionally high, ranging from 5%-90% [3]. Among the top fungal killers, *Cryptococcus* species, *Aspergillus* species and *Candida* species claim most of the annual death tolls worldwide [3].

### ***Cryptococcus neoformans* and cryptococcosis**

*C. neoformans* is ubiquitous in the environment. *C. neoformans* is often enriched in soil contaminated with pigeon guano [4]. Humans are exposed to desiccated *C. neoformans* yeast cells or spores via inhalation. Exposure to *C. neoformans* can be detected in human at a 2-year-old age [5]. In individuals with competent immune systems, *C. neoformans* cells usually do not cause disease or any symptoms, and the inhaled yeast cells or spores either get cleared or become dormant [6]. This fungus can stay dormant for decades in the lungs of immunocompetent individuals. Upon the impairment or compromise of the host immune system, *C. neoformans* cells can be reactivated and disseminate through blood, penetrate blood-brain barrier, and cause fatal meningitis. The ability to grow at the 37°C body temperature, to produce melanin and

polysaccharide capsule, and the secretion of ureases and phospholipases make this environment fungus a successful pathogen [7].

The latest estimates suggest that HIV-associated cryptococcal meningitis accounts for 150,000-200,000 deaths per year, which is about 15% of the annual total deaths among AIDS patients [8]. These deaths occur mostly in sub-Saharan Africa where the associated mortality rate remains deplorably high at around 70% at 3 months after diagnosis. The causative *Cryptococcus neoformans* species complex belongs to the phylum Basidiomycota of “higher fungi”. The species complex is composed of strains of different serotypes based on the serological tests of the capsule. Serotype A (*Cryptococcus neoformans* var. *grubii*) causes about 95% of the cryptococcosis and serotype D (*C. neoformans* var. *neoformans*) claims less than 5% of the total cryptococcal infections [9, 10].

### **Morphogenesis and virulence in *Cryptococcus neoformans***

*Cryptococcus neoformans* is able to transition from yeast growth to filamentous growth in response to nutrition depletion, mating signal pheromone, or predation stress [13-16]. Hypha formation is also essential for the production of infectious meiotic basidiospores [14]. The spores and desiccated yeast cells are the main infectious propagules for cryptococcosis. The basidiospores are as infectious and pathogenic as yeast cells in mammalian infection model, but in some cases, spores can be much more pathogenic than yeasts [11, 12].

Similar to many dimorphic fungal pathogens, like *Blastomyces* species, *Histoplasma capsulatum* and *Candida albicans*, the morphological switch between yeast and filament (hypha and pseudohypha) is tightly associated with the fungal virulence in this pathogenic fungus [17, 18]. *C. neoformans* cells grow almost exclusively in the yeast form during infection within a mammalian host and the filament form of *Cryptococcus neoformans* cells are only rarely

observed in the clinical settings, suggesting the filamentous cells are virulence attenuated.

Intravenous or intracranial infection with purified filaments from a self-filamentous *C.*

*neoformans* strain causes cryptococcosis at lower rates compared to yeast cells purified from the same strain [15, 16, 19, 20]. For example, in 1978, Neilson et al. showed that cryptococcal pseudohyphae fail to kill mice even when inoculated intracranially, while the original strains in the yeast form are lethal [16].

However, unlike other dimorphic fungal pathogens, cryptococcal dimorphic transition from yeast to hypha is mostly sex-driven [21, 22]. Under conditions like dehydration and nitrogen nutrition starvation, yeast cells with opposite mating type undergo cell fusion and initiate dikaryotic filamentous growth. That is to say, hypha is an integral part of the sexual life cycle of *Cryptococcus neoformans* and hyphal cells are less virulent.

### **The regulation of morphogenesis by transcription factor Znf2 and RAM pathway**

*Cryptococcus* can assume the pseudohyphal form in response to nutrient limitation [23, 24]. Disruption of the regulation of Ace2 and morphogenesis (RAM) pathway, however, renders this fungus in the pseudohyphal form constitutively [25]. The RAM pathway is a conserved signal transduction network among eukaryotes [26], and it has been shown to impact numerous cellular processes, such as in the best studied species *Saccharomyces cerevisiae* to include cell cycle regulation [27, 28], cell separation [29-32], mating [29, 31], and cell polarization [29, 30, 32]. Ace2, the downstream target of the RAM pathway (i.e. downstream of the Cbk1 kinase) found in *S. cerevisiae* and *S. pombe* [25], does not exist in *C. neoformans*. Thus, the downstream targets of the RAM pathway in *Cryptococcus* remain elusive. Cryptococcal mutants in the RAM pathway (*tao3Δ*, *mob2Δ*, *kic1Δ*, *cbk1Δ*, and *sog2Δ*) all have the same pseudohyphal phenotype [25]. The mutants are sterile in crosses in which both mating types carry the same mutation.

They do not make mating filaments or the terminal basidia or basidiospores. Mutations in the RAM pathway also drastically attenuate cryptococcal virulence in a mammalian model of cryptococcosis [33].

*C. neoformans* is unique among the major human fungal pathogens in that the yeast-to-hypha transition is tightly associated with mating [21, 22]. The pheromone signaling cascade triggers nonself-recognition and cell fusion during bisexual mating. The resulting dikaryotic zygote initiates hyphal growth. Therefore, yeast-to-hypha transition in *Cryptococcus* has historically been considered a pheromone-dependent process. The pheromone receptor on the membrane activates the GPCR components once bound pheromone molecules and then the conserved downstream MAPK cascade components phosphorylate and activate a transcription factor that regulates the mating process [34, 35]. The central elements of the pheromone signaling pathway are conserved among various fungal species while the downstream transcription factors are often species specific [34]. Mat2 is an HMG-box transcription factor that functions downstream of the Cpk1 MAPK pathway. Mat2 binds to the pheromone-response element present in its downstream target genes and is essential for pheromone sensing and responding [20, 36]. Overexpression of *MAT2* is sufficient to increase the pheromone transcript levels several thousand-fold, evoke shmoo cell formation, and promote cell fusion [21]. However, the pheromone sensing pathway that activates the mating process has minimal impact on cryptococcal virulence, suggesting the existence of other pathways or factors that regulate the morphogenesis independent of pheromone sensing cascade [20, 37, 38] (**see Chapter 3**).

In 2010, Lin et. al identified the transcription factor Znf2 that regulates morphogenesis in *Cryptococcus neoformans* [20]. Znf2 is a zinc-finger transcription factor that functions downstream of Mat2 [20]. Deletion of *ZNF2* confines cells in the yeast form even when cells

were cultured under mating-inducing conditions, while overexpression of *ZNF2* induces constitutive hyphal growth even when cells were cultured under mating-suppressing conditions [20, 21]. More importantly, *znf2* $\Delta$  cells are more virulent in a mammalian model of cryptococcosis compare to wild type cells, while *ZNF2*<sup>oe</sup> cells are nonpathogenic [21]. Thus, Znf2 bridges morphogenesis and pathogenesis in the fungal pathogen *Cryptococcus neoformans*. Yet, the regulatory mechanisms by which Znf2 controls morphogenesis and pathogenesis in *C. neoformans* are not yet understood (see Chapter 4).

### **The regulation of virulence by transcription factor Znf2**

Both hyphae and pseudohyphae are morphological forms that are attenuated for virulence during *Cryptococcus* infection in a mammalian host (mouse). The implication between the virulence and morphotypes had been known for more than half a century, but its underlying molecular mechanism remains a mystery. The molecular link between hyphal filamentation and virulence in *C. neoformans* was further corroborated through the characterization of Znf2 [19, 20]. Overexpression of *ZNF2* drives the cryptococcal hyphal formation and greatly attenuates virulence [20, 21]. Excitingly, when *ZNF2*<sup>oe</sup> cells are used as vaccination strain, they can provide complete protection to the mice that are subsequently challenged with otherwise lethal wild type H99 cells [19]. Furthermore, even the heat-killed *ZNF2*<sup>oe</sup> cells provide a similar level of immune-protection against a subsequent infection by wild type H99 cells [19].

It is known that efficient clearance of *Cryptococcus* is dependent on Th1-polarized cell-mediated immunity. The hallmark cytokine of Th1 responses, gamma interferon (IFN- $\gamma$ ), is associated with classical activation of macrophages and is indispensable in protection against *Cryptococcus* [39]. Inoculation with an H99 strain expressing murine IFN- $\gamma$  provides immune-protection against wild type H99 cryptococcal infection in mice [40]. CD4<sup>+</sup> T cells recovered

from the airways of the mice infected with the *ZNF2<sup>oe</sup>* strain produced significantly higher levels of Th1 and Th17 cytokines like IFN- $\gamma$  and IL-17A, indicating the activation of the host cell-mediated immune response toward the protective Th1/Th17 type by *ZNF2<sup>oe</sup>* vaccination [19]. Two known *Znf2* downstream factors *Pum1* and *Cfl1* are dispensable for the immune-protection effect elicited by *Znf2* overexpression cells [19]. The immune-protective antigen(s) on the *ZNF2<sup>oe</sup>* cells remain to be identified.

Pseudohyphal cells are also virulence attenuated in mammals. We found that the RAM pathway and *Znf2* work in parallel in regulating different types of morphogenesis (pseudohyphal and hyphal growth) (see **Chapter 2**) [41]. However, whether the pseudohyphal cells are able to provide immuno-protection against H99 infection has not yet been tested.

## Reference

1. Bruns T. Evolutionary biology: a kingdom revised. *Nature*. 2006;443(7113):758-61. Epub 2006/10/20. doi: 10.1038/443758a. PubMed PMID: 17051197.
2. Hawksworth DL, Lucking R. Fungal Diversity Revisited: 2.2 to 3.8 Million Species. *Microbiol Spectr*. 2017;5(4). Epub 2017/07/29. doi: 10.1128/microbiolspec.FUNK-0052-2016. PubMed PMID: 28752818.
3. Brown GD, Denning DW, Gow NA, Levitz SM, Netea MG, White TC. Hidden killers: human fungal infections. *Sci Transl Med*. 2012;4(165):165rv13. doi: 10.1126/scitranslmed.3004404. PubMed PMID: 23253612.
4. Casadevall A, Perfect JR. *Cryptococcus neoformans*: Citeseer; 1998.
5. Goldman DL, Khine H, Abadi J, Lindenberg DJ, Pirofski L, Niang R, et al. Serologic evidence for *Cryptococcus neoformans* infection in early childhood. *Pediatrics*. 2001;107(5):E66.

Epub 2001/05/23. PubMed PMID: 11331716.

6. Alanio A, Vernel-Pauillac F, Sturny-Leclere A, Dromer F. *Cryptococcus neoformans* host adaptation: toward biological evidence of dormancy. *MBio*. 2015;6(2). Epub 2015/04/02. doi: 10.1128/mBio.02580-14. PubMed PMID: 25827423; PubMed Central PMCID: PMC4453510.

7. Casadevall A, Steenbergen JN, Nosanchuk JD. 'Ready made' virulence and 'dual use' virulence factors in pathogenic environmental fungi - the *Cryptococcus neoformans* paradigm. *Current opinion in microbiology*. 2003;6(4):332-7. doi: 10.1016/S1369-5274(03)00082-1. PubMed PMID: WOS:000185173000003.

8. Rajasingham R, Smith RM, Park BJ, Jarvis JN, Govender NP, Chiller TM, et al. Global burden of disease of HIV-associated cryptococcal meningitis: an updated analysis. *Lancet Infect Dis*. 2017. doi: 10.1016/S1473-3099(17)30243-8. PubMed PMID: 28483415.

9. Mitchell TG, Perfect JR. Cryptococcosis in the era of AIDS--100 years after the discovery of *Cryptococcus neoformans*. *Clin Microbiol Rev*. 1995;8(4):515-48. Epub 1995/10/01. PubMed PMID: 8665468; PubMed Central PMCID: PMC172874.

10. Hagen F, Khayhan K, Theelen B, Kolecka A, Polacheck I, Sionov E, et al. Recognition of seven species in the *Cryptococcus gattii/Cryptococcus neoformans* species complex. *Fungal genetics and biology : FG & B*. 2015;78:16-48. Epub 2015/02/28. doi: 10.1016/j.fgb.2015.02.009. PubMed PMID: 25721988.

11. Velagapudi R, Hsueh YP, Geunes-Boyer S, Wright JR, Heitman J. Spores as infectious propagules of *Cryptococcus neoformans*. *Infection and immunity*. 2009;77(10):4345-55. doi: 10.1128/IAI.00542-09. PubMed PMID: 19620339; PubMed Central PMCID: PMC2747963.

12. Giles SS, Dagenais TR, Botts MR, Keller NP, Hull CM. Elucidating the pathogenesis of

spores from the human fungal pathogen *Cryptococcus neoformans*. Infection and immunity. 2009;77(8):3491-500. doi: 10.1128/IAI.00334-09. PubMed PMID: 19451235; PubMed Central PMCID: PMCPMC2715683.

13. Kwon-Chung KJ, Edman JC, Wickes BL. Genetic association of mating types and virulence in *Cryptococcus neoformans*. Infection and immunity. 1992;60(2):602-5. Epub 1992/02/01. PubMed PMID: 1730495; PubMed Central PMCID: PMCPMC257671.

14. Ellis DH, Pfeiffer TJ. Ecology, life cycle, and infectious propagule of *Cryptococcus neoformans*. Lancet. 1990;336(8720):923-5. PubMed PMID: 1976940.

15. Neilson JB, Fromtling RA, Bulmer GS. Pseudohyphal forms of *Cryptococcus neoformans*: decreased survival in vivo. Mycopathologia. 1981;73(1):57-9. PubMed PMID: 7012632.

16. Neilson JB, Ivey MH, Bulmer GS. *Cryptococcus neoformans*: pseudohyphal forms surviving culture with *Acanthamoeba polyphaga*. Infection and immunity. 1978;20(1):262-6. PubMed PMID: 352931; PubMed Central PMCID: PMC421581.

17. Li ZM, Nielsen K. Morphology Changes in Human Fungal Pathogens upon Interaction with the Host. J Fungi. 2017;3(4). doi: UNSP 66  
10.3390/jof3040066. PubMed PMID: WOS:000453177000016.

18. Goldman DL, Fries BC, Franzot SP, Montella L, Casadevall A. Phenotypic switching in the human pathogenic fungus *Cryptococcus neoformans* is associated with changes in virulence and pulmonary inflammatory response in rodents. Proceedings of the National Academy of Sciences of the United States of America. 1998;95(25):14967-72. PubMed PMID: 9843999; PubMed Central PMCID: PMCPMC24559.

19. Zhai B, Wozniak KL, Masso-Silva J, Upadhyay S, Hole C, Rivera A, et al. Development

of protective inflammation and cell-mediated immunity against *Cryptococcus neoformans* after exposure to hyphal mutants. MBio. 2015;6(5):e01433-15. doi: 10.1128/mBio.01433-15. PubMed PMID: 26443458; PubMed Central PMCID: PMC4611043.

20. Lin X, Jackson JC, Feretzaki M, Xue C, Heitman J. Transcription factors Mat2 and Znf2 operate cellular circuits orchestrating opposite- and same-sex mating in *Cryptococcus neoformans*. PLoS genetics. 2010;6(5):e1000953. doi: 10.1371/journal.pgen.1000953. PubMed PMID: 20485569; PubMed Central PMCID: PMC2869318.

21. Wang L, Zhai B, Lin X. The link between morphotype transition and virulence in *Cryptococcus neoformans*. PLoS pathogens. 2012;8(6):e1002765. doi: 10.1371/journal.ppat.1002765. PubMed PMID: 22737071; PubMed Central PMCID: PMC3380952.

22. Wang L, Tian X, Gyawali R, Upadhyay S, Foyle D, Wang G, et al. Morphotype transition and sexual reproduction are genetically associated in a ubiquitous environmental pathogen. PLoS pathogens. 2014;10(6):e1004185. doi: 10.1371/journal.ppat.1004185. PubMed PMID: 24901238; PubMed Central PMCID: PMC4047104.

23. Lee SC, Phadke S, Sun S, Heitman J. Pseudohyphal growth of *Cryptococcus neoformans* is a reversible dimorphic transition in response to ammonium that requires Amt1 and Amt2 ammonium permeases. Eukaryotic cell. 2012;11(11):1391-8. doi: 10.1128/EC.00242-12. PubMed PMID: 23002105; PubMed Central PMCID: PMC3486016.

24. Lin X. *Cryptococcus neoformans*: morphogenesis, infection, and evolution. Infect Genet Evol. 2009;9(4):401-16.

25. Walton FJ, Heitman J, Idnurm A. Conserved elements of the RAM signaling pathway establish cell polarity in the basidiomycete *Cryptococcus neoformans* in a divergent fashion from

other fungi. *Molecular biology of the cell*. 2006;17(9):3768-80. doi: 10.1091/mbc.E06-02-0125. PubMed PMID: 16775005; PubMed Central PMCID: PMC1556378.

26. Maerz S, Seiler S. Tales of RAM and MOR: NDR kinase signaling in fungal morphogenesis. *Current opinion in microbiology*. 2010;13(6):663-71. doi: 10.1016/j.mib.2010.08.010. PubMed PMID: 20869909.

27. Bogomolnaya LM, Pathak R, Guo J, Polymenis M. Roles of the RAM signaling network in cell cycle progression in *Saccharomyces cerevisiae*. *Current genetics*. 2006;49(6):384-92. doi: 10.1007/s00294-006-0069-y. PubMed PMID: 16552603.

28. Brace J, Hsu J, Weiss EL. Mitotic exit control of the *Saccharomyces cerevisiae* Ndr/LATS kinase Cbk1 regulates daughter cell separation after cytokinesis. *Molecular and cellular biology*. 2011;31(4):721-35. doi: 10.1128/MCB.00403-10. PubMed PMID: 21135117; PubMed Central PMCID: PMC3028648.

29. Nelson B, Kurischko C, Horecka J, Mody M, Nair P, Pratt L, et al. RAM: a conserved signaling network that regulates Ace2p transcriptional activity and polarized morphogenesis. *Molecular biology of the cell*. 2003;14(9):3782-803. doi: 10.1091/mbc.E03-01-0018. PubMed PMID: 12972564; PubMed Central PMCID: PMC196567.

30. Du LL, Novick P. Pag1p, a novel protein associated with protein kinase Cbk1p, is required for cell morphogenesis and proliferation in *Saccharomyces cerevisiae*. *Molecular biology of the cell*. 2002;13(2):503-14. doi: 10.1091/mbc.01-07-0365. PubMed PMID: 11854408; PubMed Central PMCID: PMC65645.

31. Bidlingmaier S, Weiss EL, Seidel C, Drubin DG, Snyder M. The Cbk1p pathway is important for polarized cell growth and cell separation in *Saccharomyces cerevisiae*. *Molecular and cellular biology*. 2001;21(7):2449-62. doi: 10.1128/MCB.21.7.2449-2462.2001. PubMed

PMID: 11259593; PubMed Central PMCID: PMC86877.

32. Racki WJ, Becam AM, Nasr F, Herbert CJ. Cbk1p, a protein similar to the human myotonic dystrophy kinase, is essential for normal morphogenesis in *Saccharomyces cerevisiae*. The EMBO journal. 2000;19(17):4524-32. doi: 10.1093/emboj/19.17.4524. PubMed PMID: 10970846; PubMed Central PMCID: PMC302079.

33. Magditch DA, Liu TB, Xue C, Idnurm A. DNA mutations mediate microevolution between host-adapted forms of the pathogenic fungus *Cryptococcus neoformans*. PLoS pathogens. 2012;8(10):e1002936. doi: 10.1371/journal.ppat.1002936. PubMed PMID: 23055925; PubMed Central PMCID: PMC3464208.

34. Jones SK, Jr., Bennett RJ. Fungal mating pheromones: choreographing the dating game. Fungal genetics and biology : FG & B. 2011;48(7):668-76. Epub 2011/04/19. doi: 10.1016/j.fgb.2011.04.001. PubMed PMID: 21496492; PubMed Central PMCID: PMC3100450.

35. Ni M, Feretzaki M, Sun S, Wang X, Heitman J. Sex in fungi. Annu Rev Genet. 2011;45:405-30. Epub 2011/09/29. doi: 10.1146/annurev-genet-110410-132536. PubMed PMID: 21942368; PubMed Central PMCID: PMC3310392.

36. Kruzel EK, Giles SS, Hull CM. Analysis of *Cryptococcus neoformans* sexual development reveals rewiring of the pheromone-response network by a change in transcription factor identity. Genetics. 2012;191(2):435-49. Epub 2012/04/03. doi: 10.1534/genetics.112.138958. PubMed PMID: 22466042; PubMed Central PMCID: PMC3374309.

37. Davidson RC, Nichols CB, Cox GM, Perfect JR, Heitman J. A MAP kinase cascade composed of cell type specific and non-specific elements controls mating and differentiation of

the fungal pathogen *Cryptococcus neoformans*. *Molecular microbiology*. 2003;49(2):469-85. PubMed PMID: 12828643.

38. Wang P, Perfect JR, Heitman J. The G-protein beta subunit GPB1 is required for mating and haploid fruiting in *Cryptococcus neoformans*. *Molecular and cellular biology*. 2000;20(1):352-62. PubMed PMID: WOS:000084227100035.

39. Arora S, Hernandez Y, Erb-Downward JR, McDonald RA, Toews GB, Huffnagle GB. Role of IFN-gamma in regulating T2 immunity and the development of alternatively activated macrophages during allergic bronchopulmonary mycosis. *Journal of immunology*. 2005;174(10):6346-56. Epub 2005/05/10. PubMed PMID: 15879135.

40. Wormley FL, Perfect JR, Steele C, Cox GM. Protection against cryptococcosis by using a murine gamma interferon-producing *Cryptococcus neoformans* strain. *Infection and immunity*. 2007;75(3):1453-62. doi: 10.1128/iai.00274-06. PubMed PMID: WOS:000244733900042.

41. Lin J, Idnurm A, Lin X. Morphology and its underlying genetic regulation impact the interaction between *Cryptococcus neoformans* and its hosts. *Med Mycol*. 2015;53(5):493-504. doi: 10.1093/mmy/myv012. PubMed PMID: 25841056; PubMed Central PMCID: PMC4577057.

## CHAPTER 2

# MORPHOLOGY AND ITS UNDERLYING GENETIC REGULATION IMPACT THE INTERACTION BETWEEN *CRYPTOCOCCUS NEOFORMANS* AND ITS HOSTS<sup>1</sup>

---

<sup>1</sup> Jianfeng Lin, Alexander Idnurm, and Xiaorong Lin, 2015. *Medical Mycology*. 53(5):493-504.  
Reprinted here with permission of the publisher.

## Abstract

*Cryptococcus neoformans* is a fungus that causes the majority of fatal cryptococcal meningitis cases worldwide. This pathogen is capable of assuming different morphotypes: yeast, pseudohypha, and hypha. The yeast form is the most common cell type observed clinically. The hyphal and pseudohyphal forms are rarely observed in the clinical setting and are considered attenuated in virulence. However, as a ubiquitous environmental pathogen, *Cryptococcus* interacts with various organisms and it is known to be parasitic to different hosts. Capitalizing on recent discoveries, morphogenesis regulators were manipulated to examine the impact of cell shape on the cryptococcal interaction with three different host systems: the soil amoeba *Acanthamoeba castellanii* (a protist), the greater wax moth *Galleria mellonella* (an insect), and the murine macrophage cell line J774A.1 (mammalian cells). The RAM pathway is a highly conserved pathway among eukaryotes that regulates cytokinesis. Disruption of any of the five RAM components in *Cryptococcus* renders cells constitutively in the pseudohyphal form. The transcription factor Znf2 is the master activator of the yeast to hyphal transition. Deletion of *ZNF2* locks cells in the yeast form while overexpression of this regulator drives hyphal growth. Genetic epistasis analyses indicate that the RAM and the Znf2 pathways regulate distinct aspects of cryptococcal morphogenesis and independently of each other. These investigations using the *Cryptococcus* RAM and *ZNF2* mutants indicate that cell shape, cell size, and likely cell surface properties weigh differently on the outcome of cryptococcal interactions with different hosts. Thus, certain traits evolved in *Cryptococcus* that are beneficial within one host might be detrimental when a different host is encountered.

## Introduction

Morphological changes are fundamental to the ability of fungi to cause disease in plants and animals. For medically-relevant species, it is evident that disrupting the ability to change cell shape results in loss of pathogenicity, illustrated by work in dimorphic species in which strains locked into one cell form have impaired ability to cause disease .[42, 43] However, in many fungi it is still not clear what advantages some alternative cell morphologies provide or if they come at a fitness cost to the organism.

*Cryptococcus neoformans* is the major etiological agent of cryptococcal meningitis, a fatal disease that has been estimated to kill more than 600,000 people worldwide each year.[44] However, as a ubiquitous environmental pathogen, the encounter of this fungus with a susceptible mammalian host is accidental. Therefore, many virulence traits in this pathogen are postulated to be selected through its interaction with the environment or its natural predators. These virulence traits include encapsulation, melanization, and thermotolerance.[45] These traits are beneficial to this pathogen under natural conditions and also during infection in a mammalian host and are thus considered “dual use” factors.[46] Besides the aforementioned traits, cell morphotype also plays an important role in cryptococcal virulence (see reviews [24, 47] and references therein), similar to what has been demonstrated in many other environmental fungal pathogens.[48] However, most of the information on the impact of cryptococcal morphotype on its interaction with different hosts was obtained with natural isolates.[16] The difference in the genotype of isolates used as well as the underlying mechanisms responsible for the morphological changes complicates the interpretation of these studies. Critical genetic components controlling cryptococcal morphotypes have been identified in the past few years (as detailed below), making it now possible to conduct comparative analyses using cryptococcal

strains in the same genetic background, carrying different mutations, and with different morphological forms.

Three morphotypes can occur in *C. neoformans*: yeast, pseudohypha, or hypha. Enlarged yeast cells have also been characterized.[49-51] The fungus typically grows as a haploid yeast. The morphological transition from the yeast form to the hyphal form takes place during both bisexual mating (**a**- $\alpha$  mating) and unisexual mating (mostly  $\alpha$ - $\alpha$  mating).[52-58] Non-mating stimuli can also trigger hyphal growth.[21, 59, 60] Regardless of the upstream stimuli, the zinc-finger transcription factor Znf2 is a key regulator for hyphal growth (Figure 2.1A). Deletion of the *ZNF2* gene restricts *Cryptococcus* in the yeast form,[20, 21, 61] whereas elevated expression of *ZNF2* drives hyphal growth irrespective of environment stimuli or mating type.[21, 22, 61] Consistent with earlier observations of a reversed relationship between filamentation and virulence (see review [24] and references therein), the *znf2* $\Delta$  mutant in H99 background that is locked in the yeast form is more virulent than the wild-type, while the strain with overexpression of the *ZNF2* gene is incapable of causing fatal infection in mice.[20, 62]

*Cryptococcus* can assume the pseudohyphal growth form in response to nutrient limitation.[23, 24] Disruption of the regulation of Ace2 and morphogenesis (RAM) pathway, however, renders this fungus in the pseudohyphal form constitutively.[25] The RAM pathway is a conserved signal transduction network among eukaryotes,[26] and it has been shown to impact numerous cellular processes, such as in the best studied species *Saccharomyces cerevisiae* to include cell cycle regulation,[27, 28] cell separation,[29-32] mating,[29, 31] and cell polarization.[29, 30, 32] Similar to the RAM pathway in *S. cerevisiae*, the RAM pathway in *C. neoformans* is composed of two serine/threonine protein kinases, Cbk1 and Kic1, and three associated proteins, Mob2, Tao3, and Sog2 (Figure 2.1A).[25, 33] Tao3 is likely the scaffold

protein in the RAM pathway,[25, 29, 30, 33] and Mob2 functions as a Cbk1-regulatory subunit.[63] Hym1, a RAM pathway component that physically associates with Kic1 in *S. cerevisiae*, has not been identified as a RAM component in *C. neoformans*. [25] The downstream targets of the RAM pathway (i.e. of the Cbk1 kinase) in *Cryptococcus* remain elusive. There is no cryptococcal homolog of Ace2, the downstream target of the RAM pathway found in *S. cerevisiae* and *S. pombe*. [25] Cryptococcal mutants in the RAM pathway (*tao3*, *mob2*, *kic1*, *cbk1*, and *sog2*) all have the same pseudohyphal phenotype. [25] In some strain backgrounds they are temperature-sensitive. [25, 33] The mutants are also sterile in crosses in which both mating types carry the same mutation in that they do not make mating filaments or the terminal basidia or basidiospores. Mutations in the RAM pathway also drastically attenuate cryptococcal virulence. [33]

Thus, both hyphae and pseudohyphae are attenuated morphological forms during *Cryptococcus* infection in a mammalian host (mouse). This reduction in virulence could be due to the inherent property of these morphological forms where the physical interconnections between cells prevent the fungus from extrapulmonary dissemination and consequently from causing fatal brain infections. Indeed, neither the *ZNF2<sup>oe</sup>* strain nor a RAM mutant in the H99 background could be detected in the brain tissue, although both were present in the lungs during infection. [33, 64] Given that *Cryptococcus* likely disseminates to the brain at least in part through a Trojan horse mechanism after being phagocytosed by host cells, [65-67] it would be interesting to test if morphotype affects phagocytosis of cryptococcal cells. The pseudohyphal form was isolated as being resistant to phagocytosis by soil amoebae in the 1970s. [16] These natural pseudohyphal isolates were later found to harbor mutations in the RAM pathway. [25] It is not known if the hyphal form of *Cryptococcus* is also resistant to the phagocytosis by soil

amoebae and if common factors affect phagocytosis of the two filamentous forms of *Cryptococcus* by amoebae, wax moth, and mammalian phagocytes.

In this study, we tested if the RAM pathway and the Znf2 pathway regulate independent or common aspects of cryptococcal morphogenesis based on genetic epistasis analyses. To investigate the impact of morphotype on cryptococcal interaction with different hosts, we used the RAM and *ZNF2* mutants (single and double mutants) that grow in different morphological forms and tested three different host systems: the soil amoeba *Acanthamoeba castellanii* (a protist), the wax moth *Galleria mellonella* (an insect), and the murine macrophage cell line J774A.1 (mammalian cells). Our results indicate that cell shape (filamentous form versus yeast form) weigh differently on the outcome of the interaction between *Cryptococcus* and different hosts. Thus, certain traits evolved in *Cryptococcus* that are beneficial against one predator might be detrimental when a different host is encountered, and the effect of morphotype is host- and condition- specific.

## **Methods and Materials**

### **Strains, growth conditions, and morphological examination**

Strains used in this study are listed in Table S2.1. The recombinant progeny between RAM pathway gene mutations and *ZNF2* alleles were isolated from crosses, and their mating type and genotype were confirmed by phenotypic assays and PCR. All *C. neoformans* cells were maintained on yeast peptone dextrose (YPD) medium or YPD + Cu<sup>2+</sup> (20 μM) for the P<sub>CTR4-2-</sub>*ZNF2* strain at 30°C unless stated otherwise. For crosses to test for amoebic predation, **a** and **α** mating pairs with equal number of cells (five microliters each at the cell concentration of 1.5 x 10<sup>7</sup> cells/mL) were cultured together on V8 agar medium in the dark at 22°C. Hallmarks of

successful mating, including the formation of mating hyphae and spores, were examined using the Olympus SZX 16 stereoscope.

For morphological examination, the wild-type and the mutant strains were inoculated into liquid media of YPD, YPD+copper (20  $\mu$ M), or YPD+ bathocuproinedisulfonic acid (BCS; 200  $\mu$ M) with the initial OD<sub>600</sub> being 0.1. After 60 hours of standing incubation, cellular morphology of these strains was examined under an Olympus CX41 light microscope. Images of these cells were captured using the QCapture software.

### **Murine macrophage phagocytosis assay**

Mouse macrophage cell line J774A.1 (ATCC<sup>®</sup> TIB-67<sup>™</sup>) was acquired from ATCC, along with the ATCC-formulated Dulbecco's Modified Eagle's Medium (DMEM, catalog no. 30-2002). Fetal bovine serum (FBS) was added into DMEM to a final concentration of 10% immediately prior to the incubation. Three hundred microliters of freshly grown J774A.1 cells were seeded into 24 well microtiter plates, with  $2.5 \times 10^5$  cells per well. The macrophage cells were cultured at 37°C with 5% CO<sub>2</sub> overnight. Old culture media were then replaced by refresh DMEM with 10% FBS. *Cryptococcus* cells of  $2.5 \times 10^6$  or more were introduced to each well for the phagocytosis assay. After 30s of rock mixing, the co-cultures were incubated at 37°C with 5% CO<sub>2</sub> for an additional two hours. The co-cultures were then washed three times with warm PBS (500  $\mu$ L/well/time) to remove medium and non-adherent cells before fixed with 300  $\mu$ L 10% formaldehyde made in PBS.

For the pre-stain approach, *Cryptococcus* cells were stained with calcofluor white (20  $\mu$ g/mL) for five minutes before the infection. For the post-stain approach, calcofluor white was used to stain the cells after phagocytosis, and then cells were fixed. The rest of the experiments were performed the same way as described in the previous paragraph. The cells were examined

under an inverted microscope (Eclipse Ti, Nikon) and the images were captured using the NIS elements AR 3.0 software.

### **Amoebic predation assays**

*Acanthamoeba castellanii* (ATCC<sup>®</sup> 30234<sup>™</sup>) purchased from ATCC was stored and grown in the PYG medium (ATCC<sup>®</sup> media 712) as described on the product sheet supplied by ATCC. In brief, 0.25 mL peak density (about two week growth) culture was transferred into five mL fresh PYG liquid media and incubated at 22°C with a 15° horizontal slant.

For the predation assay, the agar plates were cultured for 60 hours with a lawn of cryptococcal cells (original inoculum per plate: 250 µL of a culture with OD<sub>600</sub>=0.5). A 5-10 µL aliquot of a week old amoebic culture (OD<sub>600</sub>≈0.8) was dropped onto the center of the cryptococcal lawn. The diameter of the predation halo on each plate was recorded daily. Each strain had three replicates. The amoebic predation zone was defined as Dt-D0 (the diameter on the day of recording subtract the initial diameter). Because the predation zone was not in a perfectly round shape, the diameter of the predation zone was defined as the average of diameters measured with 8 different directions (see Figure S2.1 for the diagram). The amoebic predation zone was then plotted against the time using the program OriginPro 8.6.

For the amoebic predation assay on mating colonies, we first cultured the mating pair together for a week to allow the mating hyphae to be generated before dropping an aliquot of the amoeba culture on top of the mating colony. Instead of measuring the predation diameter, the amoebic cell number recovered from each cryptococcal mating colony after 2-3 weeks of co-incubation was counted using a hemocytometer.

## ***Galleria mellonella* infection**

*Galleria mellonella* at the final instar larval stage were purchased from Vanderhorst Wholesale Inc. The greater wax moth infection experiments were performed as described previously.[68] *C. neoformans* strains were grown overnight in YPD+BCS (200  $\mu$ M) liquid medium. Cells were washed three times with PBS and then resuspended in PBS buffer to the final concentration of OD<sub>600</sub>=1. Using a 10  $\mu$ l Hamilton syringe, five microliters of *Cryptococcus* cells ( $\sim 5 \times 10^4$  yeast cells) were injected into *G. mellonella* hemocoel through the last left proleg, and the control group was injected with five microliters of sterile PBS. Before injection, the area was cleaned using an alcohol swab. After four hours of incubation at 30°C, the haemolymph of infected larvae ( $\sim 5 \mu$ L) was collected into 45  $\mu$ L anti-agglutination buffer *via* gentle squeezing of a cut at the proleg as described previously.[69] The haemolymph material containing haemocytes and fungal cells were then examined microscopically.

## **Results**

### **The RAM pathway and the Znf2 pathway control distinct aspects of morphogenesis**

To investigate the relationship between the RAM pathway and the Znf2 pathway, we crossed the *znf2* $\Delta$  mutant or the conditional *ZNF2* overexpression strain (*P<sub>CTR4-2</sub>-ZNF2*) with the RAM mutants (*tao3* $\Delta$ , *mob2* $\Delta$ , *kic1* $\Delta$ , *cbk1* $\Delta$ , and *sog2* $\Delta$ ). In the *P<sub>CTR4-2</sub>-ZNF2* strain, the expression of *ZNF2* is driven by the promoter of the copper transporter *CTR4*. [70] The expression of *ZNF2* is thus suppressed by copper and induced by copper starvation in the presence of copper chelator bathocuproinedisulfonic acid (BCS). [21, 22] The isolated double mutants were examined for their morphology and other phenotypes. We found that mutations in the different RAM components in these double mutants conferred the same phenotypes (data not

shown), consistent with their established role in one complex.[25, 33] Thus, for the following experiments, we chose to use strains with the deletion in the gene encoding the kinase Cbk1 to represent the RAM complex (Figure 2.1A).

To compare the morphology of the single and double mutants, we cultured the strains in YPD liquid medium with or without supplementation of copper or BCS. As expected, the wild-type H99 strain and the *znf2* $\Delta$  mutant showed the yeast morphotype under these conditions (Figure 2.1B). The *cbk1* $\Delta$  mutant grew in the pseudohyphal form (Figure 2.1B). The  $P_{CTR4-2}$ -*ZNF2* strain grew strictly in the yeast form in the YPD+copper medium, but it became filamentous in the YPD+BCS medium when the expression of *ZNF2* was induced (Figure 2.1B). Although the majority of the  $P_{CTR4-2}$ -*ZNF2* cells were in the yeast form in the YPD medium, a few cells became filamentous during prolonged incubation, likely due to the increasingly limited copper level in the medium. It is known that the YPD medium is copper-limiting; e.g. growth of the cryptococcal strain defective in the copper regulator Mac1/Cuf1 is poor in this medium.[58] The double mutant *cbk1* $\Delta$  *znf2* $\Delta$  had the same pseudohyphal morphotype as the single *cbk1* $\Delta$  mutant. Interestingly, the *cbk1* $\Delta$   $P_{CTR4-2}$ -*ZNF2* strain grew in the hyphal form when the expression of *ZNF2* was induced (YPD+BCS). The hyphal production caused by the induction of *ZNF2* in the *cbk1* $\Delta$  mutant background was more robust than the expression of *ZNF2* alone in the wild-type background (Figure 2.1B). We speculate that driving hyphal growth from pseudohyphae might be a more efficient process than switching to hyphal growth from yeast growth. The length of the hyphae increased overtime in this *cbk1* $\Delta$   $P_{CTR4-2}$ -*ZNF2* strain under the inducing condition (Figure 2.1C). In addition, these results show that the mating defect of the RAM mutants is not due to an impediment in their capabilities for filamentous development. These observations also indicate that the mutations in *znf2* and *cbk1* have somewhat complicated

genetic interactions: *ZNF2<sup>oe</sup>* is epistatic over *cbk1Δ* in hyphal formation, while *cbk1Δ* is epistatic over *znf2Δ* for pseudohyphal formation. However, they show that the two pathways control distinct morphotype generation and that they act independently based on the phenotypes of the double mutants.

### **Murine macrophage cells can phagocytose yeasts and hyphae, but not pseudohyphae**

Although the *ZNF2<sup>oe</sup>* strain with constitutive activation of *ZNF2* is avirulent in the murine model of cryptococcosis, that strain could persist and amplify in the animal lungs during the first two weeks of infection.[20] A RAM mutant is also significantly attenuated in mouse model, but it can persist in the lungs even after 70 days post infection.[33] This is somewhat surprising given that the RAM mutants used in that experiment grow less well at 37°C *in vitro*.[25, 33] Interestingly, neither the *ZNF2<sup>oe</sup>* strain nor the RAM mutant causes infections in the brain, despite their presence in the lungs.[20, 33] As a Trojan horse mechanism is important for this facultative intracellular pathogen to spread systemically and to invade the brain,[65-67] we hypothesized that the filamentous morphotype (pseudohyphae or hyphae) might be blocked in dissemination from the lungs due to lack of phagocytosis.

To examine the impact of morphotype on the phagocytosis of *Cryptococcus* by murine macrophages, we infected the J774A.1 cell line with *Cryptococcus* cells including the wild-type H99 (yeast), the *cbk1Δ* mutant (pseudohyphae), and the *P<sub>CTR4-2</sub>-ZNF2* strain pre-cultured under the inducing condition (hyphae). After two hours of co-incubation, cells were washed with phosphate buffered saline (PBS) and fixed with formaldehyde. To distinguish extracellular from intracellular cryptococcal cells, we stained the cells with calcofluor white after phagocytosis (post-stain). Calcofluor white is a fluorochrome that binds chitin in the fungal cell wall[71] and it stains extracellular cryptococcal cells. As expected, we found both intracellular yeast cells and

adherent extracellular yeast cells of the wild type (Figure 2.2B), consistent with *Cryptococcus* being a facultative intracellular pathogen.[72] To our surprise, some hyphae produced by the *P<sub>CTR4-2-ZNF2</sub>* strain were also phagocytosed (Figure 2.2D). By contrast, no pseudohyphae of the *cbk1Δ* mutant were found either intracellularly or extracellularly (Figure 2.2F). To confirm that we did not miss any hidden cryptococcal cells, we cultured *Cryptococcus* with calcofluor white prior to the co-culture with J774A.1 cells (pre-stain). After two hours of co-culturing, cells were again washed with PBS and fixed with formaldehyde. This approach allows the clear visualization of cryptococcal cells, either intracellular or extracellular. Again, both intracellular and adherent extracellular yeast cells (H99) and hyphae (*P<sub>CTR4-2-ZNF2</sub>*) were observed (Figure 2.2A&C). Consistent with our post-stain approach, we did not find any *cbk1Δ* mutant pseudohyphae cells (Figure 2.2E&F). Taken together, the results indicate that the murine macrophage can engulf yeast and hyphae, but not pseudohyphae.

### **The hyphal and pseudohyphal, but not the yeast, forms of *Cryptococcus* are resistant to predation by amoebae**

The soil amoeba is proposed to act as one of the selective pressures for the evolution of virulence traits in *C. neoformans*. [33, 73-75] Prior observations indicate that the pseudohyphal RAM mutants are resistant to amoebic predation. [16, 25] Given the differences that we observed for the hyphae and pseudohyphae in the murine macrophage assays, we decided to examine the impact of morphotype as controlled by *Znf2* expression on cryptococcal resistance to amoebic predation.

We designed the following approach to assay amoebic predation. We first cultured a lawn of cryptococcal cells on an agar plate and then dropped the amoebic culture onto the center of the plate. The impact of the predation by amoebae is reflected by the clear zone expanded from the

center (Figure S2.1A). Conditions that favored rapid amplification of *Cryptococcus* (YPD and PYG media) were not suitable for the detection of amoebic predation (Figure S2.1B). In comparison, amoebic predation of *Cryptococcus* on nutrient-limiting V8 juice agar was easily detectable (Figure S2.1B).

We performed the amoebic predation assay with the wild-type H99 strain, the *cbk1* $\Delta$  mutant, the *znf2* $\Delta$  mutant, and the P<sub>CTR4-2</sub>-*ZNF2* strain on V8 medium with or without the addition of copper or BCS. Consistent with previous results,[16, 33] the *cbk1* $\Delta$  RAM mutant was highly resistant to the predation by amoebae and no expansion of the predation zone was detected even after three weeks of incubation (data not shown). We found cryptococcal pseudohyphal cells and amoebic cysts at the original inoculation sites, indicating that the pseudohyphal cells can indeed survive the amoebic predation under the tested conditions (data not shown). Amoebae predated the wild-type H99 strain and the *znf2* $\Delta$  mutant similarly well on these media (Figure 2.3A), both were in the yeast form under these tested conditions. Likewise, amoebae predated the P<sub>CTR4-2</sub>-*ZNF2* strain as well as the wild-type H99 on V8 medium or V8+copper medium (Figure 2.3A and Figure S2.1C). By contrast, the expansion of the amoebic predation zone on this P<sub>CTR4-2</sub>-*ZNF2* strain on the V8+BCS medium (with *ZNF2* induction) was drastically slower (Figure 2.3A and Figure S2.1C). We then used microscopy to examine closely three areas on this plate: the area outside of the predation zone, the border of the predation zone, and the area inside the predation zone. The P<sub>CTR4-2</sub>-*ZNF2* strain formed yeast colonies mixed with hyphae extending in all directions on V8+BCS medium (Figure 2.3B). At the border and inside the predation zone, yeast cells were being dismantled by amoebae, with hyphae being the “leftovers” (Figure 2.3B). Further examination of the P<sub>CTR4-2</sub>-*ZNF2* strain under a compound microscope revealed that amoebae engulfed and digested the yeast cells (Figure 2.3C). By contrast, amoebae only

wrapped around hyphae and the hyphae being attacked were still viable (Figure 2.3C). Thus, the cells of the same genetic makeup displayed difference in their resistance to amoebic predation due to their morphological difference.

The aforementioned results suggest that amoebae preferentially engulf yeast cells and leave behind hyphae or pseudohyphae. It is known that spontaneous mutations in the RAM pathway genes can occur relatively frequently under natural conditions and the reversion of these mutations also occur under conditions that select against the pseudohyphal form.[33, 64] Thus resorting to loss of RAM pathway signaling is a reasonable approach for *Cryptococcus* to resist the predation by amoebae. *Cryptococcus* is also known to naturally upregulate *ZNF2* and undergoes morphological transition from the yeast growth to hyphal growth during mating.[53, 54]

The experiments described thus far used transgenic *Cryptococcus* strains to investigate the role of morphology with different host organisms. Naturally formed mating hyphae of wild-type cells were then tested in amoebic predation assays. Mating colonies were formed by two pairs of wild-type strains: the serotype A (var. *grubii*) wild-type congenic pairs H99 $\alpha$  and KN99 $\mathbf{a}$ [76] and the serotype D (var. *neoformans*) congenic pairs XL280 $\alpha$  and XL280 $\mathbf{a}$ .[61] We included their corresponding *znf2* $\Delta$   $\mathbf{a}$  and  $\alpha$  strains as a control. It is known that *znf2* $\Delta$  mutants are capable of mating but they are specifically blocked in the hyphal morphogenesis.[29] As shown in Figure 4, the serotype D XL280 $\alpha$ -XL280 $\mathbf{a}$  pair mated robustly and produced abundant hyphae that gave the white fluffy appearance to the mating colony. The serotype A H99 $\alpha$ -KN99 $\mathbf{a}$  pair also mated and produced spotty hyphae at the periphery of the colony. As expected, the *znf2* $\Delta$  mutant mating colonies remained in the yeast form (Figure 2.4A). After the addition of amoebae, we noticed that yeast cells in the center of the H99 $\alpha$ -KN99 $\mathbf{a}$  mating colony were cleared by

amoebae. The corresponding non-filamenting mating colony of the H99 *znf2Δ* mutants was completely destroyed. Accordingly, more amoebic cells were recovered from the *znf2Δ* mutant mating colony than those from the wild-type mating colony (Figure 2.4B), most likely due to access to more digestible food source (yeast cells). Very minimal impact was observed on the XL280 $\alpha$ -XL280 $\alpha$  mating colony, where filamentation was much more robust compared to the serotype A (Figure 2.4A). Again, increased predation on the XL280 *znf2Δ* mutant mating colony was observed compared to the wild-type control (Figure 2.4A&B). Interestingly, amoebae made a much more modest impact in XL280 background compared to the H99 background, even for the *znf2Δ* mutant (Figure 2.4B). This suggests that other genetic factors, in addition to morphotype, also influence the efficiency of amoebic predation.

Collectively, the findings presented here indicate that hyphae and pseudohyphae are resistant to the amoeba *A. castellanii* while yeast cells, even genetically identical to the filamentous cells, are susceptible to this soil microbial hunter.

### **Hyphae and pseudohyphae elicit haemocyte nodulation during *Galleria mellonella* infection**

*Galleria mellonella* (the greater wax moth) has been used as an alternative host system to assess *C. neoformans* virulence traits. For example, the classic factors important for cryptococcal virulence in mammalian models, like melanin and capsule synthesis, were shown to be important also in the *G. mellonella* model.[68] Although insects do not have adaptive immune systems as mammals do, they do have sophisticated innate immune responses, including for pathogen recognition, production of antimicrobial peptides, and the formation of a multicellular complex to encapsulate invading pathogens.[77-79] Haemocytes are the major cellular defense mediator in the *G. mellonella* haemolymph and they are functionally equivalent to macrophages and neutrophils in mammals.[78] Haemocyte aggregation (haemocyte nodulation) is one of the most

important defense systems in insects to contain foreign invaders.[80, 81] Previous studies demonstrate that the pseudohyphal RAM mutants are attenuated in virulence in the *G. mellonella* model.[33] Here, we decided to analyze the impact of morphotype on the cellular responses of *G. mellonella* against *Cryptococcus*.

We infected *G. mellonella* with the wild-type H99 strain, the P<sub>CTR4-2-ZNF2</sub> strain, the *cbk1Δ* mutant, the *cbk1Δ* P<sub>CTR4-2-ZNF2</sub> strain, or the PBS control. All cryptococcal strains were pre-cultured overnight in YPD+BCS medium to induce hypha production in strains that contain the P<sub>CTR4-2-ZNF2</sub> construct (Figure 2.1C). Haemolymph samples were collected from infected larvae four hours after the injection, and they were immediately examined microscopically for haemocyte nodulation.[69, 73, 82] All strains elicited *Galleria* cellular immune responses, as haemocyte nodulation was detected for all of them (Figure 2.5). However, pseudohyphae and hyphae induced much stronger responses than yeast cells (Figure 2.5). At higher magnification, we found that yeast cells (H99) were phagocytosed by haemocytes and there was minute level of clustering of haemocytes compared to the PBS control. By contrast, hyphae and pseudohyphae caused large clustering of haemocytes, with many layers of haemocytes wrapped around the filamentous cryptococcal cells (Figure 2.5). This effective containment of hyphae and pseudohyphae by haemocyte nodulation likely contribute to this insect's resistance to the non-yeast forms.

## **Discussion**

The results presented in this study demonstrate the importance of morphotype in shaping the interaction between *Cryptococcus* and various hosts. Both hyphae and pseudohyphae confer resistance to the predation by soil amoebae (Table 2.1). Thus, being in a filamentous form is

beneficial to *Cryptococcus* in defending itself against this single-celled protist. Similarly, both hyphae and pseudohyphae are resistant to phagocytosis by haemocytes during infection in the greater wax moth. In the wax moth, however, haemocyte nodulation could effectively encase these filamentous cells and disable their infection. On the other hand, yeast cells, although vulnerable for phagocytosis, can effectively kill the infected larvae.[33, 68] Surprisingly, yeast and hyphae can both be phagocytosed by murine macrophages whereas no phagocytosis was observed for pseudohyphae (Figure 2.2). In this case, cell surface molecules differentially presented on hyphae versus pseudohyphae might be more critical than the physical shape. It is known that *Znf2* controls multiple cell surface factors in *Cryptococcus*, including proteins for cellular adhesion.[21, 22, 59] The effect of mutations in the RAM pathway on cryptococcal cell surface is unknown; however, these cells were not detected as adhered to macrophages. Nonetheless, strains in both filamentous forms are incapable of disseminating from the lungs in mouse models and are consequently unable to cause fatal brain infections.[21, 33] Thus, being in the yeast form is clearly advantageous for cryptococcal systemic spread in a mammalian host. Hence, as a facultative intracellular pathogen, resistance to phagocytosis is only part of the equation in determining the overall level of virulence of *Cryptococcus* in a multicellular host.

The physical size of the pathogen and of the phagocytes appears to be a critical factor for phagocytosis. For example, a previous study showed that haemocytes of *G. mellonella* are effective in phagocytosis of *Aspergillus fumigatus* conidia that are smaller than three micrometers.[64] Although we could easily detect phagocytosis of cryptococcal yeast cells of three to five micrometers by *G. mellonella* haemocytes (Figure 2.5), it is relatively rare to observe phagocytosis of filaments.[83] Attempts to engulf and destroy filaments are often likely to be futile as we observed for amoebae (Figure 2.3C). It is possible that *G. mellonella* resorts to

and relies primarily on haemocyte nodulation for particles of larger sizes, like hyphae or pseudohyphae (Figure 2.5). What is surprising to us is that the J774A.1 macrophage, which is of similar size as the amoebae used in this study, can efficiently engulf cryptococcal hyphae (Figure 2.2). It is unclear why macrophages failed to phagocytose pseudohyphae. Clustering of cells and/or lower adherence of the RAM mutant might be responsible for this phenomenon.

Differences in genotype, in addition to the variations in morphotype, also affect the outcome of the interaction between *Cryptococcus* and the host. For instance, yeast cells in the XL280 background are more resistant against amoebic predation than yeast cells in the H99 background (Figure 2.4). This is contrary to their virulence level in mouse models.[76, 84] Moreover, some yeasts might be digested and serve as a food source for amoebae ([85] and this study) while some other cryptococcal yeasts could revert that relationship and replicate inside amoebae after being phagocytosed.[73] In a murine model, alveolar macrophages could rapidly phagocytose yeast cells after the intratracheal infection.[72] However, yeast cells of some strains can adopt different strategies to avoid phagocytosis.[86, 87]

Often a microbial population grown under natural condition is not homogenous, even if the population is derived from a single parental cell. These cells could be heterogenous in cellular physiology, morphology, or size. The balance of different subpopulations could be shifted in response to different environmental stimuli, maximizing the community fitness or enhancing microbial survival under disparate conditions. Pigeon guano, the natural niche of *C. neoformans*, provides a stimulating environment for cryptococcal mating.[88] A cryptococcal mating colony, for example, contain yeasts, pseudohyphae, germ tubes, and hyphae. A subpopulation of the hyphae could further differentiate into fruiting bodies and generate recombinant progeny that are then distributed to new locations in the environment.[69] The stochasticity in gene expression in

cells of the same morphotype and the dynamics in morphotype transition are part of the hedge-betting strategy of this fungus to survive under changing and unpredictable selective pressures. Thus, although it is important to understand the impact of a pure morphotype on the cellular interaction between cryptococcus and the host, it is equally important to extrapolate such findings to the population level with caution. Similarly, the interpretation of the interaction of *Cryptococcus* with multicellular hosts at the cellular level should be placed in the context of the host organism as a whole.

### **Acknowledgements**

We thank Drs. Bing Zhai and Qingming Qin for their assistance with the macrophage experiments. We gratefully acknowledge the financial support from the National Institute of Allergy and Infectious Diseases (grants R21 AI094364 to AI, R01 AI097599 and R21 AI107138 to XL). AI is supported on an Australian Research Council Future Fellowship. XL holds an Investigators in the Pathogenesis of Infectious Disease Award from the Burroughs Wellcome Fund. The funders had no role in study design, data collection and analysis, decision to publish, or preparation of the manuscript.

**Conflict of interest:** We declare no competing interests exist.

## References

1. Nemecek JC, Wuthrich M, Klein BS. Global control of dimorphism and virulence in fungi. *Science* (New York, NY. 2006;312(5773):583-8. PubMed PMID: 16645097.
2. Holbrook ED, Rappleye CA. *Histoplasma capsulatum* pathogenesis: making a lifestyle switch. *Current opinion in microbiology*. 2008;11(4):318-24. PubMed PMID: 18573684.
3. Park BJ, Wannemuehler KA, Marston BJ, Govender N, Pappas PG, Chiller TM. Estimation of the current global burden of cryptococcal meningitis among persons living with HIV/AIDS. *Aids*. 2009;23(4):525-30. doi: 10.1097/QAD.0b013e328322ffac. PubMed PMID: 19182676.
4. Casadevall A, Perfect JR. *Cryptococcus neoformans*. Washington, D.C.: ASM Press; 1998.
5. Casadevall A, Steenbergen JN, Nosanchuk JD. 'Ready made' virulence and 'dual use' virulence factors in pathogenic environmental fungi--the *Cryptococcus neoformans* paradigm. *Current opinion in microbiology*. 2003;6(4):332-7. PubMed PMID: 12941400.
6. Lin X. *Cryptococcus neoformans*: morphogenesis, infection, and evolution. *Infect Genet Evol*. 2009;9(4):401-16.
7. Wang L, Lin X. Morphogenesis in fungal pathogenicity: shape, size, and surface. *PLoS pathogens*. 2012;8(12):e1003027. Epub 2012/12/14. doi: 10.1371/journal.ppat.1003027. PubMed PMID: 23236274; PubMed Central PMCID: PMC3516537.
8. Andrianopoulos A, Rodriguez-del Valle N, Klein B, Sil A. Dimorphic human fungal pathogens. In: Casadevall A, Mitchell AP, Berman J, Kwon-Chung KJ, Perfect JR, Heitman J, editors. *Human Fungal Pathogens* New York: Cold Spring Harbor Laboratory Press; in press.
9. Neilson JB, Ivey MH, Bulmer GS. *Cryptococcus neoformans*: pseudohyphal forms

surviving culture with *Acanthamoeba polyphaga*. *Infection and immunity*. 1978;20(1):262-6. PubMed PMID: 352931; PubMed Central PMCID: PMC421581.

10. Zaragoza O, Nielsen K. Titan cells in *Cryptococcus neoformans*: cells with a giant impact. *Current opinion in microbiology*. 2013;16(4):409-13. doi: 10.1016/j.mib.2013.03.006. PubMed PMID: 23588027; PubMed Central PMCID: PMC3723695.

11. Zaragoza O, Garcia-Rodas R, Nosanchuk JD, Cuenca-Estrella M, Rodriguez-Tudela JL, Casadevall A. Fungal cell gigantism during mammalian infection. *PLoS pathogens*. 2010;6(6):e1000945. Epub 2010/06/30. doi: 10.1371/journal.ppat.1000945. PubMed PMID: 20585557; PubMed Central PMCID: PMC2887474.

12. Okagaki LH, Strain AK, Nielsen JN, Charlier C, Baltes NJ, Chretien F, et al. Cryptococcal cell morphology affects host cell interactions and pathogenicity. *PLoS pathogens*. 2010;6(6):e1000953. Epub 2010/06/30. doi: 10.1371/journal.ppat.1000953. PubMed PMID: 20585559; PubMed Central PMCID: PMC2887476.

13. Kwon-Chung KJ. A new genus, *Filobasidiella*, the perfect state of *Cryptococcus neoformans*. *Mycologia*. 1975;67(6):1197-200. PubMed PMID: 765816.

14. Alspaugh JA, Davidson RC, Heitman J. Morphogenesis of *Cryptococcus neoformans*. *Contributions to microbiology*. 2000;5:217-38. PubMed PMID: 10863675.

15. Heitman J. Evolution of eukaryotic microbial pathogens via covert sexual reproduction. *Cell host & microbe*. 2010;8(1):86-99. doi: 10.1016/j.chom.2010.06.011. PubMed PMID: 20638645; PubMed Central PMCID: PMC2916653.

16. Kwon-Chung KJ. Morphogenesis of *Filobasidiella neoformans*, the sexual state of *Cryptococcus neoformans*. *Mycologia*. 1976;68(4):821-33. PubMed PMID: 790172.

17. Lin X, Hull CM, Heitman J. Sexual reproduction between partners of the same mating

- type in *Cryptococcus neoformans*. *Nature*. 2005;434(7036):1017-21. PubMed PMID: 15846346.
18. Wickes BL, Mayorga ME, Edman U, Edman JC. Dimorphism and haploid fruiting in *Cryptococcus neoformans*: association with the alpha-mating type. *Proc Natl Acad Sci USA*. 1996;93(14):7327-31. PubMed PMID: 8692992.
  19. Lin X, Huang JC, Mitchell TG, Heitman J. Virulence attributes and hyphal growth of *C. neoformans* are quantitative traits and the *MATa* allele enhances filamentation. *PLoS genetics*. 2006;2(11):e187.
  20. Wang L, Zhai B, Lin X. The link between morphotype transition and virulence in *Cryptococcus neoformans*. *PLoS pathogens*. 2012;8(6):e1002765. doi: 10.1371/journal.ppat.1002765. PubMed PMID: 22737071; PubMed Central PMCID: PMC3380952.
  21. Wang L, Tian X, Gyawali R, Lin X. Fungal adhesion protein guides community behaviors and autoinduction in a paracrine manner. *Proceedings of the National Academy of Sciences of the United States of America*. 2013;110(28):11571-6. doi: 10.1073/pnas.1308173110. PubMed PMID: 23798436; PubMed Central PMCID: PMC3710841.
  22. Fu J, Morris IR, Wickes BL. The production of monokaryotic hyphae by *Cryptococcus neoformans* can be induced by high temperature arrest of the cell cycle and is independent of same-sex mating. *PLoS pathogens*. 2013;9(5):e1003335. doi: 10.1371/journal.ppat.1003335. PubMed PMID: 23658522; PubMed Central PMCID: PMC3642078.
  23. Lin X, Jackson JC, Feretzaki M, Xue C, Heitman J. Transcription factors Mat2 and Znf2 operate cellular circuits orchestrating opposite- and same-sex mating in *Cryptococcus neoformans*. *PLoS genetics*. 2010;6(5):e1000953. doi: 10.1371/journal.pgen.1000953. PubMed PMID: 20485569; PubMed Central PMCID: PMC2869318.

24. Zhai B, Zhu P, Foyle D, Upadhyay S, Idnurm A, Lin X. Congenic strains of the filamentous form of *Cryptococcus neoformans* for studies of fungal morphogenesis and virulence. *Infection and immunity*. 2013;81(7):2626-37. doi: 10.1128/IAI.00259-13. PubMed PMID: 23670559; PubMed Central PMCID: PMC3697605.
25. Wang L, Tian X, Gyawali R, Upadhyay S, Foyle D, Wang G, et al. Morphotype transition and sexual reproduction are genetically associated in a ubiquitous environmental pathogen. *PLoS pathogens*. 2014;10(6):e1004185. doi: 10.1371/journal.ppat.1004185. PubMed PMID: 24901238; PubMed Central PMCID: PMC4047104.
26. Del Poeta M. Role of phagocytosis in the virulence of *Cryptococcus neoformans*. *Eukaryotic cell*. 2004;3(5):1067-75. doi: 10.1128/EC.3.5.1067-1075.2004. PubMed PMID: 15470235; PubMed Central PMCID: PMC522596.
27. Lee SC, Phadke S, Sun S, Heitman J. Pseudohyphal growth of *Cryptococcus neoformans* is a reversible dimorphic transition in response to ammonium that requires Amt1 and Amt2 ammonium permeases. *Eukaryotic cell*. 2012;11(11):1391-8. doi: 10.1128/EC.00242-12. PubMed PMID: 23002105; PubMed Central PMCID: PMC3486016.
28. Walton FJ, Heitman J, Idnurm A. Conserved elements of the RAM signaling pathway establish cell polarity in the basidiomycete *Cryptococcus neoformans* in a divergent fashion from other fungi. *Molecular biology of the cell*. 2006;17(9):3768-80. doi: 10.1091/mbc.E06-02-0125. PubMed PMID: 16775005; PubMed Central PMCID: PMC1556378.
29. Maerz S, Seiler S. Tales of RAM and MOR: NDR kinase signaling in fungal morphogenesis. *Current opinion in microbiology*. 2010;13(6):663-71. doi: 10.1016/j.mib.2010.08.010. PubMed PMID: 20869909.
30. Bogomolnaya LM, Pathak R, Guo J, Polymenis M. Roles of the RAM signaling network

in cell cycle progression in *Saccharomyces cerevisiae*. *Current genetics*. 2006;49(6):384-92. doi: 10.1007/s00294-006-0069-y. PubMed PMID: 16552603.

31. Brace J, Hsu J, Weiss EL. Mitotic exit control of the *Saccharomyces cerevisiae* Ndr/LATS kinase Cbk1 regulates daughter cell separation after cytokinesis. *Molecular and cellular biology*. 2011;31(4):721-35. doi: 10.1128/MCB.00403-10. PubMed PMID: 21135117; PubMed Central PMCID: PMC3028648.

32. Nelson B, Kurischko C, Horecka J, Mody M, Nair P, Pratt L, et al. RAM: a conserved signaling network that regulates Ace2p transcriptional activity and polarized morphogenesis. *Molecular biology of the cell*. 2003;14(9):3782-803. doi: 10.1091/mbc.E03-01-0018. PubMed PMID: 12972564; PubMed Central PMCID: PMC196567.

33. Du LL, Novick P. Pag1p, a novel protein associated with protein kinase Cbk1p, is required for cell morphogenesis and proliferation in *Saccharomyces cerevisiae*. *Molecular biology of the cell*. 2002;13(2):503-14. doi: 10.1091/mbc.01-07-0365. PubMed PMID: 11854408; PubMed Central PMCID: PMC65645.

34. Bidlingmaier S, Weiss EL, Seidel C, Drubin DG, Snyder M. The Cbk1p pathway is important for polarized cell growth and cell separation in *Saccharomyces cerevisiae*. *Molecular and cellular biology*. 2001;21(7):2449-62. doi: 10.1128/MCB.21.7.2449-2462.2001. PubMed PMID: 11259593; PubMed Central PMCID: PMC86877.

35. Racki WJ, Becam AM, Nasr F, Herbert CJ. Cbk1p, a protein similar to the human myotonic dystrophy kinase, is essential for normal morphogenesis in *Saccharomyces cerevisiae*. *The EMBO journal*. 2000;19(17):4524-32. doi: 10.1093/emboj/19.17.4524. PubMed PMID: 10970846; PubMed Central PMCID: PMC302079.

36. Magditch DA, Liu TB, Xue C, Idnurm A. DNA mutations mediate microevolution

between host-adapted forms of the pathogenic fungus *Cryptococcus neoformans*. PLoS pathogens. 2012;8(10):e1002936. doi: 10.1371/journal.ppat.1002936. PubMed PMID: 23055925; PubMed Central PMCID: PMC3464208.

37. Colman-Lerner A, Chin TE, Brent R. Yeast Cbk1 and Mob2 activate daughter-specific genetic programs to induce asymmetric cell fates. Cell. 2001;107(6):739-50. PubMed PMID: 11747810.

38. Renwick J, Daly P, Reeves EP, Kavanagh K. Susceptibility of larvae of *Galleria mellonella* to infection by *Aspergillus fumigatus* is dependent upon stage of conidial germination. Mycopathologia. 2006;161(6):377-84. doi: 10.1007/s11046-006-0021-1. PubMed PMID: 16761185.

39. Kechichian TB, Shea J, Del Poeta M. Depletion of alveolar macrophages decreases the dissemination of a glucosylceramide-deficient mutant of *Cryptococcus neoformans* in immunodeficient mice. Infection and immunity. 2007;75(10):4792-8. PubMed PMID: 17664261.

40. Charlier C, Nielsen K, Daou S, Brigitte M, Chretien F, Dromer F. Evidence of a role for monocytes in dissemination and brain invasion by *Cryptococcus neoformans*. Infection and immunity. 2009;77(1):120-7. PubMed PMID: 18936186.

41. Sabiiti W, Robertson E, Beale MA, Johnston SA, Brouwer AE, Loyse A, et al. Efficient phagocytosis and laccase activity affect the outcome of HIV-associated cryptococcosis. The Journal of clinical investigation. 2014;124(5):2000-8. Epub 2014/04/20. doi: 10.1172/JCI72950. PubMed PMID: 24743149; PubMed Central PMCID: PMC4001551.

42. Mylonakis E, Moreno R, El Khoury JB, Idnurm A, Heitman J, Calderwood SB, et al. *Galleria mellonella* as a model system to study *Cryptococcus neoformans* pathogenesis. Infection and immunity. 2005;73(7):3842-50. doi: 10.1128/IAI.73.7.3842-3850.2005. PubMed

PMID: 15972469; PubMed Central PMCID: PMC1168598.

43. Upadhyay S, Torres G, Lin X. Laccases involved in 1,8-dihydroxynaphthalene melanin biosynthesis in *Aspergillus fumigatus* are regulated by developmental factors and copper homeostasis. *Eukaryotic cell*. 2013;12(12):1641-52. Epub 2013/10/15. doi: 10.1128/EC.00217-13. PubMed PMID: 24123270; PubMed Central PMCID: PMC3889567.

44. Ory JJ, Griffith CL, Doering TL. An efficiently regulated promoter system for *Cryptococcus neoformans* utilizing the *CTR4* promoter. *Yeast*. 2004;21(11):919-26. doi: 10.1002/yea.1139. PubMed PMID: 15334556.

45. Herth W, Schnepf E. The fluorochrome, calcofluor white, binds oriented to structural polysaccharide fibrils. *Protoplasma*. 1980;105(1-2):129-33. doi: Doi 10.1007/Bf01279855. PubMed PMID: ISI:A1980KV58200011.

46. Feldmesser M, Kress Y, Novikoff P, Casadevall A. *Cryptococcus neoformans* is a facultative intracellular pathogen in murine pulmonary infection. *Infection and immunity*. 2000;68(7):4225-37. PubMed PMID: 10858240; PubMed Central PMCID: PMC101732.

47. Steenbergen JN, Shuman HA, Casadevall A. *Cryptococcus neoformans* interactions with amoebae suggest an explanation for its virulence and intracellular pathogenic strategy in macrophages. *Proceedings of the National Academy of Sciences of the United States of America*. 2001;98(26):15245-50. doi: 10.1073/pnas.261418798. PubMed PMID: 11742090; PubMed Central PMCID: PMC65014.

48. Kwon-Chung KJ, Fraser JA, Doering TL, Wang Z, Janbon G, Idnurm A, et al. *Cryptococcus neoformans* and *Cryptococcus gattii*, the Etiologic Agents of Cryptococcosis. *Cold Spring Harbor perspectives in medicine*. 2014;4(7). doi: 10.1101/cshperspect.a019760. PubMed PMID: 24985132.

49. Casadevall A. Amoeba provide insight into the origin of virulence in pathogenic fungi. *Advances in experimental medicine and biology*. 2012;710:1-10. doi: 10.1007/978-1-4419-5638-5\_1. PubMed PMID: 22127880.
50. Nielsen K, Cox GM, Wang P, Toffaletti DL, Perfect JR, Heitman J. Sexual cycle of *Cryptococcus neoformans* var. *grubii* and virulence of congenic **a** and **a** isolates. *Infection and immunity*. 2003;71(9):4831-41. PubMed PMID: 12933823.
51. Mak P, Zdybicka-Barabas A, Cytrynska M. A different repertoire of *Galleria mellonella* antimicrobial peptides in larvae challenged with bacteria and fungi. *Developmental and comparative immunology*. 2010;34(10):1129-36. doi: 10.1016/j.dci.2010.06.005. PubMed PMID: 20558200.
52. Lavine MD, Strand MR. Insect hemocytes and their role in immunity. *Insect biochemistry and molecular biology*. 2002;32(10):1295-309. PubMed PMID: 12225920.
53. Cytrynska M, Mak P, Zdybicka-Barabas A, Suder P, Jakubowicz T. Purification and characterization of eight peptides from *Galleria mellonella* immune hemolymph. *Peptides*. 2007;28(3):533-46. doi: 10.1016/j.peptides.2006.11.010. PubMed PMID: 17194500.
54. Lavine MD, Strand MR. Insect hemocytes and their role in immunity. *Insect Biochemistry and Molecular Biology*. 2002;32(10):1295-309. doi: [http://dx.doi.org/10.1016/S0965-1748\(02\)00092-9](http://dx.doi.org/10.1016/S0965-1748(02)00092-9).
55. Bogus MI, Kedra E, Bania J, Szczepanik M, Czygier M, Jablonski P, et al. Different defense strategies of *Dendrolimus pini*, *Galleria mellonella*, and *Calliphora vicina* against fungal infection. *Journal of insect physiology*. 2007. PubMed PMID: 17512001.
56. Strand MR, Pech LL. Immunological basis for compatibility in parasitoid-host relationships. *Annual review of entomology*. 1995;40:31-56. doi:

10.1146/annurev.en.40.010195.000335. PubMed PMID: 7810989.

57. Jackson JC, Higgins LA, Lin X. Conidiation color mutants of *Aspergillus fumigatus* are highly pathogenic to the heterologous insect host *Galleria mellonella*. PloS one. 2009;4(1):e4224. Epub 2009/01/22. doi: 10.1371/journal.pone.0004224. PubMed PMID: 19156203; PubMed Central PMCID: PMC2625396.

58. Perfect JR, Lang SD, Durack DT. Chronic cryptococcal meningitis: a new experimental model in rabbits. The American journal of pathology. 1980;101(1):177-94. PubMed PMID: 7004196; PubMed Central PMCID: PMC1903580.

59. Bunting LA, Neilson JB, Bulmer GS. *Cryptococcus neoformans*: gastronomic delight of a soil ameba. Sabouraudia. 1979;17(3):225-32. PubMed PMID: 394365.

60. Luberto C, Martinez-Marino B, Taraskiewicz D, Bolanos B, Chitano P, Toffaletti DL, et al. Identification of *App1* as a regulator of phagocytosis and virulence of *Cryptococcus neoformans*. The Journal of clinical investigation. 2003;112(7):1080-94. doi: 10.1172/JCI18309. PubMed PMID: 14523045; PubMed Central PMCID: PMC198528.

61. Kozel TR, Gotschlich EC. The capsule of *Cryptococcus neoformans* passively inhibits phagocytosis of the yeast by macrophages. Journal of immunology. 1982;129(4):1675-80. PubMed PMID: 7050244.

62. Nielsen K, De Obaldia AL, Heitman J. *Cryptococcus neoformans* mates on pigeon guano: implications for the realized ecological niche and globalization. Eukaryotic cell. 2007;6(6):949-59. PubMed PMID: 17449657.

**Table 2.1. Morphotype affects the interaction between *C. neoformans* and its hosts.**

	<b>YEAST</b>	<b>PSEUDOHYPHAE</b>	<b>HYPHAE</b>
<b><i>ACANTHAMOEBA CASTELLANII</i></b>	Phagocytosed	Survived	Survived
<b><i>GALLERIA MELLONELLA</i></b>	Phagocytosed	Contained by aggregated haemocytes	Contained by aggregated haemocytes
<b>MURINE MACROPHAGE CELL J774A.1</b>	Phagocytosed	No adherence or phagocytosis	Phagocytosed

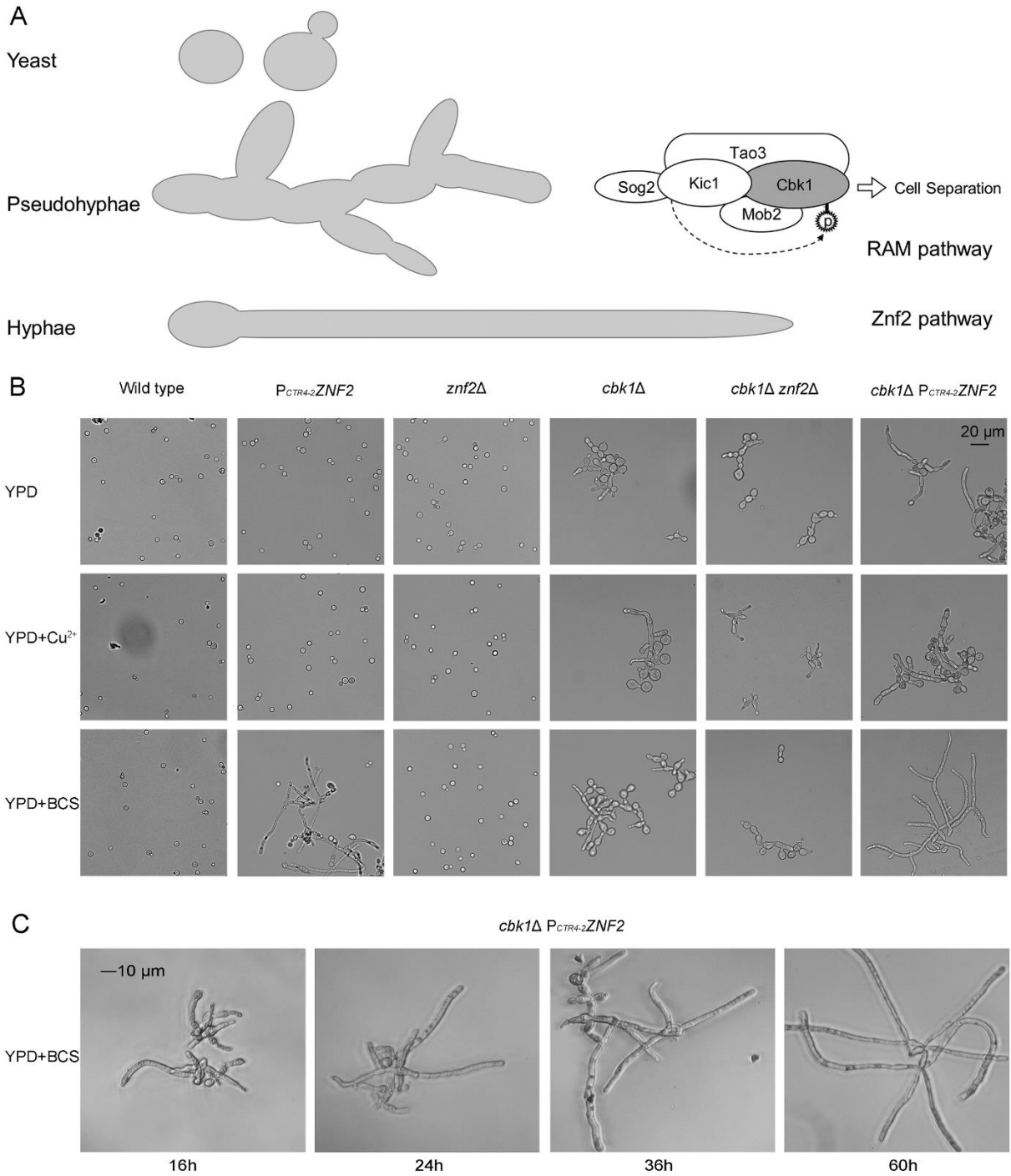


**Figure 2.1.** The Znf2 and the RAM pathways control distinct aspects of morphogenesis. (A) Diagram of the three morphotypes of *Cryptococcus* and the Znf2 and RAM pathways. The five RAM pathway components, Cbk1, Kic1, Mob2, Tao3 and Sog2, are depicted, with Cbk1 being

the ultimate kinase of this complex [25]. Znf2 is a master activator of filamentation. **(B)** The cellular morphology of the wild-type H99 strain, the  $P_{CTR4-2}ZNF2$  strain, the  $znf2\Delta$  mutant, the  $cbk1\Delta$  mutant, the  $cbk1\Delta znf2\Delta$  double mutant, and the  $cbk1\Delta P_{CTR4-2}ZNF2$  strain was examined from cultures in YPD, YPD+copper, and YPD+BCS media. **(C)** The cellular morphology of the  $cbk1\Delta P_{CTR4-2}ZNF2$  strain was examined microscopically after the induction of  $ZNF2$  expression for the indicated time periods.

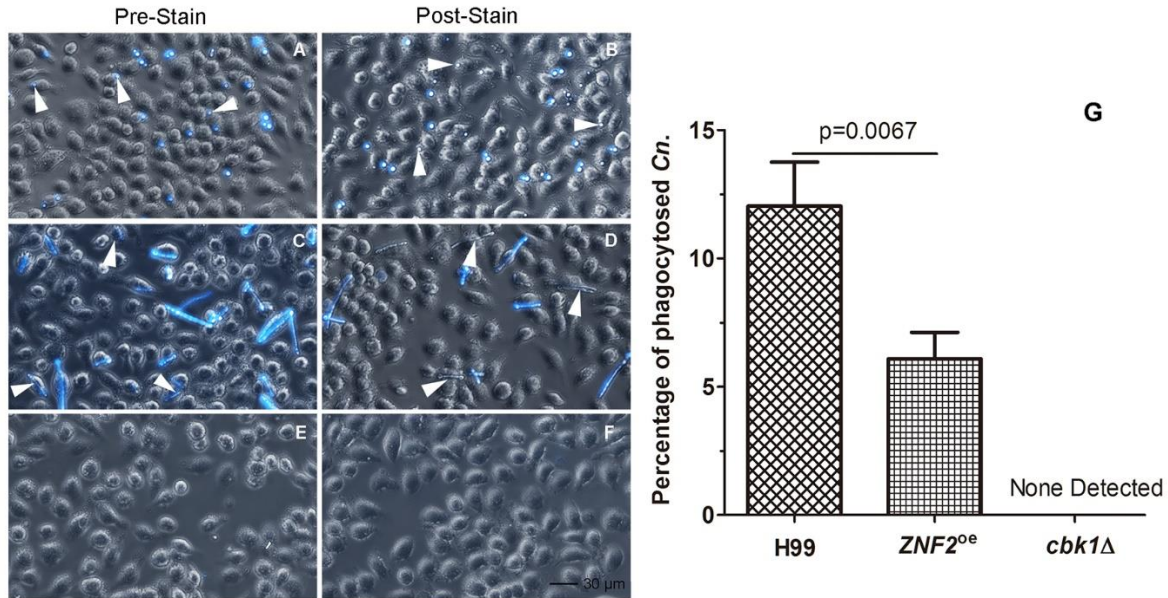


**Figure 2.2.** Phagocytosis of cryptococcal cells of different morphology by murine macrophage cells. Murine J774A.1 cells were infected by *C. neoformans* wild-type strain H99 (A&B), the *P<sub>CTR4-2</sub>ZNF2* strain (C&D), and the *cbk1Δ* mutant (E&F) for two hours and then fixed. The left panel images were taken with cryptococcal cells stained with calcofluor white prior to the infection (A, C, &D). The right panel images were taken with the co-culture stained with calcofluor white after fixation (B, D, &F).

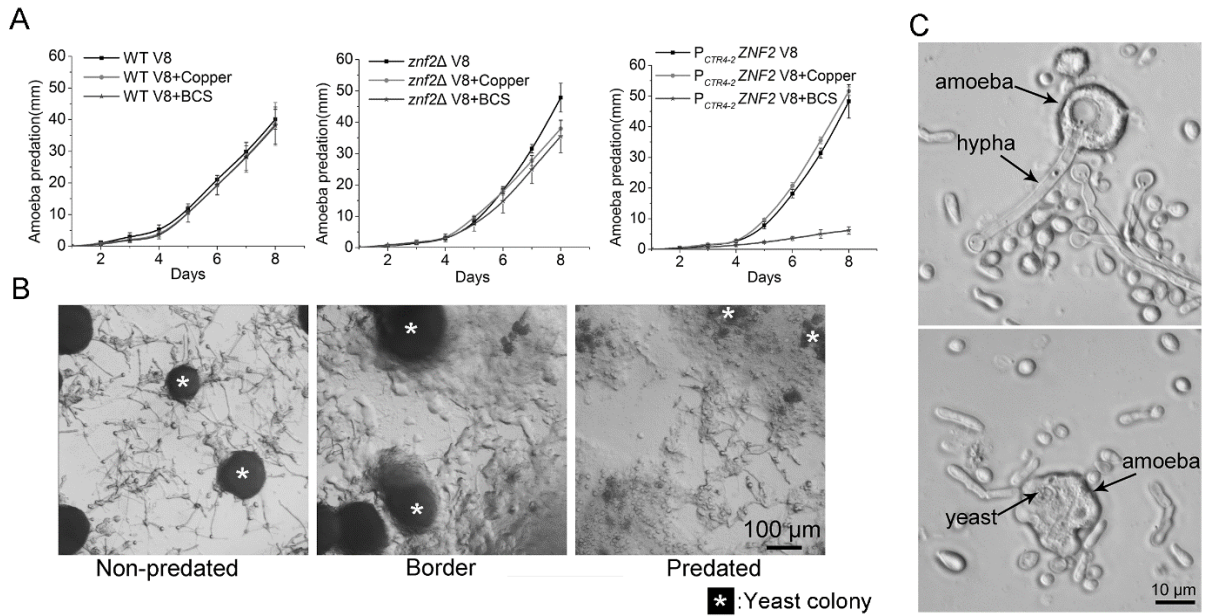


**Figure 2.3.** Amoebic predation of *Cryptococcus*. **(A)** The dynamics of amoebic predation of *Cryptococcus* wild-type strain H99, the *znf2Δ* mutant, and the  $P_{CTR4-2}ZNF2$  strain on V8 juice agar, V8+copper, and V8+BCS was recorded for 8 days. No expansion of predation zone on the *cbk1Δ* mutant was observed even after three weeks (not shown). **(B)** The area outside of the predation zone, at the front of the predation, and inside the predation zone of the  $P_{CTR4-2}ZNF2$  strain on V8+BCS agar medium. \* indicate the yeast colonies. **(C)** From the predation zone of the  $P_{CTR4-2}ZNF2$  strain on V8+BCS agar medium, amoebae with attempts to phagocytose hyphae were observed (upper image) and amoebae with completely phagocytosed yeast cells were observed (lower image).

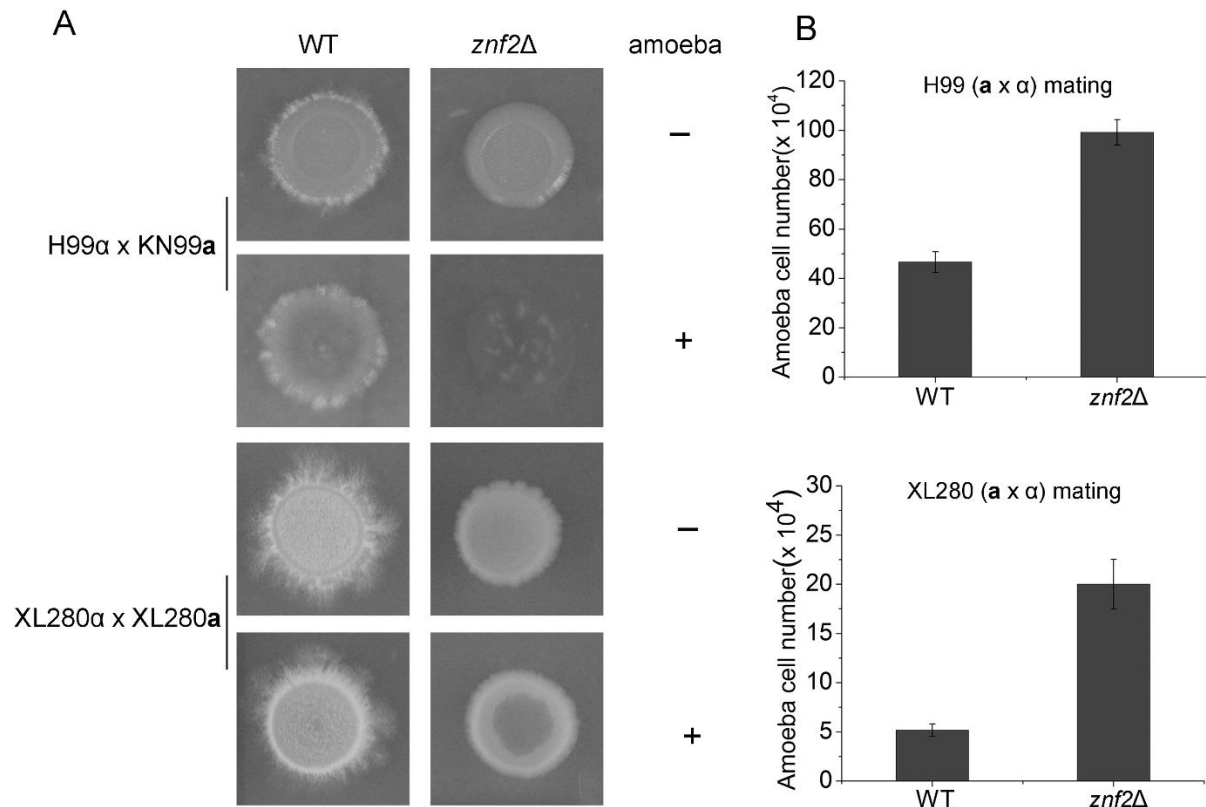
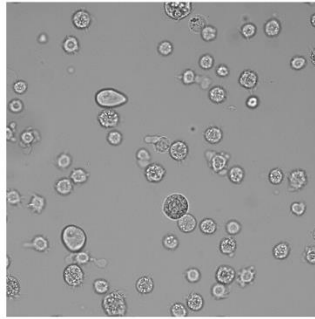
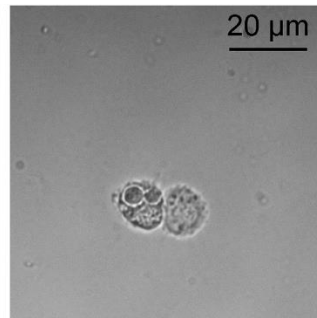
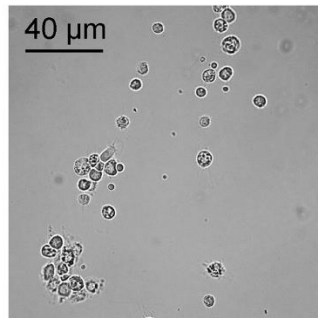


**Figure 2.4.** Amoebic predation of mating colonies. **(A)** The wild-type strain pairs (H99α x KN99α and XL280α x XL280α) and their corresponding *znf2Δ* mutant pairs were mated on V8 medium. The images of intact colonies and colonies with amoebae predation are shown. **(B)** Amoebae cells recovered from the mating colonies were quantified.

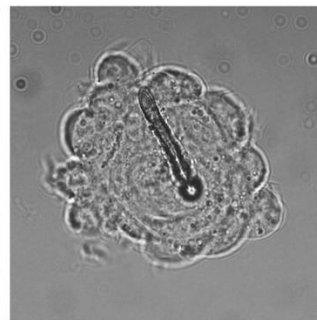
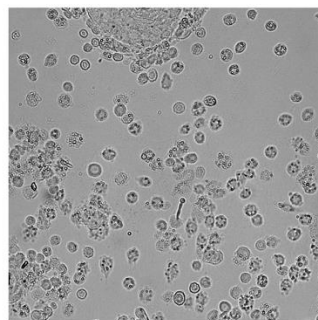
PBS



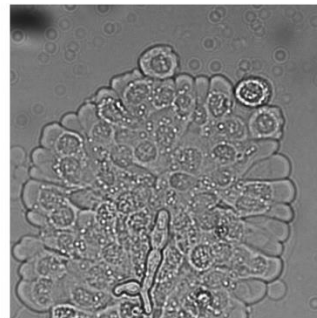
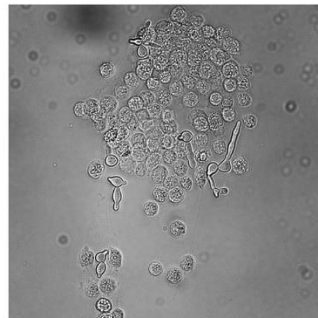
H99 $\alpha$



P<sub>CTR4-2</sub>ZNF2



*cbk1* $\Delta$



*cbk1* $\Delta$  P<sub>CTR4-2</sub>ZNF2

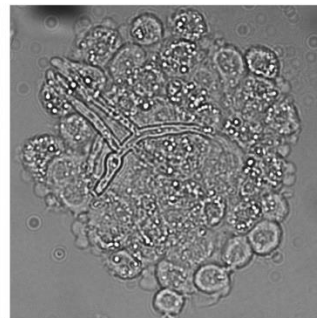
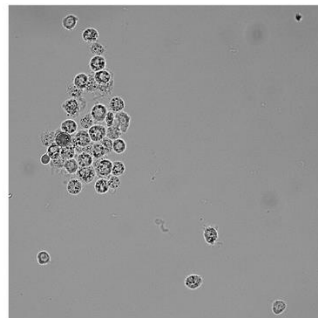


**Figure 2.5.** *Galleria mellonella* haemocyte nodulation induced by cryptococcal infections.

Larvae were infected by cryptococcal cells (wild-type H99, the *znf2*Δ mutant, and the P<sub>CTR4-ZNF2</sub> strain) precultured overnight in YPD+BCS liquid medium. Haemolymph from infected larvae was collected at 4 hours post inoculation and was immediately observed microscopically.

**Table S2.1.** Strains used in this study.

Name	Genotype	Source
H99 <sup>a</sup>	<i>MAT</i> $\alpha$ , WT, Serotype A	[84]
KN99a <sup>a</sup>	<i>MAT</i> <b>a</b> , WT, Serotype A	[89]
XL280 <sup>b</sup>	<i>MAT</i> $\alpha$ , WT, Serotype D	[90]
AIJ18 <sup>b</sup>	<i>MAT</i> <b>a</b> , WT, Serotype D	[61]
LW30 <sup>a</sup>	<i>MAT</i> $\alpha$ , P <sub>CTR-4-2</sub> :: <i>ZNF2A</i> -NEO	[21]
XL1601 <sup>a</sup>	<i>MAT</i> $\alpha$ , <i>znf2</i> ::NEO	[20]
XL1637 <sup>a</sup>	<i>MAT</i> <b>a</b> , <i>znf2</i> ::NEO	[20]
FJW9 <sup>a</sup>	<i>MAT</i> $\alpha$ , <i>cbk1</i> ::NAT	[25]
AIJ18 <sup>b</sup>	<i>MAT</i> <b>a</b> (= XL280 <b>a</b> )	[61]
AIJ9 <sup>b</sup>	<i>MAT</i> $\alpha$ (= XL280 $\alpha$ )	[61]
BZXL4 <sup>b</sup>	<i>MAT</i> $\alpha$ , <i>znf2</i> ::NAT	Obtained from a cross between XL280 <b>a</b> and XL574
BZXL5 <sup>b</sup>	<i>MAT</i> <b>a</b> , <i>znf2</i> ::NAT	Obtained from a cross between XL280 <b>a</b> and XL574
FJW8 <sup>a</sup>	<i>MAT</i> $\alpha$ , <i>kic1</i> ::NAT	[25]
FJW10 <sup>a</sup>	<i>MAT</i> $\alpha$ , <i>mob2</i> ::NAT	[25]
AI131 <sup>a</sup>	<i>MAT</i> $\alpha$ , <i>sog2</i> , T-DNA NAT	[25]
RM2 <sup>a</sup>	<i>MAT</i> $\alpha$ , <i>tao3</i> , T-DNA NAT	[25]
XL1653 <sup>a</sup>	<i>MAT</i> <b>a</b> , <i>kic1</i> ::NAT, <i>znf2</i> ::NEO	Obtained from a cross between FJW8 and XL1601.
XL1655 <sup>a</sup>	<i>MAT</i> $\alpha$ , <i>cbk1</i> ::NAT, <i>znf2</i> ::NEO	Obtained from a cross between FJW9 with XL1637.
XL1657 <sup>a</sup>	<i>MAT</i> $\alpha$ , <i>mob2</i> ::NAT, <i>znf2</i> ::NEO	Obtained from a cross between FJW10 and XL1637.
XL1658 <sup>a</sup>	<i>MAT</i> $\alpha$ , <i>tao3</i> ::NAT, <i>znf2</i> ::NEO	Obtained from a cross between AI136 and XL1637.
XL1659 <sup>a</sup>	<i>sog2</i> ::NAT, <i>znf2</i> ::NEO	Obtained from a cross between AI131 and XL1601.
XL1734 <sup>a</sup>	<i>MAT</i> $\alpha$ , P <sub>CTR-4-2</sub> - <i>ZNF2</i> -NEO, <i>cbk1</i> ::NAT	Obtained from a cross between LW30 and FJW9 <b>a</b> .
XL1731 <sup>a</sup>	<i>MAT</i> $\alpha$ , P <sub>CTR-4-2</sub> - <i>ZNF2</i> -G418, <i>kic1</i> ::NAT	Obtained from a cross between LW30 and FJW8 <b>a</b> .
XL1739 <sup>a</sup>	<i>MAT</i> $\alpha$ , P <sub>CTR-4-2</sub> - <i>ZNF2</i> -G418, <i>mob2</i> ::NAT	Obtained from a cross between LW30 and FJW10 <b>a</b>
XL1743 <sup>a</sup>	<i>MAT</i> $\alpha$ , P <sub>CTR-4-2</sub> - <i>ZNF2</i> -G418, <i>sog2-1</i> , T-DNA NAT	Obtained from a cross between LW30 and AI131 <b>a</b>

<sup>a</sup>: Strains in H99 $\alpha$ /KN99**a** background (Serotype A)  
<sup>b</sup>: Strains in XL280 background (Serotype D)

1. Perfect JR, Lang SD, Durack DT. Chronic cryptococcal meningitis: a new experimental

- model in rabbits. *The American journal of pathology*. 1980;101(1):177-194.
2. Nielsen K, Cox GM, Wang P, Toffaletti DL, Perfect JR, Heitman J. Sexual cycle of *Cryptococcus neoformans* var. *grubii* and virulence of congenic **a** and alpha isolates. *Infection and immunity*. 2003;71(9):4831-4841.
  3. Lin X, Huang JC, Mitchell TG, Heitman J. Virulence attributes and hyphal growth of *C. neoformans* are quantitative traits and the *MAT*alpha allele enhances filamentation. *PLoS genetics*. 2006;2(11):e187.
  4. Zhai B, Zhu P, Foyle D, Upadhyay S, Idnurm A, Lin X. Congenic strains of the filamentous form of *Cryptococcus neoformans* for studies of fungal morphogenesis and virulence. *Infection and immunity*. 2013;81(7):2626-2637.
  5. Wang L, Zhai B, Lin X. The link between morphotype transition and virulence in *Cryptococcus neoformans*. *PLoS pathogens*. 2012;8(6):e1002765.
  6. Lin X, Jackson JC, Feretzaki M, Xue C, Heitman J. Transcription factors Mat2 and Znf2 operate cellular circuits orchestrating opposite- and same-sex mating in *Cryptococcus neoformans*. *PLoS genetics*. 2010;6(5):e1000953.
  7. Walton FJ, Heitman J, Idnurm A. Conserved elements of the RAM signaling pathway establish cell polarity in the basidiomycete *Cryptococcus neoformans* in a divergent fashion from other fungi. *Molecular biology of the cell*. 2006;17(9):3768-3780.

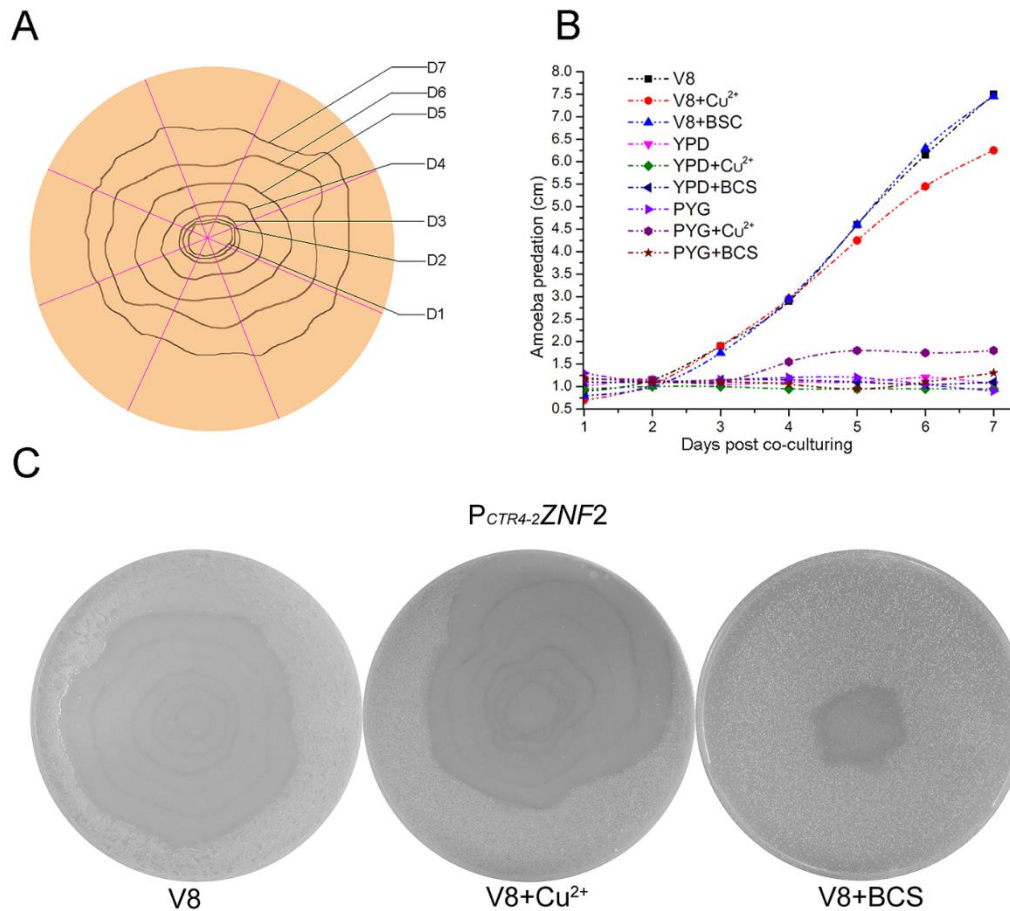


**Figure S2.1.** (A) Diagram for the amoebic predation zone measurement. The edge of the predation zone was delineated each day. The diameters in 8 indicated directions were measured, with 3 plate replicates for each sample. The predation zone formed after 24 hours was used as the baseline to eliminate the irregularity of the amoebae drops on different plates. (B) The dynamics of amoebic predation of *C. neoformans* on V8 juice agar, YPD agar, and PYG agar with or without the addition of copper or BCS. (C) The images of amoebic predation of the P<sub>CTR4-2</sub>ZNF2 strain on V8 juice agar, V8+copper, and V8+BCS were taken at the time of termination due to the fact that the amoebic predation zone reached the edge of the plate.

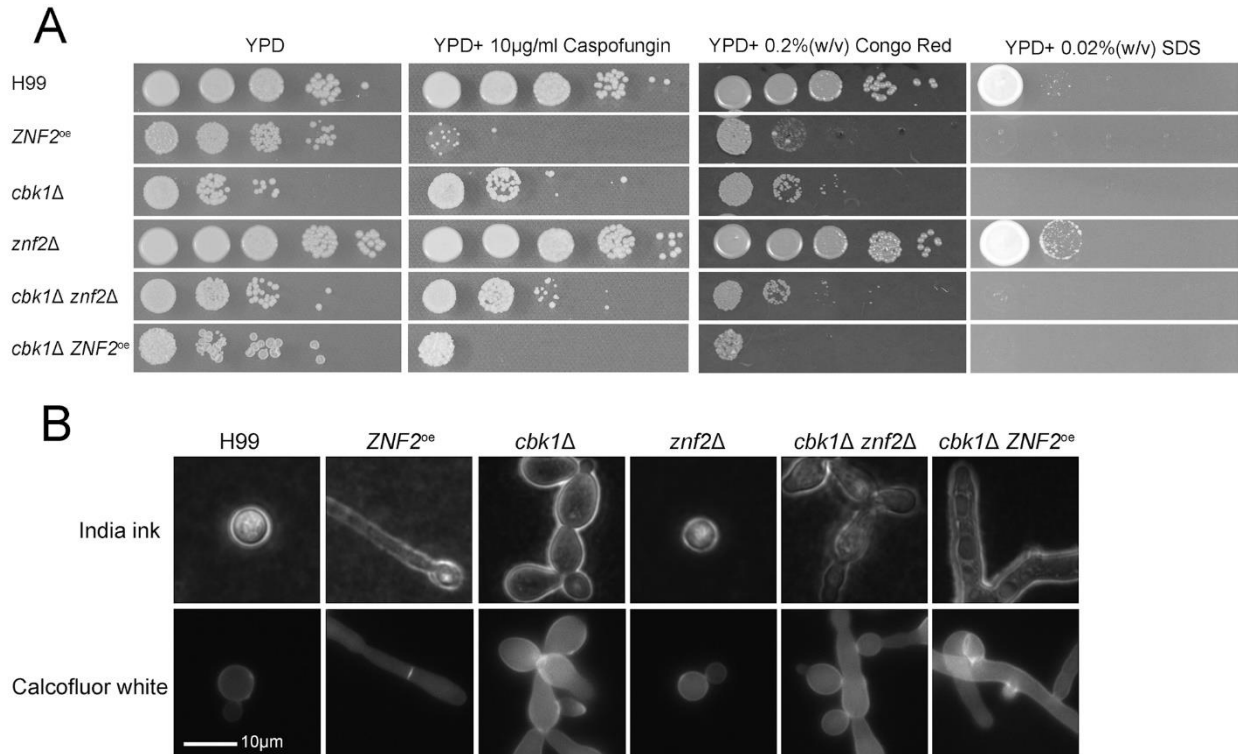


**Figure S2.2.** (A) Overnight cultures of the mutants and the wild type in YPD+ BCS liquid medium were diluted to an  $OD_{600}=1.0$ . Three microliters of tenfold serial dilutions of each strain was spotted onto YPD plates with or without cell wall perturbing agents. The strains were grown for additional 2 days at 30°C. (B) Mutants and the wild type were cultured overnight in YPD+ BCS liquid medium. Cells were then stained with Calcofluor white or India ink. Calcofluor white staining results were observed under a fluorescent microscope and India ink staining were observed under a compound microscope.

CHAPTER 3

GLUCOSAMINE STIMULATES PHEROMONE-INDEPENDENT DIMORPHIC  
TRANSITION IN *CRYPTOCOCCUS NEOFORMANS* BY PROMOTING CRZ1 NUCLEAR  
TRANSLOCATION<sup>2</sup>

---

<sup>2</sup> Xinpeng Xu\*, Jianfeng Lin\*, Youbao Zhao, Elyssa Kirkman, Yee-Seul So, Yong-Sun Bahn, and Xiaorong Lin, 2017. *PLoS Genetics*. 13(9):e1006982.

Reprinted here with permission of the publisher.

## Abstract

Morphotype switch is a cellular response to external and internal cues. The *Cryptococcus neoformans* species complex can undergo morphological transitions between the yeast and the hypha form, and such morphological changes profoundly affect cryptococcal interaction with various hosts. Filamentation in *Cryptococcus* was historically considered a mating response towards pheromone. Recent studies indicate the existence of pheromone-independent signaling pathways but their identity or the effectors remain unknown. Here, we demonstrated that glucosamine stimulated the *C. neoformans* species complex to undergo self-filamentation. Glucosamine-stimulated filamentation was independent of the key components of the pheromone pathway, which is distinct from pheromone-elicited filamentation. Glucosamine stimulated self-filamentation in H99, a highly virulent serotype A clinical isolate and a widely used reference strain. Through a genetic screen of the deletion sets made in the H99 background, we found that Crz1, a transcription factor downstream of calcineurin, was essential for glucosamine-stimulated filamentation despite its dispensability for pheromone-mediated filamentation. Glucosamine promoted Crz1 translocation from the cytoplasm to the nucleus. Interestingly, multiple components of the high osmolality glycerol response (HOG) pathway, consisting of the phosphorelay system and some of the Hog1 MAPK module, acted as repressors of glucosamine-elicited filamentation through their calcineurin-opposing effect on Crz1's nuclear translocation. Surprisingly, glucosamine-stimulated filamentation did not require Hog1 itself and was distinct from the conventional general stress response. The results demonstrate that *Cryptococcus* can resort to multiple genetic pathways for morphological transition in response to different stimuli. Given that the filamentous form attenuates cryptococcal virulence and is immune-stimulatory in

mammalian models, the findings suggest that morphogenesis is a fertile ground for future investigation into novel means to compromise cryptococcal pathogenesis.

### **Author Summary**

Cryptococcal meningitis claims half a million lives each year. There is no clinically available vaccine and the current antifungal therapies have serious limitations. Thus, identifying cryptococcal specific programs that can be targeted for antifungal or vaccine development is of great value. We have shown previously that switching from the yeast to the hypha form drastically attenuates/abolishes cryptococcal virulence. Cryptococcal cells in the filamentous form also trigger host immune responses that can protect the host from a subsequent lethal challenge. However, self-filamentation is rarely observed in serotype A isolates that are responsible for the vast majority of cryptococcosis cases. In this study, we found that glucosamine stimulated self-filamentation in genetically distinct strains of the *Cryptococcus* species complex, including the most commonly used serotype A reference strain H99. We demonstrated that filamentation elicited by glucosamine did not depend on the pheromone pathway, but it requires the calcineurin transcription factor Crz1. Glucosamine promotes nuclear translocation of Crz1, which is positively controlled by the phosphatase calcineurin and is suppressed by the HOG pathway. These findings raise the possibility of manipulating genetic pathways controlling fungal morphogenesis against diseases caused by the *Cryptococcus* species complex.

## Introduction

The opportunistic environmental fungal pathogen, *Cryptococcus neoformans*, is a leading killer of HIV-infected patients worldwide [44, 45]. It causes 1 million infections and more than half a million deaths each year worldwide [44]. *C. neoformans* is a species complex containing several serotypes (A, D, and AD hybrids) [91]. Among these serotypes, serotype A (*C. neoformans* var. *grubii*) causes approximately 95% of all cryptococcosis cases [92, 93], whereas serotype D (*C. neoformans* var. *neoformans*) is responsible for about 5% of the cases. The current anti-cryptococcal treatments rely primarily on azole antifungals with or without the induction therapy with amphotericin B [94]. The mortality rates of cryptococcosis are unacceptably high (~10-75%) [44, 95-97]. To further compound the problem, the emergence of resistance to azole drugs has been observed in multiple regions around the world [98-102] and relapse frequently occurs following treatment largely due to failure to clear the original infection [100, 103]. Thus, it is of great value to identify cryptococcal specific programs that can be used for new antifungal or vaccine development.

Morphotype switch between yeast and hypha is a cellular adaptation tightly linked to the virulence of dimorphic fungal pathogens [104-106]. In *Candida albicans*, proteins associated with hyphal growth are shown to impact its pathogenicity and some of them provide the bases for vaccine development [107-111]. Our previous studies in *C. neoformans* demonstrated that morphotypes (yeast or filament) are tightly linked to pathogenicity of this fungus as well [19-21]. Znf2, the master regulator of filamentation, is a potent anti-virulent factor. Deletion of this zinc finger transcription factor locks cells in yeast form and enhances fungal virulence in a murine model of cryptococcosis. Conversely, overexpression of *ZNF2* drives cells to the hyphal form and attenuates/abolishes the ability of *C. neoformans* to cause fatal infections [19-21].

*Cryptococcus* cells with *ZNF2* overexpression stimulate protective immune responses in the host and provide protection to the animal against a subsequent challenge by the highly virulent serotype A clinical isolate H99 [19]. These findings indicate that activation of the filamentation program could drastically compromise cryptococcal virulence. Thus, the yeast-to-hypha morphological transition provides an important avenue to explore alternative measures for the prevention and/or treatment of cryptococcal infections.

*C. neoformans* species is not considered a conventional dimorphic fungus due to the historical association of the yeast-to-hypha transition with mating. The mating response is controlled by the pheromone pathway composed of the pheromone, the pheromone receptor, the Cpk1 mitogen-activated protein kinase (MAPK) module, and the ultimate HMG domain transcription factor Mat2 [20, 37, 112-116]. The pheromone pathway promotes self-filamentation during unisexual development or dikaryotic filamentation during **a**-**α** bisexual development. As expected, the pheromone pathway is activated under mating-inducing conditions (e.g. dehydration, nutrition limitation, V8 juice, and darkness). However, the host environment is not favorable for mating and the pheromone pathway exerts no or minimal impact on virulence [20, 114, 117, 118]. Recent studies with *C. neoformans* serotype D isolates indicate that the pheromone pathway is essential for filamentation during **a**-**α** bisexual mating [20, 21, 90, 119, 120], but it is not necessary for self-filamentation in a unisexual population under certain conditions [121-124]. Given the largely unisexual population of *C. neoformans* (**α** >99%, **a** <1%), it is important to identify pheromone-independent pathways that can control self-filamentation.

Although all serotypes of the *C. neoformans* species complex are expected to possess the ability to undergo self-filamentation, self-filamentation is often observed in serotype D isolates

and rarely in serotype A isolates [56, 61, 125, 126], including the highly virulent clinical isolate and the most widely used serotype A reference strain H99 [84, 89, 127]. This hinders the investigation of morphological transition in *C. neoformans* as many resources are generated for the H99 background, including a congenic pair, gene deletion sets, a well-annotated genome, and vast literatures about cryptococcal biology and pathology [74, 128-130]. The rarity of self-filamentation in serotype A isolates challenge the possibility of mitigating the diseases caused by the *C. neoformans* species complex through activating the filamentation program.

Here, we found that glucosamine stimulated self-filamentation in both serotype D and serotype A strains, including H99. Although we found that both N-acetyl-glucosamine (GlcNAc) and glucosamine could stimulate filamentation in another fungal pathogen *C. albicans*, GlcNAc showed no effect on filamentation in *C. neoformans*. We demonstrated that filamentation in *C. neoformans* evoked by glucosamine was independent of the pheromone pathway. By genetic screens, we discovered that Crz1, a transcription factor downstream of calcineurin, was required for this process. The requirement of Crz1 for filamentation is specific to the response elicited by glucosamine, as Crz1 is not critical for filamentation elicited by pheromone [121]. We demonstrated that glucosamine promoted the translocation of Crz1 from the cytoplasm to the nucleus where it could exert its function as a transcription factor. Not surprisingly, we found that the catalytic and regulatory subunits of the phosphatase calcineurin, Cna1 and Cnb1, were essential for the nuclear translocation of Crz1 and for filamentation. Interestingly, multiple components in the HOG pathway, except Hog1 itself, acted as repressors of glucosamine-elicited filamentation through their calcineurin-opposing effect on Crz1's nuclear translocation. Deletion of these kinases increased the basal level of nucleus-localized Crz1. These findings indicate that *C. neoformans* can resort to different genetic pathways for morphological transition in response

to different stimuli, paving the way for future investigation to identify signals and targets that can be used to manipulate morphogenesis of this fungal pathogen *in vivo*.

## Results

### Glucosamine stimulates H99 and other strains to undergo self-filamentation

Wild-type H99 does not undergo self-filamentation under all mating-inducing conditions. Here, we decided to test the effect of different carbon sources based on previous studies in other dimorphic fungal pathogens such as *Candida albicans* [131-134], *Histoplasma capsulatum*, and *Blastomyces dermatitidis* [135] where N-acetyl-glucosamine (GlcNAc) activates hyphal growth. Here, we used YP medium (1% yeast extract and 2% peptone) as the base medium and supplemented it with different carbon sources at the final concentrations of 2%. We included 6-carbon sugars (glucose, galactose, and inositol), amino sugars (N-methyl-glucosamine, N-acetyl glucosamine, and glucosamine), and other carbon sources (glycerol, ethanol, and sodium acetate). None of the carbon sources tested stimulated filamentation in H99, with the exception of glucosamine (Figure 3.1A). Filamentation induced by glucosamine was unlikely to be an effect of carbon repression, as the non-metabolizable glucose analog 2-deoxyl glucose did not trigger filamentation in H99 (Figure 3.1A). The filamentation stimulated by glucosamine was also unlikely to be a general effect due to the activation of the hexamine metabolism pathway, as N-methyl-glucosamine and N-acetyl glucosamine both failed to stimulate filamentation in H99 (Figure 3.1A).

The effect of glucosamine on filamentation was dose-dependent, as glucosamine at lower concentrations (<0.5%) did not evoke obvious hyphal growth in H99 (Figure 3.1B). Robust filamentation was observed when glucosamine was present at concentrations higher than 1%

(Figure 3.1B). The addition of other carbon sources (e.g. glucose, galactose, or GlcNAc) inhibited filamentation in H99 (Figure 3.1C). This suggests potential competitive inhibition of glucosamine by other carbon sources. Although not all strains could produce hyphae on the glucosamine medium, glucosamine-stimulated filamentation was not limited to H99. Some other isolates of either serotype A or serotype D (e.g. XL280) self-filamented on glucosamine medium (Figure 3.1D). Interestingly, glucosamine-stimulated filamentation not only in *C. neoformans*, but also in some *C. albicans* strains (Figure S3.1). This suggests that glucosamine could be a general signal for fungal morphogenesis.

### **Glucosamine-stimulated filamentation requires Znf2 but not the pheromone sensing pathway controlled by Mat2**

*C. neoformans* typically undergoes yeast-to-hypha transition during  $\mathbf{a}\text{-}\alpha$  bisexual mating or during unisexual development. Two transcription factors, Mat2 and Znf2, were demonstrated to be critical for hyphal growth during sexual development [20, 21, 120]. Mat2 controls the pheromone pathway and plays a central role in cell fusion [20]. Under mating-inducing conditions (e.g. on V8 medium), Mat2 activates Znf2, the master regulator of filamentation [20, 21]. However, under mating-suppressing conditions (e.g. on YPD medium), overexpression of *MAT2* fails to activate Znf2 despite high levels of pheromone and *C. neoformans* remains in the yeast form [21].

We first examined the effect of glucosamine on the activity of Mat2 and Znf2 in wild-type H99. We measured the transcript levels of their target genes, which reflected the activities of these transcription factors. The pheromone gene *MF $\alpha$*  is the most upregulated gene controlled by Mat2 during both bisexual and unisexual development [20, 120]. The filamentation marker gene *CFL1* is one of the highly expressed genes upregulated by Znf2 [21, 59, 136]. We found

that the transcript levels of *MF $\alpha$*  and *CFLI* increased more than 100 and 300 folds respectively when H99 was cultured on glucosamine medium compared to that of the base medium at 96 hours (Figure 3.2A), indicating the activation of both Mat2 and Znf2.

To examine if self-filamentation in H99 evoked by glucosamine relies on Mat2 or/and Znf2, we tested the *znf2 $\Delta$*  mutant and the *mat2 $\Delta$*  mutant on glucosamine medium. As expected, the *MF $\alpha$*  transcript level was no longer induced by glucosamine in the *mat2 $\Delta$*  mutant (Figure 3.2A). By contrast, a strong induction of the filamentation marker *CFLI* at a level comparable to that in wild-type H99 was observed in the *mat2 $\Delta$*  mutant (Figure 3.2A). Consistent with the expression of the filamentation marker *CFLI*, the *mat2 $\Delta$*  mutant self-filamented on glucosamine medium (Figure 3.2B). A strain overexpressing *MAT2* (*MAT2<sup>oe</sup>*) also self-filamented on glucosamine medium. The result indicates that Mat2 is not essential for glucosamine-stimulated filamentation.

In contrast to the *mat2 $\Delta$*  mutant, there was no increase but rather a modest reduction in the *CFLI* transcript level in the *znf2 $\Delta$*  mutant on glucosamine medium compared to that of the base medium (Figure 3.2A). The *MF $\alpha$*  transcript level increased slightly (~4 fold) in this mutant (Figure 3.2A). The low level of *CFLI* in the *znf2 $\Delta$*  mutant was consistent with its non-filamentous phenotype on glucosamine medium (Figure 3.2B). Collectively, these observations indicate that Znf2, but not Mat2, is required for glucosamine-stimulated filamentation in H99. The self-filamentation observed in H99 and the *mat2 $\Delta$*  mutant was a response to glucosamine. The wild-type H99, the *mat2 $\Delta$*  mutant, or the *znf2 $\Delta$*  mutant is incapable of self-filamentation on V8 medium (Figure S3.2).

To determine if the dispensability of Mat2 and the essentiality of Znf2 in glucosamine-stimulated filamentation are conserved in *C. neoformans*, we further tested the *mat2 $\Delta$*  mutant and

the *znf2* $\Delta$  mutant made in the serotype D XL280 background. No hyphal growth was observed in the *znf2* $\Delta$  mutant while the *mat2* $\Delta$  mutant filamented similarly as the wild-type control on glucosamine medium (Figure S3.2). This is again different from filamentation observed on mating-inducing V8 medium where Mat2 is required (Figure S3.2)[20, 121]. This result corroborates the conclusion that filamentation elicited by glucosamine requires the morphogenesis regulator Znf2, but not the pheromone pathway regulator Mat2.

To further verify that the pheromone pathway is not critical for glucosamine-stimulated filamentation, we tested additional mutants in the H99 background with disruption in the following key components of this pathway (Figure 3.2C), namely the pheromone receptor Ste3 [137, 138], the pheromone receptor like protein Cpr2 [139], G $\alpha$  subunit Gpa1 [140], G $\beta$  subunit Gpb1 [141], a PAK kinase Ste20 $\alpha$  [142], the MAPK kinase kinase Ste11 $\alpha$  [117], the MAPK kinase Ste7 [37], and the MAPK Cpk1 [37]. Except for the *ste3* $\alpha$  $\Delta$  and the *ste7* $\Delta$  mutants, all other gene deletion mutants tested filamented on glucosamine medium (Figure 3.2C). The *ste3* $\alpha$  $\Delta$  could eventually produce some filaments after prolonged incubation. To verify that the blocked filamentation observed in the *ste7* $\Delta$  mutant is not an artifact, we tested multiple *ste7* $\Delta$  isolates generated in both mating type **a** and  $\alpha$  backgrounds. All the *ste7* $\Delta$  mutants tested showed only yeast growth on glucosamine medium, indicating the unique role of Ste7 in filamentation compared to other components of the pheromone pathway. Collectively, the results indicate that the pheromone pathway overall is dispensable for filamentation induced by glucosamine.

### **Identify the possible pathways involved in glucosamine-stimulated self-filamentation through genetic screens**

To identify genes that are involved in filamentation triggered by glucosamine, we screened approximately 2500 gene deletion mutants made in the H99 background for altered filamentation

on glucosamine medium. The strains screened included the partial genome deletion set generated by Dr. Hiten Madhani's group in 2015, and the transcription factor and the kinase deletion sets generated by Dr. Yong-Sun Bahn's group [143, 144]. Among the deletion mutants tested, two genes encoding the glucosamine-6-phosphate deaminase Gnd1 (gene locus # CNAG\_06098) and the glucosamine 6-phosphate N-acetyltransferase Gnat1 (gene locus # CNAG\_05695) are involved in the hexamine metabolism pathway (Figure S3.3A). The *gnd1* $\Delta$  mutant was unable to grow in the presence of glucosamine (even at concentrations lower than 0.1%) (Figure S3.3B), suggesting that the Gnd1 is essential for the growth of *C. neoformans* under such conditions. *GNAT1* was not essential for growth on glucosamine medium. However, the *gnat1* $\Delta$  mutant filamented as well as, if not better than, the wild-type H99 on glucosamine medium (Figure S3.3C). The result suggests that the hexamine metabolism is unlikely to be responsible for the filamentous growth elicited by glucosamine.

We classified the mutants screened with altered filamentation into four groups: non-filamentous group, decreased filamentation, increased filamentation, and hyper-filamentation (Figure S3.4 and Table S3.1). The fact that mutants with reduced/abolished filamentation and mutants with enhanced filamentation were recovered from the screen indicates that there are both repressors and activators of filamentation in response to glucosamine. Among mutants with enhanced filamentation, several were in the HOG pathway [145, 146] (Figure 3.3A), including the *tco1* $\Delta$ , *ssk1* $\Delta$ , *ssk2* $\Delta$ , and *pbs2* $\Delta$  mutants (Figure 3.3B). However, disruption of Hog1 itself, the downstream MAPK of this pathway, did not impact filamentation (Figure 3.3B). This observation suggests that glucosamine may not trigger the same response as osmotic stress. Consistent with this idea, the *crz1* $\Delta$  mutant is as resistant to osmotic stress caused by NaCl as the wild type (more details later. See Figure S3.8).

Among the gene deletion mutants that showed blocked filamentation on glucosamine medium were the calcineurin mutants. These include the mutants with disruption in genes encoding the calcineurin catalytic subunit *Cna1* [147, 148], the calcineurin regulatory subunit *Cnb1* [147, 149], and the calcineurin downstream zinc finger transcription factor *Crz1* (aka *Sp1*) [150-152] (Figure 3.4A-B, Table S3.1). The mutant defective in the calcineurin binding protein *Cbp1* [153, 154] showed reduced filamentation (Figure 3.4B). Treatment with the calcineurin inhibitor FK506 blocked the wild-type H99 from undergoing filamentation on glucosamine medium (Figure 3.4C), a phenotype similar to the *cna1Δ*, *cnb1Δ*, and *crz1Δ* mutants (Figure 3.4B).

Thus, the two pathways appear to exert opposing effects on glucosamine-stimulated self-filamentation in H99: the phosphorelay system and Ssk2-Pbs2 upstream of the Hog1 MAPK pathway suppress filamentation while the calcineurin pathway is required for filamentation.

### **Crz1 controls glucosamine-stimulated filamentation and functions upstream of Znf2**

Calcineurin transduces signals (e.g. elevated level of calcium) by dephosphorylating the downstream targets (Figure 3.4A). The transcription factor *Crz1* is one of the targets of calcineurin, and not all responses controlled by calcineurin depend on *Crz1* [155, 156]. For instance, the *cna1Δ* and *cnb1Δ* mutants displayed severe growth defect at 37°C and these mutants were hyper-sensitive to cell wall stress induced by Calcofluor White or Congo red [150-152, 155] (Figure S3.5). By contrast, the *crz1Δ* mutant showed only slightly increased sensitivity to cell wall stress and heat stress (Figure S3.5). Nonetheless, the *crz1Δ* mutant, like the calcineurin mutants (*cna1Δ* and *cnb1Δ*), was abolished in filamentation induced by glucosamine (Figure 3.4B). This suggests that *Crz1* is a major effector of the calcineurin pathway in regulating filamentation in response to glucosamine.

We then examined if overexpression of *CRZI* could promote filamentation on glucosamine medium. To this end, we placed the *CRZI* gene under the control of the constitutively active *GPD1* promoter [21, 22]. We introduced these constructs into the wild-type H99 or the *crz1Δ* mutant. We found that overexpression of *CRZI* enhanced filamentation (Figure 3.4D and Figure 3.5B). The enhancement in filamentation by *CRZI* overexpression was specific to the induction by glucosamine, as *CRZI* overexpression did not confer self-filamentation to either wild-type H99 or the corresponding *crz1Δ* mutant when cells were cultured alone on V8 medium (Figure S3.6A). Furthermore, the deletion of *CRZI* or the overexpression of *CRZI* did not affect the ability of the strain to cross with a wild-type partner of the opposite mating type based on the observation that there was no notable difference between the crosses *crz1Δ*  $\alpha$  x **a**, *CRZI*<sup>oc</sup>  $\alpha$  x **a**, and  $\alpha$  x **a** (Figure S3.6B). These findings suggest that alteration of the expression level of *CRZI* does not impact mating efficiency controlled by the pheromone pathway, consistent with the recent finding in a serotype D strain [157].

To examine the genetic relationship between Crz1 and Znf2 in the regulation of filamentation in response to glucosamine, we first measured the transcript levels of *ZNF2* and *CRZI* in the *znf2Δ* mutant and the *crz1Δ* mutant. The *CRZI* transcript level on glucosamine medium was comparable to that of the base medium in wild type and its transcript level was also comparable between the wild type and the *znf2Δ* mutant (Figure 3.5A). This result indicates that neither Znf2 nor glucosamine has much impact on *CRZI* at the transcript level. On the other hand, the *ZNF2* transcript level in wild-type H99 increased more than 6 fold on glucosamine medium and the degree of induction was much reduced in the *crz1Δ* mutant (2-3 fold) (Figure 3.5A). This suggests that deletion of *CRZI* attenuated the induction of *ZNF2* elicited by glucosamine. Furthermore, overexpression of *CRZI* failed to confer filamentation to the *znf2Δ*

mutant while overexpression of *ZNF2* restored filamentation in the *crz1Δ* mutant on glucosamine medium (Figure 3.5B). Collectively, these epistatic results indicate that Crz1 functions upstream of Znf2 in response to glucosamine.

We then examined if disruption of Crz1 affects the subcellular localization of Znf2 after the Znf2 protein is made. For this purpose, we introduced the  $P_{CTR4}$ -mCherry-*ZNF2* construct into the *crz1Δ* mutant and the wild-type H99 background. The mCherry-Znf2 signal was localized to the nucleus in both the *crz1Δ* mutant background and the wild-type background (Figure 3.5C). Collectively, the results suggest that Crz1 regulates *ZNF2* at the transcript level and it functions upstream of Znf2, and Crz1 does not affect the subcellular localization of the Znf2 protein.

### **Crz1 translocates from the cytosol to the nucleus in response to glucosamine**

Calcineurin is known to dephosphorylate Crz1 in response to certain stimuli like calcium or heat shock. Dephosphorylation causes the translocation of Crz1 from the cytosol to the nucleus for it to function as a transcription factor in *C. neoformans* [150-152] (Figure 3.4A). To examine if glucosamine affects the subcellular translocation of Crz1, we placed mCherry tagged Crz1 under the control of the constitutively active *GPD1* promoter. The exposure to either calcium or high temperature, two known stimuli of calcineurin, indeed stimulated mCherry-Crz1 in this overexpression strain to relocate from the cytosol into the nucleus (Figure 3.6A). As reported previously [152], NaCl induced granular localization of Crz1 in the cytosol (Figure 3.6A), indicating that the nuclear translocation of Crz1 is stimulus-specific. We then tested the effect of glucosamine on the subcellular localization of Crz1. Remarkably, greater than 90% of the cryptococcal population showed nuclear localization of Crz1 in the presence of glucosamine (Figure 3.6A-B). This indicates that glucosamine, like calcium, greatly increases the

translocation of Crz1 from the cytosol into the nucleus. The translocation of Crz1 to the nucleus in response to calcium and glucosamine was not affected by Znf2 (Figure 3.6C-D), consistent with Crz1 functioning upstream of Znf2. To verify that the nuclear translocation effect of glucosamine was not an artifact due to *CRZI* overexpression, we tested Crz1-mCherry placed under the control of its native promoter that was used in a recent study [156]. Again, glucosamine greatly increased the population of cryptococcal cells with nucleus-localized Crz1, as did calcium and the exposure to high temperature (Figure S3.7). This finding indicates that glucosamine enhances nuclear translocation of the Crz1 protein regardless its gene expression level.

If glucosamine activates filamentation through its effect on the translocation of Crz1, we hypothesized that overexpression of *CRZI* would be futile in the absence of a functional calcineurin. Indeed, no filamentation was observed when *CRZI* was overexpressed in the *cna1Δ* mutant or the *cnb1Δ* mutant (Figure 3.7A). Similarly, overexpression of *CRZI* did not restore the temperature sensitivity of the *cna1Δ* mutant (Figure S3.8). Consistent with our hypothesis, Crz1 showed only cytoplasmic localization in the calcineurin *cna1Δ* and *cnb1Δ* mutants, regardless whether the cells were cultured in YPD medium or in glucosamine medium (Figure 3.7B-C). The *cbp1Δ* mutant showed reduced filamentation and overexpression of *CRZI* in *cbp1Δ* restored filamentation (Figure 3.7A). Consistently, Crz1 was more concentrated in the nucleus in this mutant background (Figure 3.7B-C). The results demonstrate the essential role of calcineurin in controlling the nuclear translocation of Crz1, which correlates with robustness in filamentation.

## **Components of the HOG pathway suppress filamentation by regulating the subcellular localization of Crz1**

Multiple components of the HOG pathway, namely Tco1 (hybrid histidine kinase), Ssk1 (response regulator), Ssk2 (MAPKKK), and Pbs2 (MAPKK), suppress glucosamine-stimulated filamentation given that disruption of these components enhanced filamentation (Figure 3.3). We decided to examine if the HOG pathway components suppress filamentation through Crz1. For this purpose, we made double gene deletion mutants *ssk2Δcrz1Δ* and *pbs2Δcrz1Δ* and examined their phenotypes on glucosamine medium. The *ssk2Δ* and *pbs2Δ* single mutants showed enhanced filamentation on glucosamine medium (Figure 3.3, Figure 3.8A-B). The *ssk2Δcrz1Δ* and *pbs2Δcrz1Δ* double mutants were non-filamentous on glucosamine medium (Figure 3.8A), similar to the *crz1Δ* single mutant. This result suggests that Crz1 is essential in the regulation of filamentation in response to glucosamine and it functions downstream of Ssk2 and Pbs2.

We postulate that the HOG pathway components may oppose the effect of calcineurin and suppress the nuclear translocation of Crz1. If this hypothesis is valid, then disruption of the HOG pathway components would increase the level of nucleus-localized Crz1. To test this hypothesis, we constructed mCherry labeled Crz1 in the *ssk1Δ* mutant, the *ssk2Δ* mutant, and the *pbs2Δ* mutant by crossing these strains to XW252 (P<sub>CRZ1</sub>-Crz1-mCherry, GFP-Nop1) [156]. We then examined the subcellular localization of Crz1-mCherry in the absence of these HOG pathway components. We found that most cells showed nuclear localized Crz1-mCherry next to the nucleolus marker GFP-Nop1 in the absence of Ssk1, Ssk2, or Pbs2 even when these cells were cultured in YPD medium at 22°C without any stimulus (Figure 3.8C). Upon induction with glucosamine, almost all cells showed nuclear localized Crz1, regardless whether the *SSK1*, *SSK2*, or *PBS2* gene was intact or not (Figure 3.8C). Thus, the absence of the HOG pathway upstream

components increased the basal level of nuclear localized Crz1, which may have enhanced the initiation of filamentation in the *ssk1Δ*, *ssk2Δ*, or *pbs2Δ* mutant on glucosamine medium. In contrast to the deletion of *SSK1*, *SSK2*, or *PBS2*, the deletion of *HOG1* gene did not significantly enhance the basal level of nuclear-translocation in the absence of glucosamine compared to the wild type (generated by crossing  $P_{GPD1}$ -mCherry-*CRZ1* to *hog1Δ*) (left panel in Figure 3.8D). Nonetheless, the treatment of glucosamine stimulated the translocation of cytosolic Crz1 into the nucleus in the *hog1Δ* strain, just like the wild type (right panel in Figure 3.8D). Thus, Hog1, the downstream MAPK of the HOG pathway, appears to be dispensable for glucosamine-stimulated filamentation. In the wild-type H99 strain, Hog1 is known to be highly phosphorylated under normal growth conditions and it undergoes dephosphorylation in response to osmotic shock [158]. Indeed, we observed reduced level of phosphorylation of Hog1 in response to osmotic stress caused by NaCl (Figure 3.8E). However, no apparent change in Hog1 phosphorylation was observed in response to glucosamine (Figure 3.8E). This result indicates that Hog1 phosphorylation is not affected by glucosamine, which corroborates the dispensability of Hog1 in glucosamine-stimulated filamentation.

## Discussion

*C. neoformans* could undergo yeast-to-hypha transition and this morphotype switch is linked to its virulence potential. Yeast is the virulent form, whereas the filamentous form is attenuated in virulence in mammalian models of cryptococcosis ([24] and references therein). Our previous studies demonstrated that upregulation of *ZNF2* is sufficient to drive *C. neoformans* to undergo filamentation and to abolish/attenuate virulence [19-21]. Thus, activation of filamentation could potentially be used to mitigate cryptococcosis if suitable effectors that can

trigger cryptococcal filamentation program *in vivo* can be identified. In addition, the filamentous form of *Cryptococcus* elicits protective immune-responses in a mammalian host [19], providing a platform for future vaccine development.

Because the pheromone pathway has no or minimal impact on virulence and *C. neoformans* infections are largely caused by serotype A  $\alpha$  isolates ( $\alpha >99\%$  among serotype A isolates), it is of great value to identify conserved signals and pathways that control self-filamentation independent of the pheromone pathway. Self-filamentation in *C. neoformans* is mostly observed in serotype D isolates and rarely in serotype A isolates. The widely used and highly virulent serotype A reference strain H99, for instance, has not been observed to undergo self-filamentation under laboratory conditions despite numerous attempts. Here we found that H99 can undergo self-filamentation in response to glucosamine and this morphological transition is independent of the pheromone pathway. Why glucosamine, but not any other carbon-source tested, triggers self-filamentation in H99 remains mysterious. Glucosamine is the subunit of chitosan from *Cryptococcus* cell wall. Chitosan is the deacetylated form of chitin, and chitin is a common cell wall component in fungi and in the exoskeletons of arthropods, such as the shells of crustaceans and the outer coverings of insects. It is possible that the presence of glucosamine, rather than N-acetyl glucosamine, the subunit of chitin, serves as a unique danger signal to *Cryptococcus*. Alternatively, unknown secondary signals triggered by glucosamine are the real signals stimuli of filamentation. Regardless of the true biological meaning of glucosamine, the identification of pathways that control self-filamentation in natural serotype A strains like H99 represents an important advance in the endeavors to understand the regulation of cryptococcal dimorphism, which was primarily considered a response to pheromone.

By screening approximately 2500 gene deletion mutants for altered filamentation on glucosamine medium, we found that the transcription factor Crz1 was critical for glucosamine-induced filamentation: deletion of *CRZ1* abolished filamentation and overexpression of *CRZ1* enhanced filamentation on glucosamine medium. Crz1 appears to regulate filamentation specifically in response to glucosamine, as neither deletion nor overexpression of *CRZ1* showed any effect on cryptococcal yeast-to-hypha transition during mating on V8 medium (Figure S3.6)[157]. We found that the pheromone pathway responding to mating cues was overall dispensable for filamentation in response to glucosamine (Figure 3.2). Glucosamine strongly induced Crz1 to translocate from the cytosol to the nucleus, where it can exert its function as a transcription factor. Two pathways converged on Crz1 and play important but opposing roles. One pathway is the expected calcineurin pathway known to dephosphorylate Crz1, which required for its nuclear translocation [152, 156]. Indeed, Crz1 was retained in the cytoplasm in the absence of calcineurin catalytic subunit Cna1 or the regulatory subunit Cnb1 (Figure 3.7B-C). Interestingly, the absence of Cbp1 didn't affect Crz1's translocation into the nucleus (Figure 3.7C). This offers a plausible explanation for the lack of dramatic phenotype of the *cbp1Δ* mutant, in contrast to the non-filamentous phenotype of the *cna1Δ* and the *cnb1Δ* mutant on glucosamine medium (Figure 3.4B). The other pathway is the HOG components upstream of the Hog1 MAPK, which is known for their regulation of a variety of environmental stress responses. We found that the HOG components inhibited filamentation on glucosamine medium and suppressed the nuclear translocation of Crz1 (Figure 3.8C), likely through their direct or indirect effect on Crz1 phosphorylation that counter-balances the phosphatase activity of calcineurin (Figure 3.9).

In another fungal pathogen *Aspergillus fumigatus*, CrzA (Crz1 homolog) translocates to the nucleus upon osmotic stress caused by NaCl or sorbitol [159]. CrzA also directly upregulates the expression of the histidine kinase PhkB and the MAPKKK SskB of the osmotic sensing pathway by binding to their promoters [159]. Thus in *A. fumigatus*, CrzA plays a role in osmotic stress response [159], and there appears to be a positive feedback regulation between the osmotic sensing pathway and CrzA in *A. fumigatus*. Unlike CrzA in *A. fumigatus*, Crz1 in *Cryptococcus* translocates to granule-like structures in the cytoplasm after osmotic stress [89] (Figure 3.6). Consistent with its cytoplasmic localization in response to osmotic stress, the *crz1* $\Delta$  mutant was as resistant to the osmotic stress caused by NaCl as the wild type (Figure S3.8). Overexpression of *CRZ1* in the *pbs2* $\Delta$  mutant also failed to restore *pbs2* $\Delta$ 's sensitivity to osmotic stress (Figure S3.8). These findings are consistent with the idea that Crz1 is not critical for the osmotic stress response in *C. neoformans* (Figure S3.8).

The calcineurin pathway is known to control growth, stress responses, morphogenesis and pathogenicity in various fungal species [147-149, 155, 160-166]. However, Crz1, the established downstream target of calcineurin, appears to be more specific in promoting hyphal growth than the adaptation to the general stresses based on previous studies in *A. fumigatus* [167, 168] and *Candida* species [161, 169]. Interestingly, the HOG pathway plays a more suppressive role in hyphal growth as demonstrated in *Candida* species [170-172]) and in *Cryptococcus neoformans* during bisexual mating [146, 158]. Thus the opposing effect between the calcineurin pathway and the HOG pathway on hyphal growth might be conserved in multiple fungal species. Whether Crz1 is the conserved conjunction of these two pathways in regulating filamentation in these fungal species is yet to be determined.

We believe that the upstream components of the HOG pathway normally suppress the translocation of Crz1 to the nucleus based on the elevated basal level of nuclear Crz1 in the corresponding deletion mutants in the absence of any stimuli (Figure 3.8C). This suggests that the upstream components of the HOG pathway inactivate Crz1, possibly by enabling the phosphorylation of Crz1 either directly or indirectly, and consequently opposing the activity of calcineurin. It is important to note that nuclear localization of Crz1 is necessary, but not sufficient to drive filamentation in the absence of glucosamine. This is evident given that some cells showed nuclear localized Crz1 even in YPD medium, but all cells grew in the yeast form under that condition. This is also consistent with the observation that heat-shock and calcium, although both stimulate nuclear translocation of Crz1, were unable to elicit filamentation in H99 in the absence of glucosamine. Thus, a yet unknown factor affected by glucosamine, in addition to the requirement of Crz1 nuclear translocation, has to be involved to enable filamentation.

One interesting observation is that not all components in a well-established pathway behave in the same fashion. For example, most key components in the pheromone pathway, including the transcription factor Mat2, are dispensable for self-filamentation induced by glucosamine. However, *ste7* $\Delta$  is non-filamentous on glucosamine medium. This finding is surprising given that *ste7* $\Delta$  and *mat2* $\Delta$  are both non-filamentous with identical transcriptomes under mating-inducing conditions during both bisexual and unisexual development [20, 37, 173]. Thus, the distinct phenotype of *ste7* $\Delta$  on glucosamine medium suggests that Ste7 might have additional functions besides its established role in pheromone sensing and response. Another example is Hog1 in the HOG pathway. Most upstream components of the HOG pathway suppress filamentation on glucosamine medium, but the MAPK Hog1 itself shows no or minimal involvement in this process. We postulate that there is a divergence in the downstream effectors

of this phosphorelay system in response to osmotic stress or glucosamine. Hog1 is activated in response to osmotic stress when Crz1 is being concentrated in granules in the cytoplasm in *Cryptococcus* [152] (Figure 3.6A). In contrast, Crz1 is localized to the nucleus in response to glucosamine. How different effectors are activated by the same phosphorelay system, what controls the multiple distinct subcellular localizations of Crz1, and what prevents cross-activation of the downstream effectors remain to be investigated.

## **Materials and Methods**

### **Media and growth conditions**

Strains were stored as glycerol stocks in  $-80^{\circ}\text{C}$ . Freshly streaked cells were used for experiments. The three deletion sets made in the H99 background were obtained from the Fungal Genetics Stock Center (FGSC) and the information about these strains can be obtained from the FGSC website (<http://www.fgsc.net/crypto/crypto.htm>). Other strains were listed in Table S3.2. Cryptococcal cells were maintained on YPD medium (20 peptone, 10 yeast extract, 20 glucose, 20 agar, gram/liter) unless stated otherwise.

### **Filamentation assay**

For the filamentation assay, the YP medium (20 peptone, 10 yeast extract, 20 agar, gram/liter) was used as the base medium. All the different carbon sources tested were made to the final concentration of 2%. When testing filamentation on YPGlcN medium (20 peptone, 10 yeast extract, 20 glucosamine, 20 agar, gram/liter), 3  $\mu\text{l}$  of cells (optical density  $\text{OD}_{600}=1$ ) of the tested strains were dropped onto the agar medium. Cells were cultured at  $30^{\circ}\text{C}$  for two days before being transferred to  $22^{\circ}\text{C}$  for additional incubation of 4 to 7 days in the dark. To test the effect of the calcineurin inhibitor FK506 on filamentation, FK506 was added to the YPGlcN

medium at the final concentration of 1 µg/ml. To test the dose-dependent effects of glucosamine on filamentation, glucosamine were added to the YP base medium to the final concentration of 0, 0.2%, 0.5%, 1%, and 2%. To test the effect of the addition of another carbon source to the YPGlcN medium on filamentation, 2% galactose, glycerol, or xylose was added to the YPGlcN medium (2% glucosamine).

### **Phenotypical assays**

To test thermo-tolerance, cells of the tested strains with 5x serial dilutions ( $OD_{600}$ = 10, 2, 0.4, 0.08, 0.016, and 0.0032) were dropped onto YPD medium and incubated at 30°C or 37°C for 2 days. To test the susceptibility to cell wall stress, cells of the indicated strains were serial diluted and spotted onto YPD medium, YPD with 0.2% Congo Red, or YPD medium with 10 µg/ml of Calcofluor white. Cells were then incubated at 30°C for 2 days.

### **RNA extraction and qPCR**

RNA extraction and qPCR were performed as we described previously [21]. For the transcript measurements used in Figure 2, strains H99, *mat2Δ*, and *znf2Δ* were cultured on YPD medium or glucosamine medium at 30°C for 2 days, and then were transferred to 22°C for additional 2 days before cells were harvested. For the transcript measurements used in Figure 5, Strains H99, *crz1Δ*, and *znf2Δ* were cultured on the YP-glucosamine or YP base medium at 30°C for 2 days, and then incubated at 22°C for additional incubation. Cells were harvested at the time points (0, 2 days, 4 days, and 6 days) as indicated in the figures.

Harvested cells were washed with cold water, frozen in liquid nitrogen, and then lyophilized. Lyophilized cells were broken into fine powder with glass beads and total RNA was extracted with the PureLink® RNA Mini Kit (life technology) according to the manufacture's instruction. First strand cDNA was synthesized with Superscript III cDNA synthesis kit

(Invitrogen) according to the manufacture's instruction. The house-keeping gene *TEF1* was used as the endogenous control. The relative transcript levels were determined using the comparative  $\Delta\Delta C_t$  method as described previously [21]. Three biological replicates were performed for each sample and their values were used to calculate the mean and the standard error. Primers used for realtime PCR were listed in Table S3.

### **Genetic screen of the gene deletion mutants on glucosamine medium**

All the gene deletion mutants in the serotype A background used in this study generated by the Lin's group or Bahn's group were made in the same H99 background (see Table S3.2 for strains used in this study). The 2015 gene deletion set deposited by Dr. Hiten Madhani's lab and the transcription factor and kinase gene deletion sets deposited by Dr. Bahn's lab are available from the Fungal Genetics Stock Center. <http://www.fgsc.net/crypto/crypto.htm>). These mutants were also generated in the same H99 background. The mutants were screened on the YP-glucosamine (2%) medium after replicating from 96 well plates as described earlier for the filamentation assays. Strains with altered filamentation were selected based on comparison with other strains on the same plate during the initial screen. These mutant phenotypes were further confirmed in the secondary screen with the wild type H99 control. For the genes and pathways that were further characterized in this study, including the pheromone pathway, the calcineurin pathway, and the Hog1 pathway, separate mutants were obtained from the original sources where the mutations were verified in the previously published work. These strains and their sources/references were listed in Table S3.2.

### **Gene deletion and gene overexpression**

To generate the knockout construct, 1 kb of the 5' and 3' flanking sequences bordering the open reading frame of the gene of interest were amplified using the genomic DNA of the

wild-type strain as the template. They were then fused with the NEO or NAT dominant drug marker amplified from the plasmid pAI1 or pJAF1 by overlap PCR as we described previously [174]. The knockout constructs were introduced into appropriate recipient strains by biolistic transformation as described previously [175]. The transformants grown on selective medium (YPD+NAT or YPD+G418/NEO) were then screened for gene replacement *via* homologous recombination events by diagnostic PCR as described previously [174]. To generate *CRZ1* or *ZNF2* overexpression strains, the open reading frame of the *CRZ1* or the *ZNF2* gene were first amplified by PCR with specifically designed primers with *FseI/PacI* cut sites at the ends. After digestion, the digested products were ligated into the P<sub>GPD1</sub> vector or the P<sub>CTR4</sub> vector where the ORF was placed downstream of the *GPD1* or the *CTR4* promoter, as we described previously [59, 136]. The resulting plasmids were then linearized and introduced into the recipient strains as indicated in the text by biolistic transformation. All the primers used for constructing or confirming gene deletion or gene overexpression were listed in Table S3.3.

### **Mating and genetic crosses**

Yeast cells of  $\alpha$  and **a** mating partners were mixed together on V8 juice agar medium (5% V8 juice, 0.5 g/L KH<sub>2</sub>PO<sub>4</sub>, 4% agar, pH adjusted to 5). The mixed culture was then incubated for 2 weeks at 22°C in the dark until spores were produced following filamentation. Cells from V8 medium were transferred to fresh YPD agar medium and spores were micro-manipulated with a dissecting microscope. The mating type of the germinated spores was determined by successful mating of their derived colonies with either JEC20**a** or JEC21**a**. Genetic linkage between the presence of the drug marker and the observed mutant phenotype was established by analyzing the dissected spores as we described previously [61].

## Protein Tagging

To characterize the subcellular localization of Znf2 and Crz1, mCherry was fused to the N-terminus of Znf2 or Crz1 in frame. The ORF of *CRZ1* or *ZNF2* with *PacI* recognition site at 3' end was amplified by PCR and then fused at the N-terminus with mCherry carrying *FseI* recognition site at its 5' end. The fragment mCherry-*CRZ1* and mCherry-*ZNF2* was digested with *FseI* and *PacI* and then ligated into the  $P_{GPD1}$  vector or the  $P_{CTR4}$  vector. The construct of the mCherry tagged protein controlled by the *GPD1* or the *CTR4* promoter ( $P_{GPD1}$ -mCherry-*CRZ1* and  $P_{CTR4}$ -mCherry-*ZNF2*) were then introduced into the recipient strains by biolistic transformation as described previously [175]. The N-terminal tagged Crz1 and Znf2 are functional based on the observation that they could restore the filamentation defect observed in the corresponding gene deletion mutants.

## Microscopic examination

Colony morphology was examined with a SZX16 stereoscope (Olympus). Colony images were captured with a GO-21 camera and acquired using the QIMAGINE software. To determine the subcellular localization of mCherry-Crz1 or mCherry-Znf2, cells were observed with a Zeiss M2 epi-fluorescence microscope and images were acquired with the AxioCam MRm camera and processed with the software Zen 11 (Carl Zeiss Microscopy). The filter used for visualizing mCherry was the FL filter set 43 HE cy3 (Carl Zeiss Microscopy). GFP was visualized using the filter FL filter set 38 HE GFP (Carl Zeiss Microscopy). To visualize the nuclei, cells were fixed in a fixer solution (3.7% formaldehyde; 1X PBS; 1% Triton X) for 10 min and then stained with DAPI (0.4  $\mu\text{g/ml}$ ) for 15 min. The filter used to visualize DAPI was FL Filter Set 49 DAPI (Carl Zeiss Microscopy).

### **Crz1-mCherry translocation assay**

To examine the effect of temperature on Crz1 localization, cells of the tested strains were cultured in the YPD medium at 22°C, 30°C, or 37°C overnight. To test the effects of different conditions or mutations on the subcellular localization of mCherry tagged Crz1, *Cryptococcus* cells were grown in liquid media at 22°C for 10 hours. To examine the impact of glucosamine on Crz1's subcellular localization, cells were cultured in the YP-glucosamine (2%) liquid medium at 30°C for 10 hrs. To examine the impact of calcium or salt on the localization of Crz1, cells were cultured first in YPD at 22°C, centrifuged, washed with PBS, and then suspended in 100 mM CaCl<sub>2</sub> or 1.5 M NaCl for 10-30 minutes. To test the impact on Crz1's subcellular localization by the deletion of *SSK1*, *SSK2*, *PBS2*, *CNA1*, *CNBI* or *CBP1*, the corresponding *Cryptococcus* strains were cultured in either YPD or glucosamine medium at 22°C for 10 hours. To quantify the percentage of cells with Crz1 localized to the nucleus, the numbers of cells with Crz1 in the nucleus and the total cells with fluorescence signals were determined and the ratio was calculated in three replicated samples. The data were used to calculate the mean value of the population with nuclear localization and the standard errors.

### **Western blot analysis of Hog1 phosphorylation.**

The overnight culture of wild-type strain H99 was inoculated in fresh YPD liquid medium (250 ml) and incubated at 30°C until the culture reached the optical density of approximately 0.9-1.0 at 600 nm (OD<sub>600</sub>). Cells were harvested by centrifugation, washed two times in PBS, and resuspended in YPD medium containing 1 M NaCl or in YP medium containing 2% glucosamine. At each designated time point, an aliquot of 50 ml of the culture was mixed with an equal volume of ice-cold stop solution (0.9% NaCl, 1 mM NaN<sub>3</sub>, 10 mM EDTA, 50 mM NaF). The cells were then collected by centrifugation and resuspended in lysis

buffer [50 mM Tris-Cl (pH 7.5), 1% sodium deoxycholate, 5 mM sodium pyrophosphate, 0.2 mM sodium orthovanadate, 50 mM NaF, 0.1% SDS, 1% Triton X-100, 0.5 mM phenylmethylsulfonyl fluoride, and 2.5× protease inhibitor cocktail solution (Calbiochem)]. The resuspended cells were disrupted using a bead-beater for 6 cycles (30 sec bead beating with 2 min rest intervals). Protein concentrations were determined with the Pierce BCA protein assay kit (Thermo Fisher Scientific). A total of 5 µg of proteins were loaded into 10% SDS-polyacrylamide gel and analyzed by western blot using a primary antibody of rabbit P-p38 MAPK specific antibody (Cell Signalling Technology) to detect phosphorylated Hog1 and polyclonal anti-Hog1 antibody (Santa Cruz) for the detection of Hog1 as a loading control. Anti-rabbit IgG horseradish peroxidase-conjugated antibody (Santa Cruz) was used as a secondary antibody. The blot was developed using the ECL western blotting detection system according to the instruction of the manufacture (Bio-Rad).

### **Statistical analysis**

Statistical significance of different groups in terms of Crz1 localization was assessed by the *t*-test. The statistical analyses were performed using the Graphpad Prism 5 program, with *p* values lower than 0.05 considered statistically significant.

### **Acknowledgement**

This work was supported by National Institutes of Health (<http://www.niaid.nih.gov>) (R01AI097599 to XL). Dr. Lin holds an Investigator Award in the Pathogenesis of Infectious Disease from the Burroughs Wellcome Fund (<http://www.bwfund.org/>) (#1012445). Additional financial support came from the Biology department of Texas A&M University (<http://www.bio.tamu.edu/>) and the Microbiology department of the University of Georgia (<http://mib.uga.edu/>). The funders had no role in study design, data collection and interpretation,

or the decision to submit the work for publication. We thank Dr. Heitman (Duke) and Dr. Madhani (UCSF) for their generous gifts of strains, and the fungal genetics stock center (FGSC, <http://www.fgsc.net/>) for providing the service for the storage and maintenance of the deletion sets.

## References

1. Nemecek JC, Wuthrich M, Klein BS. Global control of dimorphism and virulence in fungi. *Science* (New York, NY. 2006;312(5773):583-8. PubMed PMID: 16645097.
2. Holbrook ED, Rappleye CA. *Histoplasma capsulatum* pathogenesis: making a lifestyle switch. *Current opinion in microbiology*. 2008;11(4):318-24. PubMed PMID: 18573684.
3. Park BJ, Wannemuehler KA, Marston BJ, Govender N, Pappas PG, Chiller TM. Estimation of the current global burden of cryptococcal meningitis among persons living with HIV/AIDS. *Aids*. 2009;23(4):525-30. doi: 10.1097/QAD.0b013e328322ffac. PubMed PMID: 19182676.
4. Casadevall A, Perfect JR. *Cryptococcus neoformans*. Washington, D.C.: ASM Press; 1998.
5. Casadevall A, Steenbergen JN, Nosanchuk JD. 'Ready made' virulence and 'dual use' virulence factors in pathogenic environmental fungi--the *Cryptococcus neoformans* paradigm. *Current opinion in microbiology*. 2003;6(4):332-7. PubMed PMID: 12941400.
6. Lin X. *Cryptococcus neoformans*: morphogenesis, infection, and evolution. *Infect Genet Evol*. 2009;9(4):401-16.
7. Wang L, Lin X. Morphogenesis in fungal pathogenicity: shape, size, and surface. *PLoS pathogens*. 2012;8(12):e1003027. Epub 2012/12/14. doi: 10.1371/journal.ppat.1003027. PubMed

PMID: 23236274; PubMed Central PMCID: PMC3516537.

8. Andrianopoulos A, Rodriguez-del Valle N, Klein B, Sil A. Dimorphic human fungal pathogens. In: Casadevall A, Mitchell AP, Berman J, Kwon-Chung KJ, Perfect JR, Heitman J, editors. Human Fungal Pathogens New York: Cold Spring Harbor Laboratory Press; in press.
9. Neilson JB, Ivey MH, Bulmer GS. *Cryptococcus neoformans*: pseudohyphal forms surviving culture with *Acanthamoeba polyphaga*. Infection and immunity. 1978;20(1):262-6. PubMed PMID: 352931; PubMed Central PMCID: PMC421581.
10. Zaragoza O, Nielsen K. Titan cells in *Cryptococcus neoformans*: cells with a giant impact. Current opinion in microbiology. 2013;16(4):409-13. doi: 10.1016/j.mib.2013.03.006. PubMed PMID: 23588027; PubMed Central PMCID: PMC3723695.
11. Zaragoza O, Garcia-Rodas R, Nosanchuk JD, Cuenca-Estrella M, Rodriguez-Tudela JL, Casadevall A. Fungal cell gigantism during mammalian infection. PLoS pathogens. 2010;6(6):e1000945. Epub 2010/06/30. doi: 10.1371/journal.ppat.1000945. PubMed PMID: 20585557; PubMed Central PMCID: PMC2887474.
12. Okagaki LH, Strain AK, Nielsen JN, Charlier C, Baltes NJ, Chretien F, et al. Cryptococcal cell morphology affects host cell interactions and pathogenicity. PLoS pathogens. 2010;6(6):e1000953. Epub 2010/06/30. doi: 10.1371/journal.ppat.1000953. PubMed PMID: 20585559; PubMed Central PMCID: PMC2887476.
13. Kwon-Chung KJ. A new genus, *filobasidiella*, the perfect state of *Cryptococcus neoformans*. Mycologia. 1975;67(6):1197-200. PubMed PMID: 765816.
14. Alspaugh JA, Davidson RC, Heitman J. Morphogenesis of *Cryptococcus neoformans*. Contributions to microbiology. 2000;5:217-38. PubMed PMID: 10863675.
15. Heitman J. Evolution of eukaryotic microbial pathogens via covert sexual reproduction.

Cell host & microbe. 2010;8(1):86-99. doi: 10.1016/j.chom.2010.06.011. PubMed PMID: 20638645; PubMed Central PMCID: PMC2916653.

16. Kwon-Chung KJ. Morphogenesis of *Filobasidiella neoformans*, the sexual state of *Cryptococcus neoformans*. Mycologia. 1976;68(4):821-33. PubMed PMID: 790172.

17. Lin X, Hull CM, Heitman J. Sexual reproduction between partners of the same mating type in *Cryptococcus neoformans*. Nature. 2005;434(7036):1017-21. PubMed PMID: 15846346.

18. Wickes BL, Mayorga ME, Edman U, Edman JC. Dimorphism and haploid fruiting in *Cryptococcus neoformans*: association with the alpha-mating type. Proc Natl Acad Sci USA. 1996;93(14):7327-31. PubMed PMID: 8692992.

19. Lin X, Huang JC, Mitchell TG, Heitman J. Virulence attributes and hyphal growth of *C. neoformans* are quantitative traits and the *MATa* allele enhances filamentation. PLoS genetics. 2006;2(11):e187.

20. Wang L, Zhai B, Lin X. The link between morphotype transition and virulence in *Cryptococcus neoformans*. PLoS pathogens. 2012;8(6):e1002765. doi: 10.1371/journal.ppat.1002765. PubMed PMID: 22737071; PubMed Central PMCID: PMC3380952.

21. Wang L, Tian X, Gyawali R, Lin X. Fungal adhesion protein guides community behaviors and autoinduction in a paracrine manner. Proceedings of the National Academy of Sciences of the United States of America. 2013;110(28):11571-6. doi: 10.1073/pnas.1308173110. PubMed PMID: 23798436; PubMed Central PMCID: PMC3710841.

22. Fu J, Morris IR, Wickes BL. The production of monokaryotic hyphae by *Cryptococcus neoformans* can be induced by high temperature arrest of the cell cycle and is independent of same-sex mating. PLoS pathogens. 2013;9(5):e1003335. doi: 10.1371/journal.ppat.1003335.

PubMed PMID: 23658522; PubMed Central PMCID: PMCPMC3642078.

23. Lin X, Jackson JC, Feretzaki M, Xue C, Heitman J. Transcription factors Mat2 and Znf2 operate cellular circuits orchestrating opposite- and same-sex mating in *Cryptococcus neoformans*. PLoS genetics. 2010;6(5):e1000953. doi: 10.1371/journal.pgen.1000953. PubMed PMID: 20485569; PubMed Central PMCID: PMC2869318.

24. Zhai B, Zhu P, Foyle D, Upadhyay S, Idnurm A, Lin X. Congenic strains of the filamentous form of *Cryptococcus neoformans* for studies of fungal morphogenesis and virulence. Infection and immunity. 2013;81(7):2626-37. doi: 10.1128/IAI.00259-13. PubMed PMID: 23670559; PubMed Central PMCID: PMC3697605.

25. Wang L, Tian X, Gyawali R, Upadhyay S, Foyle D, Wang G, et al. Morphotype transition and sexual reproduction are genetically associated in a ubiquitous environmental pathogen. PLoS pathogens. 2014;10(6):e1004185. doi: 10.1371/journal.ppat.1004185. PubMed PMID: 24901238; PubMed Central PMCID: PMC4047104.

26. Del Poeta M. Role of phagocytosis in the virulence of *Cryptococcus neoformans*. Eukaryotic cell. 2004;3(5):1067-75. doi: 10.1128/EC.3.5.1067-1075.2004. PubMed PMID: 15470235; PubMed Central PMCID: PMC522596.

27. Lee SC, Phadke S, Sun S, Heitman J. Pseudohyphal growth of *Cryptococcus neoformans* is a reversible dimorphic transition in response to ammonium that requires Amt1 and Amt2 ammonium permeases. Eukaryotic cell. 2012;11(11):1391-8. doi: 10.1128/EC.00242-12. PubMed PMID: 23002105; PubMed Central PMCID: PMC3486016.

28. Walton FJ, Heitman J, Idnurm A. Conserved elements of the RAM signaling pathway establish cell polarity in the basidiomycete *Cryptococcus neoformans* in a divergent fashion from other fungi. Molecular biology of the cell. 2006;17(9):3768-80. doi: 10.1091/mbc.E06-02-0125.

PubMed PMID: 16775005; PubMed Central PMCID: PMC1556378.

29. Maerz S, Seiler S. Tales of RAM and MOR: NDR kinase signaling in fungal morphogenesis. *Current opinion in microbiology*. 2010;13(6):663-71. doi: 10.1016/j.mib.2010.08.010. PubMed PMID: 20869909.

30. Bogomolnaya LM, Pathak R, Guo J, Polymenis M. Roles of the RAM signaling network in cell cycle progression in *Saccharomyces cerevisiae*. *Current genetics*. 2006;49(6):384-92. doi: 10.1007/s00294-006-0069-y. PubMed PMID: 16552603.

31. Brace J, Hsu J, Weiss EL. Mitotic exit control of the *Saccharomyces cerevisiae* Ndr/LATS kinase Cbk1 regulates daughter cell separation after cytokinesis. *Molecular and cellular biology*. 2011;31(4):721-35. doi: 10.1128/MCB.00403-10. PubMed PMID: 21135117; PubMed Central PMCID: PMC3028648.

32. Nelson B, Kurischko C, Horecka J, Mody M, Nair P, Pratt L, et al. RAM: a conserved signaling network that regulates Ace2p transcriptional activity and polarized morphogenesis. *Molecular biology of the cell*. 2003;14(9):3782-803. doi: 10.1091/mbc.E03-01-0018. PubMed PMID: 12972564; PubMed Central PMCID: PMC196567.

33. Du LL, Novick P. Pag1p, a novel protein associated with protein kinase Cbk1p, is required for cell morphogenesis and proliferation in *Saccharomyces cerevisiae*. *Molecular biology of the cell*. 2002;13(2):503-14. doi: 10.1091/mbc.01-07-0365. PubMed PMID: 11854408; PubMed Central PMCID: PMC65645.

34. Bidlingmaier S, Weiss EL, Seidel C, Drubin DG, Snyder M. The Cbk1p pathway is important for polarized cell growth and cell separation in *Saccharomyces cerevisiae*. *Molecular and cellular biology*. 2001;21(7):2449-62. doi: 10.1128/MCB.21.7.2449-2462.2001. PubMed PMID: 11259593; PubMed Central PMCID: PMC86877.

35. Racki WJ, Becam AM, Nasr F, Herbert CJ. Cbk1p, a protein similar to the human myotonic dystrophy kinase, is essential for normal morphogenesis in *Saccharomyces cerevisiae*. *The EMBO journal*. 2000;19(17):4524-32. doi: 10.1093/emboj/19.17.4524. PubMed PMID: 10970846; PubMed Central PMCID: PMC302079.
36. Magditch DA, Liu TB, Xue C, Idnurm A. DNA mutations mediate microevolution between host-adapted forms of the pathogenic fungus *Cryptococcus neoformans*. *PLoS pathogens*. 2012;8(10):e1002936. doi: 10.1371/journal.ppat.1002936. PubMed PMID: 23055925; PubMed Central PMCID: PMC3464208.
37. Colman-Lerner A, Chin TE, Brent R. Yeast Cbk1 and Mob2 activate daughter-specific genetic programs to induce asymmetric cell fates. *Cell*. 2001;107(6):739-50. PubMed PMID: 11747810.
38. Renwick J, Daly P, Reeves EP, Kavanagh K. Susceptibility of larvae of *Galleria mellonella* to infection by *Aspergillus fumigatus* is dependent upon stage of conidial germination. *Mycopathologia*. 2006;161(6):377-84. doi: 10.1007/s11046-006-0021-1. PubMed PMID: 16761185.
39. Kechichian TB, Shea J, Del Poeta M. Depletion of alveolar macrophages decreases the dissemination of a glucosylceramide-deficient mutant of *Cryptococcus neoformans* in immunodeficient mice. *Infection and immunity*. 2007;75(10):4792-8. PubMed PMID: 17664261.
40. Charlier C, Nielsen K, Daou S, Brigitte M, Chretien F, Dromer F. Evidence of a role for monocytes in dissemination and brain invasion by *Cryptococcus neoformans*. *Infection and immunity*. 2009;77(1):120-7. PubMed PMID: 18936186.
41. Sabiiti W, Robertson E, Beale MA, Johnston SA, Brouwer AE, Loyse A, et al. Efficient phagocytosis and laccase activity affect the outcome of HIV-associated cryptococcosis. *The*

Journal of clinical investigation. 2014;124(5):2000-8. Epub 2014/04/20. doi: 10.1172/JCI72950. PubMed PMID: 24743149; PubMed Central PMCID: PMC4001551.

42. Mylonakis E, Moreno R, El Khoury JB, Idnurm A, Heitman J, Calderwood SB, et al. *Galleria mellonella* as a model system to study *Cryptococcus neoformans* pathogenesis. Infection and immunity. 2005;73(7):3842-50. doi: 10.1128/IAI.73.7.3842-3850.2005. PubMed PMID: 15972469; PubMed Central PMCID: PMC1168598.

43. Upadhyay S, Torres G, Lin X. Laccases involved in 1,8-dihydroxynaphthalene melanin biosynthesis in *Aspergillus fumigatus* are regulated by developmental factors and copper homeostasis. Eukaryotic cell. 2013;12(12):1641-52. Epub 2013/10/15. doi: 10.1128/EC.00217-13. PubMed PMID: 24123270; PubMed Central PMCID: PMC3889567.

44. Ory JJ, Griffith CL, Doering TL. An efficiently regulated promoter system for *Cryptococcus neoformans* utilizing the *CTR4* promoter. Yeast. 2004;21(11):919-26. doi: 10.1002/yea.1139. PubMed PMID: 15334556.

45. Herth W, Schnepf E. The fluorochrome, calcofluor white, binds oriented to structural polysaccharide fibrils. Protoplasma. 1980;105(1-2):129-33. doi: Doi 10.1007/Bf01279855. PubMed PMID: ISI:A1980KV58200011.

46. Feldmesser M, Kress Y, Novikoff P, Casadevall A. *Cryptococcus neoformans* is a facultative intracellular pathogen in murine pulmonary infection. Infection and immunity. 2000;68(7):4225-37. PubMed PMID: 10858240; PubMed Central PMCID: PMC101732.

47. Steenbergen JN, Shuman HA, Casadevall A. *Cryptococcus neoformans* interactions with amoebae suggest an explanation for its virulence and intracellular pathogenic strategy in macrophages. Proceedings of the National Academy of Sciences of the United States of America. 2001;98(26):15245-50. doi: 10.1073/pnas.261418798. PubMed PMID: 11742090; PubMed

Central PMCID: PMC65014.

48. Kwon-Chung KJ, Fraser JA, Doering TL, Wang Z, Janbon G, Idnurm A, et al. *Cryptococcus neoformans* and *Cryptococcus gattii*, the Etiologic Agents of Cryptococcosis. Cold Spring Harbor perspectives in medicine. 2014;4(7). doi: 10.1101/cshperspect.a019760. PubMed PMID: 24985132.
49. Casadevall A. Amoeba provide insight into the origin of virulence in pathogenic fungi. Advances in experimental medicine and biology. 2012;710:1-10. doi: 10.1007/978-1-4419-5638-5\_1. PubMed PMID: 22127880.
50. Nielsen K, Cox GM, Wang P, Toffaletti DL, Perfect JR, Heitman J. Sexual cycle of *Cryptococcus neoformans* var. *grubii* and virulence of congenic **a** and **a** isolates. Infection and immunity. 2003;71(9):4831-41. PubMed PMID: 12933823.
51. Mak P, Zdybicka-Barabas A, Cytrynska M. A different repertoire of *Galleria mellonella* antimicrobial peptides in larvae challenged with bacteria and fungi. Developmental and comparative immunology. 2010;34(10):1129-36. doi: 10.1016/j.dci.2010.06.005. PubMed PMID: 20558200.
52. Lavine MD, Strand MR. Insect hemocytes and their role in immunity. Insect biochemistry and molecular biology. 2002;32(10):1295-309. PubMed PMID: 12225920.
53. Cytrynska M, Mak P, Zdybicka-Barabas A, Suder P, Jakubowicz T. Purification and characterization of eight peptides from *Galleria mellonella* immune hemolymph. Peptides. 2007;28(3):533-46. doi: 10.1016/j.peptides.2006.11.010. PubMed PMID: 17194500.
54. Lavine MD, Strand MR. Insect hemocytes and their role in immunity. Insect Biochemistry and Molecular Biology. 2002;32(10):1295-309. doi: [http://dx.doi.org/10.1016/S0965-1748\(02\)00092-9](http://dx.doi.org/10.1016/S0965-1748(02)00092-9).

55. Bogus MI, Kedra E, Bania J, Szczepanik M, Czygier M, Jablonski P, et al. Different defense strategies of *Dendrolimus pini*, *Galleria mellonella*, and *Calliphora vicina* against fungal infection. *Journal of insect physiology*. 2007. PubMed PMID: 17512001.
56. Strand MR, Pech LL. Immunological basis for compatibility in parasitoid-host relationships. *Annual review of entomology*. 1995;40:31-56. doi: 10.1146/annurev.en.40.010195.000335. PubMed PMID: 7810989.
57. Jackson JC, Higgins LA, Lin X. Conidiation color mutants of *Aspergillus fumigatus* are highly pathogenic to the heterologous insect host *Galleria mellonella*. *PLoS one*. 2009;4(1):e4224. Epub 2009/01/22. doi: 10.1371/journal.pone.0004224. PubMed PMID: 19156203; PubMed Central PMCID: PMC2625396.
58. Perfect JR, Lang SD, Durack DT. Chronic cryptococcal meningitis: a new experimental model in rabbits. *The American journal of pathology*. 1980;101(1):177-94. PubMed PMID: 7004196; PubMed Central PMCID: PMC1903580.
59. Bunting LA, Neilson JB, Bulmer GS. *Cryptococcus neoformans*: gastronomic delight of a soil amoeba. *Sabouraudia*. 1979;17(3):225-32. PubMed PMID: 394365.
60. Luberto C, Martinez-Marino B, Taraskiewicz D, Bolanos B, Chitano P, Toffaletti DL, et al. Identification of App1 as a regulator of phagocytosis and virulence of *Cryptococcus neoformans*. *The Journal of clinical investigation*. 2003;112(7):1080-94. doi: 10.1172/JCI18309. PubMed PMID: 14523045; PubMed Central PMCID: PMC198528.
61. Kozel TR, Gotschlich EC. The capsule of *Cryptococcus neoformans* passively inhibits phagocytosis of the yeast by macrophages. *Journal of immunology*. 1982;129(4):1675-80. PubMed PMID: 7050244.
62. Nielsen K, De Obaldia AL, Heitman J. *Cryptococcus neoformans* mates on pigeon guano:

- implications for the realized ecological niche and globalization. *Eukaryotic cell*. 2007;6(6):949-59. PubMed PMID: 17449657.
63. Nielsen K, Cox GM, Wang P, Toffaletti DL, Perfect JR, Heitman J. Sexual cycle of *Cryptococcus neoformans* var. *grubii* and virulence of congenic **a** and alpha isolates. *Infection and immunity*. 2003;71(9):4831-41. PubMed PMID: 12933823.
64. Lin X, Huang JC, Mitchell TG, Heitman J. Virulence attributes and hyphal growth of *C. neoformans* are quantitative traits and the *MAT*alpha allele enhances filamentation. *PLoS genetics*. 2006;2(11):e187. doi: 10.1371/journal.pgen.0020187. PubMed PMID: 17112316; PubMed Central PMCID: PMC1636697.
65. Belay T, Cherniak R, O'Neill EB, Kozel TR. Serotyping of *Cryptococcus neoformans* by dot enzyme assay. *Journal of clinical microbiology*. 1996;34(2):466-70. PubMed PMID: 8789042.
66. Kwon-Chung KJ, Bennett JE. Epidemiologic differences between the two varieties of *Cryptococcus neoformans*. *Am J Epidemiol*. 1984;120(1):123-30. PubMed PMID: 6377880.
67. Franzot SP, Salkin IF, Casadevall A. *Cryptococcus neoformans* var. *grubii*: separate varietal status for *Cryptococcus neoformans* serotype A isolates. *Journal of clinical microbiology*. 1999;37(3):838-40. PubMed PMID: 9986871.
68. Perfect JR, Dismukes WE, Dromer F, Goldman DL, Graybill JR, Hamill RJ, et al. Clinical practice guidelines for the management of cryptococcal disease: 2010 update by the infectious diseases society of america. *Clin Infect Dis*. 2010;50(3):291-322. PubMed PMID: 20047480.
69. Rhein J, Morawski BM, Hullsiek KH, Nabeta HW, Kiggundu R, Tugume L, et al. Efficacy of adjunctive sertraline for the treatment of HIV-associated cryptococcal meningitis: an

- open-label dose-ranging study. *Lancet Infect Dis.* 2016;16(7):809-18. doi: 10.1016/S1473-3099(16)00074-8. PubMed PMID: 26971081; PubMed Central PMCID: PMC4927382.
70. Day JN, Chau TT, Wolbers M, Mai PP, Dung NT, Mai NH, et al. Combination antifungal therapy for cryptococcal meningitis. *N Engl J Med.* 2013;368(14):1291-302. doi: 10.1056/NEJMoa1110404. PubMed PMID: 23550668; PubMed Central PMCID: PMC3978204.
71. Jarvis JN, Bicanic T, Loyse A, Namarika D, Jackson A, Nussbaum JC, et al. Determinants of mortality in a combined cohort of 501 patients with HIV-associated Cryptococcal meningitis: implications for improving outcomes. *Clin Infect Dis.* 2014;58(5):736-45. doi: 10.1093/cid/cit794. PubMed PMID: 24319084; PubMed Central PMCID: PMC3922213.
72. Smith KD, Achan B, Huppler Hullsiek K, McDonald T, Okagaki LH, Akampurira A, et al. Increased antifungal drug resistance in Ugandan clinical isolates of *Cryptococcus neoformans*. *Antimicrobial agents and chemotherapy.* 2015. doi: 10.1128/AAC.01299-15. PubMed PMID: 26324276.
73. Sionov E, Chang YC, Kwon-Chung KJ. Azole heteroresistance in *Cryptococcus neoformans*: emergence of resistant clones with chromosomal disomy in the mouse brain during fluconazole treatment. *Antimicrobial agents and chemotherapy.* 2013;57(10):5127-30. doi: 10.1128/AAC.00694-13. PubMed PMID: 23836187; PubMed Central PMCID: PMC3811407.
74. Van Wyk M, Govender NP, Mitchell TG, Litvintseva AP. Multilocus sequence typing of serially collected isolates of *Cryptococcus* from HIV-infected patients in South Africa. *Journal of clinical microbiology.* 2014;52(6):1921-31. Epub 2014/03/22. doi: 10.1128/JCM.03177-13. PubMed PMID: 24648562.

75. Pfaller MA, Diekema DJ, Gibbs DL, Newell VA, Bijie H, Dzierzanowska D, et al. Results from the ARTEMIS DISK Global Antifungal Surveillance Study, 1997 to 2007: 10.5-year analysis of susceptibilities of noncandidal yeast species to fluconazole and voriconazole determined by CLSI standardized disk diffusion testing. *Journal of clinical microbiology*. 2009;47(1):117-23. PubMed PMID: 19005141.
76. Chen YC, Chang TY, Liu JW, Chen FJ, Chien CC, Lee CH, et al. Increasing trend of fluconazole-non-susceptible *Cryptococcus neoformans* in patients with invasive cryptococcosis: a 12-year longitudinal study. *BMC Infect Dis*. 2015;15(1):277. doi: 10.1186/s12879-015-1023-8. PubMed PMID: 26194004.
77. Powderly WG, Saag MS, Cloud GA, Robinson P, Meyer RD, Jacobson JM, et al. A controlled trial of fluconazole or amphotericin B to prevent relapse of cryptococcal meningitis in patients with the acquired immunodeficiency syndrome. The NIAID AIDS Clinical Trials Group and Mycoses Study Group. *N Engl J Med*. 1992;326(12):793-8. PubMed PMID: 1538722.
78. Sil A, Andrianopoulos A. Thermally dimorphic human fungal pathogens-polyphyletic pathogens with a convergent pathogenicity trait. *Cold Spring Harbor perspectives in medicine*. 2014. doi: 10.1101/cshperspect.a019794. PubMed PMID: 25384771.
79. Mitchell AP. Dimorphism and virulence in *Candida albicans*. *Current opinion in microbiology*. 1998;1(6):687-92. PubMed PMID: 10066539.
80. Klein BS, Tebbets B. Dimorphism and virulence in fungi. *Current opinion in microbiology*. 2007;10(4):314-9. PubMed PMID: 17719267.
81. Ibrahim AS, Luo G, Gebremariam T, Lee H, Schmidt CS, Hennessey JP, Jr., et al. NDV-3 protects mice from vulvovaginal candidiasis through T- and B-cell immune response. *Vaccine*. 2013;31(47):5549-56. doi: 10.1016/j.vaccine.2013.09.016. PubMed PMID: 24063977; PubMed

Central PMCID: PMCPMC3866209.

82. Liu Y, Filler SG. *Candida albicans* Als3, a multifunctional adhesin and invasin. *Eukaryotic cell*. 2011;10(2):168-73. Epub 2010/12/01. doi: EC.00279-10 [pii]

10.1128/EC.00279-10. PubMed PMID: 21115738; PubMed Central PMCID: PMC3067396.

83. Moyes DL, Wilson D, Richardson JP, Mogavero S, Tang SX, Wernecke J, et al. Candidalysin is a fungal peptide toxin critical for mucosal infection. *Nature*. 2016;532(7597):64-8. doi: 10.1038/nature17625. PubMed PMID: 27027296; PubMed Central PMCID: PMCPMC4851236.

84. Staab JF, Bradway SD, Fidel PL, Sundstrom P. Adhesive and mammalian transglutaminase substrate properties of *Candida albicans* Hwp1. *Science* (New York, NY. 1999;283(5407):1535-8. Epub 1999/03/05. PubMed PMID: 10066176.

85. Ibrahim AS, Spellberg BJ, Avanesian V, Fu Y, Edwards JE, Jr. The anti-*Candida* vaccine based on the recombinant N-terminal domain of Als1p is broadly active against disseminated candidiasis. *Infection and immunity*. 2006;74(5):3039-41. Epub 2006/04/20. PubMed PMID: 16622247; PubMed Central PMCID: PMC1459699.

86. Zhai B, Wozniak KL, Masso-Silva J, Upadhyay S, Hole C, Rivera A, et al. Development of protective inflammation and cell-mediated immunity against *Cryptococcus neoformans* after exposure to hyphal mutants. *MBio*. 2015;6(5):e01433-15. doi: 10.1128/mBio.01433-15. PubMed PMID: 26443458; PubMed Central PMCID: PMCPMC4611043.

87. Wang P, Heitman J. Signal transduction cascades regulating mating, filamentation, and virulence in *Cryptococcus neoformans*. *Current opinion in microbiology*. 1999;2(4):358-62. PubMed PMID: 10458985.

88. Chung S, Karos M, Chang YC, Lukszo J, Wickes BL, Kwon-Chung KJ. Molecular

analysis of CPRalpha, a MATalpha-specific pheromone receptor gene of *Cryptococcus neoformans*. *Eukaryotic cell*. 2002;1(3):432-9. Epub 2002/11/29. PubMed PMID: 12455991; PubMed Central PMCID: PMC118017.

89. Shen WC, Davidson RC, Cox GM, Heitman J. Pheromones stimulate mating and differentiation *via* paracrine and autocrine signaling in *Cryptococcus neoformans*. *Eukaryotic cell*. 2002;1(3):366-77. PubMed PMID: 12455985.

90. Waugh MS, Vallim MA, Heitman J, Alspaugh JA. Ras1 controls pheromone expression and response during mating in *Cryptococcus neoformans*. *Fungal genetics and biology : FG & B*. 2003;38(1):110-21. PubMed PMID: 12553941.

91. Hsueh YP, Shen WC. A homolog of Ste6, the  $\alpha$ -factor transporter in *Saccharomyces cerevisiae*, is required for mating but not for monokaryotic fruiting in *Cryptococcus neoformans*. *Eukaryotic cell*. 2005;4(1):147-55. Epub 2005/01/12. PubMed PMID: 15643070; PubMed Central PMCID: PMC544149.

92. Davidson RC, Nichols CB, Cox GM, Perfect JR, Heitman J. A MAP kinase cascade composed of cell type specific and non-specific elements controls mating and differentiation of the fungal pathogen *Cryptococcus neoformans*. *Molecular microbiology*. 2003;49(2):469-85. PubMed PMID: 12828643.

93. Clarke DL, Woodlee GL, McClelland CM, Seymour TS, Wickes BL. The *Cryptococcus neoformans* STE11a gene is similar to other fungal mitogen-activated protein kinase kinase kinase (MAPKKK) genes but is mating type specific. *Molecular microbiology*. 2001;40(1):200-13. PubMed PMID: 11298287.

94. Lengeler KB, Davidson RC, D'Souza C, Harashima T, Shen WC, Wang P, et al. Signal transduction cascades regulating fungal development and virulence. *Microbiol Mol Biol Rev*.

2000;64(4):746-85. PubMed PMID: 11104818; PubMed Central PMCID: PMCPMC99013.

95. Kozubowski L, Heitman J. Profiling a killer, the development of *Cryptococcus neoformans*. FEMS Microbiol Rev. 2012;36(1):78-94. doi: 10.1111/j.1574-6976.2011.00286.x.

PubMed PMID: 21658085; PubMed Central PMCID: PMCPMC3318972.

96. Kruzel EK, Giles SS, Hull CM. Analysis of *Cryptococcus neoformans* sexual development reveals rewiring of the pheromone response network by a change in transcription factor identity. Genetics. 2012. Epub 2012/04/03. doi: genetics.112.138958 [pii]

10.1534/genetics.112.138958. PubMed PMID: 22466042.

97. Gyawali R, Zhao Y, Lin J, Fan Y, Xu X, Upadhyay S, et al. Pheromone Independent Unisexual Development in *Cryptococcus neoformans*. PLoS genetics. in revision.

98. Chung S, Karos M, Chang YC, Lukszo J, Wickes BL, Kwon-Chung KJ. Molecular Analysis of *CPR $\alpha$* , a *MAT $\alpha$* -Specific Pheromone Receptor Gene of *Cryptococcus neoformans*. Eukaryotic Cell. 2002;1(3):432-9. doi: 10.1128/EC.1.3.432-439.2002. PubMed PMID: PMC118017.

99. Hsueh Y-P, Shen W-C. A Homolog of Ste6, the  $\alpha$ -Factor Transporter in *Saccharomyces cerevisiae*, Is Required for Mating but Not for Monokaryotic Fruiting in *Cryptococcus neoformans*. Eukaryotic Cell. 2005;4(1):147-55. doi: 10.1128/EC.4.1.147-155.2005. PubMed PMID: PMC544149.

100. Hsueh Y-P, Xue C, Heitman J. G protein signaling governing cell fate decisions involves opposing  $G\alpha$  subunits in *Cryptococcus neoformans*. Mol Biol Cell. 2007;18(9):3237-49. doi: 10.1091/mbc.E07-02-0133. PubMed PMID: PMC1951760.

101. Yan Z, Li X, Xu J. Geographic distribution of mating type alleles of *Cryptococcus neoformans* in four areas of the United States. Journal of clinical microbiology. 2002;40(3):965-

72. PubMed PMID: 11880424.

102. Frazzitta AE, Vora H, Price MS, Tenor JL, Betancourt-Quiroz M, Toffaletti DL, et al. Nitrogen source-dependent capsule induction in human-pathogenic *Cryptococcus* species. *Eukaryotic cell*. 2013;12(11):1439-50. doi: 10.1128/EC.00169-13. PubMed PMID: 23975889; PubMed Central PMCID: PMC3837930.

103. Janbon G, Ormerod KL, Paulet D, Byrnes EJ, 3rd, Yadav V, Chatterjee G, et al. Analysis of the genome and transcriptome of *Cryptococcus neoformans* var. *grubii* reveals complex RNA expression and microevolution leading to virulence attenuation. *PLoS genetics*. 2014;10(4):e1004261. doi: 10.1371/journal.pgen.1004261. PubMed PMID: 24743168; PubMed Central PMCID: PMC3990503.

104. Idnurm A, Bahn YS, Nielsen K, Lin X, Fraser JA, Heitman J. Deciphering the model pathogenic fungus *Cryptococcus neoformans*. *Nature reviews*. 2005;3(10):753-64. PubMed PMID: 16132036.

105. Santiago-Tirado FH, Doering TL. All about that fat: Lipid modification of proteins in *Cryptococcus neoformans*. *J Microbiol*. 2016;54(3):212-22. doi: 10.1007/s12275-016-5626-6. PubMed PMID: 26920881; PubMed Central PMCID: PMC4851765.

106. Srikanta D, Santiago-Tirado FH, Doering TL. *Cryptococcus neoformans*: historical curiosity to modern pathogen. *Yeast*. 2014;31(2):47-60. doi: 10.1002/yea.2997. PubMed PMID: 24375706; PubMed Central PMCID: PMC3938112.

107. Alvarez FJ, Konopka JB. Identification of an N-acetylglucosamine transporter that mediates hyphal induction in *Candida albicans*. *Molecular biology of the cell*. 2007;18(3):965-75. doi: 10.1091/mbc.E06-10-0931. PubMed PMID: 17192409; PubMed Central PMCID: PMC1805087.

108. Castilla R, Passeron S, Cantore ML. N-acetyl-D-glucosamine induces germination in *Candida albicans* through a mechanism sensitive to inhibitors of cAMP-dependent protein kinase. *Cell Signal*. 1998;10(10):713-9. PubMed PMID: 9884022.
109. Huang G, Yi S, Sahni N, Daniels KJ, Srikantha T, Soll DR. N-acetylglucosamine induces white to opaque switching, a mating prerequisite in *Candida albicans*. *PLoS pathogens*. 2010;6(3):e1000806. doi: 10.1371/journal.ppat.1000806. PubMed PMID: 20300604; PubMed Central PMCID: PMC2837409.
110. Simonetti N, Strippoli V, Cassone A. Yeast-mycelial conversion induced by N-acetyl-D-glucosamine in *Candida albicans*. *Nature*. 1974;250(464):344-6. Epub 1974/07/26. PubMed PMID: 4605454.
111. Gilmore SA, Naseem S, Konopka JB, Sil A. N-acetylglucosamine (GlcNAc) triggers a rapid, temperature-responsive morphogenetic program in thermally dimorphic fungi. *PLoS genetics*. 2013;9(9):e1003799. doi: 10.1371/journal.pgen.1003799. PubMed PMID: 24068964; PubMed Central PMCID: PMC3778022.
112. Gyawali R, Upadhyay S, Way J, Lin X. Characterizing a family of secretory proteins associated with different morphotypes in *Cryptococcus neoformans*. *Applied and environmental microbiology*. 2016. doi: 10.1128/AEM.02967-16. PubMed PMID: 28039134.
113. Karos M, Chang YC, McClelland CM, Clarke DL, Fu J, Wickes BL, et al. Mapping of the *Cryptococcus neoformans* MATa locus: presence of mating type-specific mitogen-activated protein kinase cascade homologs. *Journal of bacteriology*. 2000;182(21):6222-7. PubMed PMID: 11029445.
114. Chang YC, Miller GF, Kwon-Chung KJ. Importance of a developmentally regulated pheromone receptor of *Cryptococcus neoformans* for virulence. *Infection and immunity*.

2003;71(9):4953-60. PubMed PMID: 12933837.

115. Hsueh YP, Xue C, Heitman J. A constitutively active GPCR governs morphogenic transitions in *Cryptococcus neoformans*. The EMBO journal. 2009;28(9):1220-33. doi: 10.1038/emboj.2009.68. PubMed PMID: 19322200; PubMed Central PMCID: PMC2683048.

116. Alspaugh JA, Perfect JR, Heitman J. *Cryptococcus neoformans* mating and virulence are regulated by the G-protein alpha subunit *GPA1* and cAMP. Genes Dev. 1997;11(23):3206-17. PubMed PMID: 9389652; PubMed Central PMCID: PMC316752.

117. Wang P, Perfect JR, Heitman J. The G-protein beta subunit Gpb1 is required for mating and haploid fruiting in *Cryptococcus neoformans*. Mol Cell Biol. 2000;20(1):352-62. PubMed PMID: 10594037.

118. Wang P, Nichols CB, Lengeler KB, Cardenas ME, Cox GM, Perfect JR, et al. Mating-type-specific and nonspecific PAK kinases play shared and divergent roles in *Cryptococcus neoformans*. Eukaryotic cell. 2002;1(2):257-72. PubMed PMID: 12455960.

119. Jung KW, Yang DH, Maeng S, Lee KT, So YS, Hong J, et al. Systematic functional profiling of transcription factor networks in *Cryptococcus neoformans*. Nature communications. 2015;6:6757. doi: 10.1038/ncomms7757. PubMed PMID: 25849373; PubMed Central PMCID: PMC4391232.

120. Lee KT, So YS, Yang DH, Jung KW, Choi J, Lee DG, et al. Systematic functional analysis of kinases in the fungal pathogen *Cryptococcus neoformans*. Nat Commun. 2016;7:12766. doi: 10.1038/ncomms12766. PubMed PMID: 27677328; PubMed Central PMCID: PMC5052723.

121. Bahn YS, Geunes-Boyer S, Heitman J. Ssk2 mitogen-activated protein kinase kinase

kinase governs divergent patterns of the stress-activated Hog1 signaling pathway in *Cryptococcus neoformans*. Eukaryotic cell. 2007;6(12):2278-89. PubMed PMID: 17951522.

122. Bahn YS, Kojima K, Cox GM, Heitman J. A unique fungal two-component system regulates stress responses, drug sensitivity, sexual development, and virulence of *Cryptococcus neoformans*. Molecular biology of the cell. 2006;17(7):3122-35. PubMed PMID: 16672377.

123. Cruz MC, Fox DS, Heitman J. Calcineurin is required for hyphal elongation during mating and haploid fruiting in *Cryptococcus neoformans*. The EMBO journal. 2001;20(5):1020-32. PubMed PMID: 11230126.

124. Odom A, Muir S, Lim E, Toffaletti DL, Perfect J, Heitman J. Calcineurin is required for virulence of *Cryptococcus neoformans*. The EMBO journal. 1997;16(10):2576-89. PubMed PMID: 9184205.

125. Fox DS, Cruz MC, Sia RA, Ke H, Cox GM, Cardenas ME, et al. Calcineurin regulatory subunit is essential for virulence and mediates interactions with FKBP12-FK506 in *Cryptococcus neoformans*. Molecular microbiology. 2001;39(4):835-49. PubMed PMID: 11251806.

126. Moranova Z, Virtudazo E, Hricova K, Ohkusu M, Kawamoto S, Husickova V, et al. The *CRZI/SPI*-like gene links survival under limited aeration, cell integrity and biofilm formation in the pathogenic yeast *Cryptococcus neoformans*. Biomed Pap Med Fac Univ Palacky Olomouc Czech Repub. 2014;158(2):212-20. doi: 10.5507/bp.2013.024. PubMed PMID: 23640031.

127. Adler A, Park YD, Larsen P, Nagarajan V, Wollenberg K, Qiu J, et al. A novel specificity protein 1 (*SPI*)-like gene regulating protein kinase C-1 (*Pkc1*)-dependent cell wall integrity and virulence factors in *Cryptococcus neoformans*. J Biol Chem. 2011;286(23):20977-90. doi: 10.1074/jbc.M111.230268. PubMed PMID: 21487010; PubMed Central PMCID:

PMCPMC3121451.

128. Lev S, Desmarini D, Chayakulkeeree M, Sorrell TC, Djordjevic JT. The Crz1/Sp1 transcription factor of *Cryptococcus neoformans* is activated by calcineurin and regulates cell wall integrity. *PloS one*. 2012;7(12):e51403. doi: 10.1371/journal.pone.0051403. PubMed PMID: 23251520; PubMed Central PMCID: PMCPMC3520850.

129. Gorlach J, Fox DS, Cutler NS, Cox GM, Perfect JR, Heitman J. Identification and characterization of a highly conserved calcineurin binding protein, CBP1/calciressin, in *Cryptococcus neoformans*. *The EMBO journal*. 2000;19(14):3618-29. doi: 10.1093/emboj/19.14.3618. PubMed PMID: 10899116; PubMed Central PMCID: PMCPMC313974.

130. Fox DS, Heitman J. Calcineurin-binding protein Cbp1 directs the specificity of calcineurin-dependent hyphal elongation during mating in *Cryptococcus neoformans*. *Eukaryotic cell*. 2005;4(9):1526-38. doi: 10.1128/EC.4.9.1526-1538.2005. PubMed PMID: 16151246; PubMed Central PMCID: PMCPMC1214203.

131. Chow EW, Clancey SA, Billmyre RB, Averette AF, Granek JA, Mieczkowski P, et al. Elucidation of the calcineurin-Crz1 stress response transcriptional network in the human fungal pathogen *Cryptococcus neoformans*. *PLoS genetics*. 2017;13(4):e1006667. doi: 10.1371/journal.pgen.1006667. PubMed PMID: 28376087; PubMed Central PMCID: PMCPMC5380312.

132. Park HS, Chow EW, Fu C, Soderblom EJ, Moseley MA, Heitman J, et al. Calcineurin Targets Involved in Stress Survival and Fungal Virulence. *PLoS pathogens*. 2016;12(9):e1005873. doi: 10.1371/journal.ppat.1005873. PubMed PMID: 27611567; PubMed Central PMCID: PMCPMC5017699.

133. Gyawali R, Zhao Y, Lin J, Fan Y, Xu X, Upadhyay S, et al. Pheromone independent unisexual development in *Cryptococcus neoformans*. PLoS genetics. 2017;13(5):e1006772. doi: 10.1371/journal.pgen.1006772. PubMed PMID: 28467481; PubMed Central PMCID: PMC5435349.
134. Bahn YS, Kojima K, Cox GM, Heitman J. Specialization of the HOG pathway and its impact on differentiation and virulence of *Cryptococcus neoformans*. Molecular biology of the cell. 2005;16(5):2285-300. doi: 10.1091/mbc.e04-11-0987. PubMed PMID: 15728721; PubMed Central PMCID: PMC1087235.
135. de Castro PA, Chen C, de Almeida RS, Freitas FZ, Bertolini MC, Morais ER, et al. ChIP-seq reveals a role for CrzA in the *Aspergillus fumigatus* high-osmolarity glycerol response (HOG) signalling pathway. Molecular microbiology. 2014;94(3):655-74. doi: 10.1111/mmi.12785. PubMed PMID: 25196896.
136. Yu SJ, Chang YL, Chen YL. Calcineurin signaling: lessons from *Candida* species. FEMS yeast research. 2015;15(4):fov016. doi: 10.1093/femsyr/fov016. PubMed PMID: 25878052.
137. Chen YL, Brand A, Morrison EL, Silao FG, Bigol UG, Malbas FF, Jr., et al. Calcineurin controls drug tolerance, hyphal growth, and virulence in *Candida dubliniensis*. Eukaryotic cell. 2011;10(6):803-19. Epub 2011/05/03. doi: EC.00310-10 [pii] 10.1128/EC.00310-10. PubMed PMID: 21531874; PubMed Central PMCID: PMC3127677.
138. Steinbach WJ, Cramer RA, Jr., Perfect BZ, Asfaw YG, Sauer TC, Najvar LK, et al. Calcineurin controls growth, morphology, and pathogenicity in *Aspergillus fumigatus*. Eukaryotic cell. 2006;5(7):1091-103. PubMed PMID: 16835453.
139. Tamuli R, Deka R, Borkovich KA. Calcineurin Subunits A and B Interact to Regulate Growth and Asexual and Sexual Development in *Neurospora crassa*. PloS one.

2016;11(3):e0151867. doi: 10.1371/journal.pone.0151867. PubMed PMID: 27019426; PubMed Central PMCID: PMC4809485.

140. Bader T, Schroppel K, Bentink S, Agabian N, Kohler G, Morschhauser J. Role of calcineurin in stress resistance, morphogenesis, and virulence of a *Candida albicans* wild-type strain. *Infection and immunity*. 2006;74(7):4366-9. doi: 10.1128/IAI.00142-06. PubMed PMID: 16790813; PubMed Central PMCID: PMC1489686.

141. Kontoyiannis DP, Lewis RE, Alexander BD, Lortholary O, Dromer F, Gupta KL, et al. Calcineurin inhibitor agents interact synergistically with antifungal agents *in vitro* against *Cryptococcus neoformans* isolates: correlation with outcome in solid organ transplant recipients with cryptococcosis. *Antimicrobial agents and chemotherapy*. 2008;52(2):735-8. PubMed PMID: 18070977.

142. Chen YL, Lehman VN, Lewit Y, Averette AF, Heitman J. Calcineurin governs thermotolerance and virulence of *Cryptococcus gattii*. *G3 (Bethesda)*. 2013;3(3):527-39. Epub 2013/03/02. doi: 10.1534/g3.112.004242. PubMed PMID: 23450261; PubMed Central PMCID: PMC3583459.

143. Cramer RA, Jr., Perfect BZ, Pinchai N, Park S, Perlin DS, Asfaw YG, et al. Calcineurin target CrzA regulates conidial germination, hyphal growth, and pathogenesis of *Aspergillus fumigatus*. *Eukaryotic cell*. 2008;7(7):1085-97. PubMed PMID: 18456861.

144. Soriani FM, Malavazi I, da Silva Ferreira ME, Savoldi M, Von Zeska Kress MR, de Souza Goldman MH, et al. Functional characterization of the *Aspergillus fumigatus* CRZI homologue, CrzA. *Molecular microbiology*. 2008;67(6):1274-91. doi: 10.1111/j.1365-2958.2008.06122.x. PubMed PMID: 18298443.

145. Karababa M, Valentino E, Pardini G, Coste AT, Bille J, Sanglard D. CRZI, a target of the

- calcineurin pathway in *Candida albicans*. *Molecular microbiology*. 2006;59(5):1429-51. doi: 10.1111/j.1365-2958.2005.05037.x. PubMed PMID: 16468987.
146. Alonso-Monge R, Roman E, Arana DM, Prieto D, Urrialde V, Nombela C, et al. The Sko1 protein represses the yeast-to-hypha transition and regulates the oxidative stress response in *Candida albicans*. *Fungal Genet Biol*. 2010;47(7):587-601. doi: 10.1016/j.fgb.2010.03.009. PubMed PMID: 20388546.
147. Alonso-Monge R, Navarro-Garcia F, Molero G, Diez-Orejas R, Gustin M, Pla J, et al. Role of the mitogen-activated protein kinase Hog1p in morphogenesis and virulence of *Candida albicans*. *Journal of bacteriology*. 1999;181(10):3058-68. PubMed PMID: 10322006.
148. Day AM, Smith DA, Ikeh MA, Haider M, Herrero-de-Dios CM, Brown AJ, et al. Blocking two-component signalling enhances *Candida albicans* virulence and reveals adaptive mechanisms that counteract sustained SAPK activation. *PLoS pathogens*. 2017;13(1):e1006131. doi: 10.1371/journal.ppat.1006131. PubMed PMID: 28135328; PubMed Central PMCID: PMC5300278.
149. Feretzaki M, Heitman J. Genetic circuits that govern bisexual and unisexual reproduction in *Cryptococcus neoformans*. *PLoS genetics*. 2013;9(8):e1003688. doi: 10.1371/journal.pgen.1003688. PubMed PMID: 23966871; PubMed Central PMCID: PMC3744442.
150. Lin X, Chacko N, Wang L, Pavuluri Y. Generation of stable mutants and targeted gene deletion strains in *Cryptococcus neoformans* through electroporation. *Med Mycol*. 2015;53(3):225-34. doi: 10.1093/mmy/myu083. PubMed PMID: 25541555; PubMed Central PMCID: PMC4574871.

151. Toffaletti DL, Rude TH, Johnston SA, Durack DT, Perfect JR. Gene transfer in *Cryptococcus neoformans* by use of biolistic delivery of DNA. Journal of bacteriology. 1993;175(5):1405-11. PubMed PMID: 8444802; PubMed Central PMCID: PMC193227.

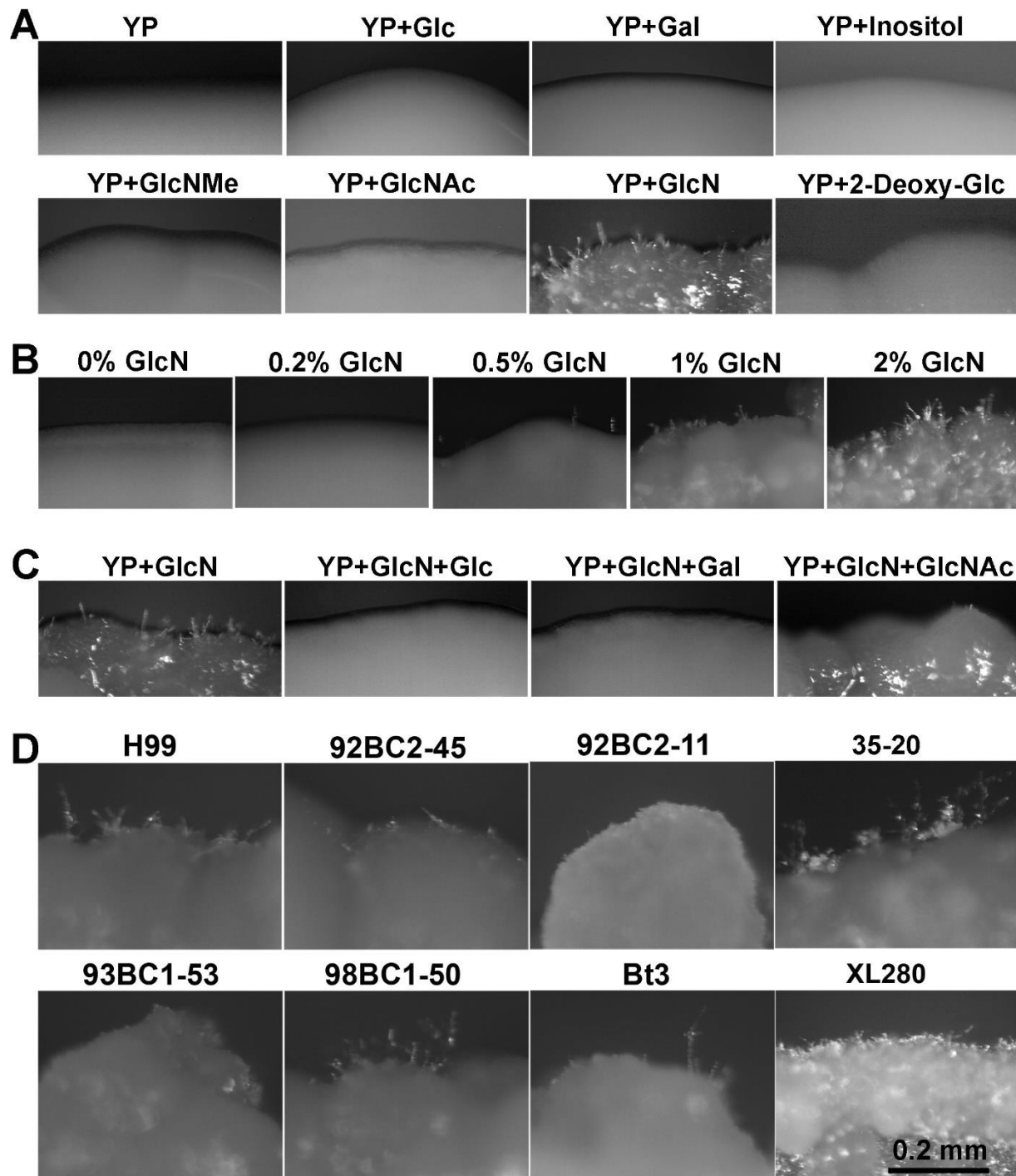


**Figure 3.1. Glucosamine stimulates self-filamentation in H99 and other cryptococcal isolates.** (A) The effect of the addition of different six-carbon sugars and hexamines at 2% to YP base medium. H99 was cultured on YP, YP+Glc (glucose), YP+Gal (galactose), YP+Inositol, YP+GlcNMe (N-Methyl-glucosamine), YP+GlcNAc (N-Acetyl-glucosamine), YP+GlcN

(glucosamine), and YP+2-Deoxyl-Glc (2-Deoxyl-glucose) for 7 days. **(B)** The dose-dependent effect of glucosamine on self-filamentation in H99. H99 was cultured on YP+GlcN at final concentration of 0, 0.2%, 0.5%, 1%, and 2% for 7 days. **(C)** The inhibitory effect of other carbon sources on GlcN-induced filamentation. H99 was cultured on the indicated media for 7 days. H99 cultured on YP+GlcN (2%) was used as control. Other carbon sources, such as glucose, galactose, or N-Acetyl-glucosamine (2%) were added to the YP+GlcN medium. **(D)** The effect of glucosamine on filamentation is not specific to H99. 92BC2-45 (serotype A), 92BC2-11 (serotype A), 93BC1-53 (serotype D), 35-20 VNI (serotype A), 98BC1-50 (serotype D), Bt3 strain (serotype A), and XL280 $\alpha$  (serotype D) were cultured on YP+GlcN medium for 7 days.

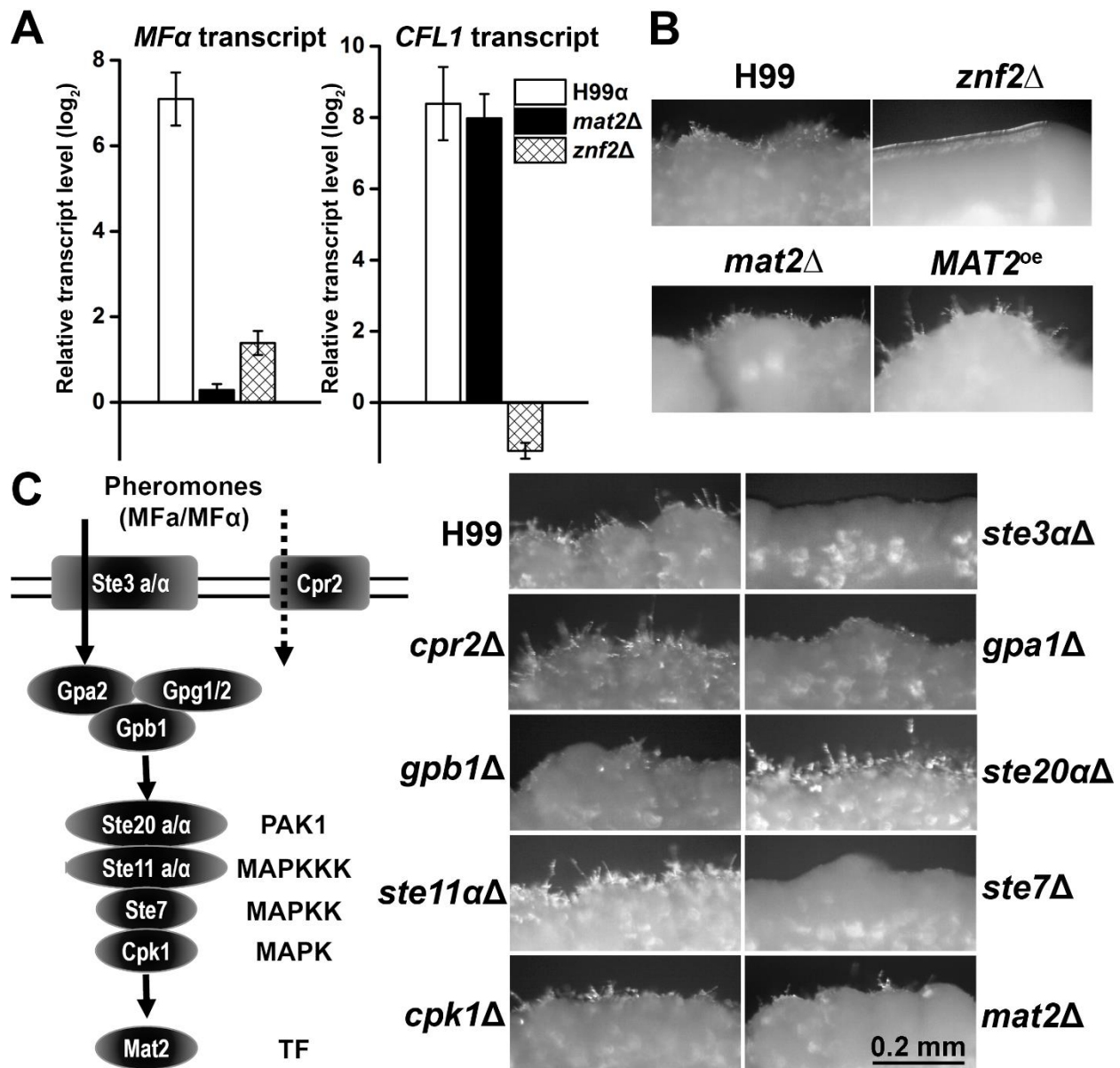


**Figure 3.2. Glucosamine-stimulated filamentation is independent of the Mat2-controlled pheromone pathway but requires the morphogenesis regulator Znf2.** (A) The *CFL1* and *MFα* transcript levels in wild-type H99, the *znf2Δ* mutant, and the *mat2Δ* mutant on glucosamine medium for 4 days relative to those on the control YP medium. The house keeping gene *TEF1* is used as the internal control. (B) The wild-type H99 strain, the *znf2Δ* mutant, the *mat2Δ* mutant, and the *MAT2<sup>oe</sup>* strain were cultured on YP+GlcN medium for 6 days. (C) The left panel depicts some of the key components of the pheromone pathway. The right panel shows images of

colonies of wild-type H99, the *ste3* $\Delta$  mutant, the *cpr2* $\Delta$  mutant, the *gpa1* $\Delta$  mutant, the *gpb1* $\Delta$  mutant, the *ste20 $\alpha$*  $\Delta$  mutant, the *ste11 $\alpha$*  $\Delta$  mutant, the *ste7* $\Delta$  mutant, the *cpk1* $\Delta$  mutant, and the *mat2* $\Delta$  mutant cultured on medium for 7 days.

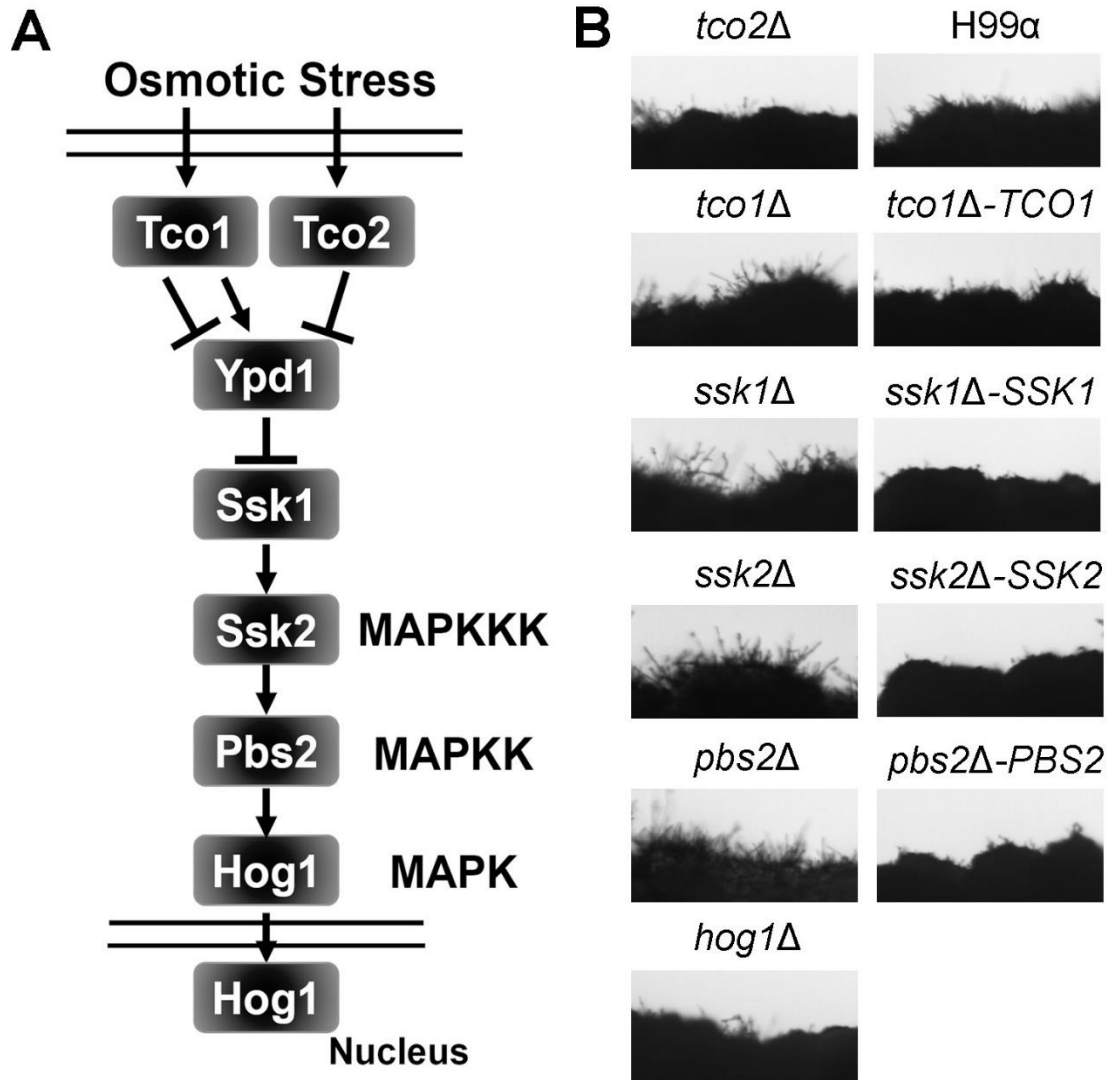


**Figure 3.3. Multiple components of the HOG pathway suppress filamentation on glucosamine medium.** (A) A diagram depicting the major components of the osmotic sensing HOG pathway in *Cryptococcus*. (B) The wild-type H99, the *tco1Δ* mutant, the *tco1Δ-TCO1* complemented strain, the *tco2Δ* mutant, the *ssk1Δ* mutant, the *ssk1Δ-SSK1* complemented strain, the *ssk2Δ* mutant, the *ssk2Δ-SSK2* complemented strain, the *pbs2Δ* mutant, the *pbs2Δ-PBS2* complemented strain, and the *hog1Δ* mutant were cultured on glucosamine medium (1.6% glucosamine) for 7 days.

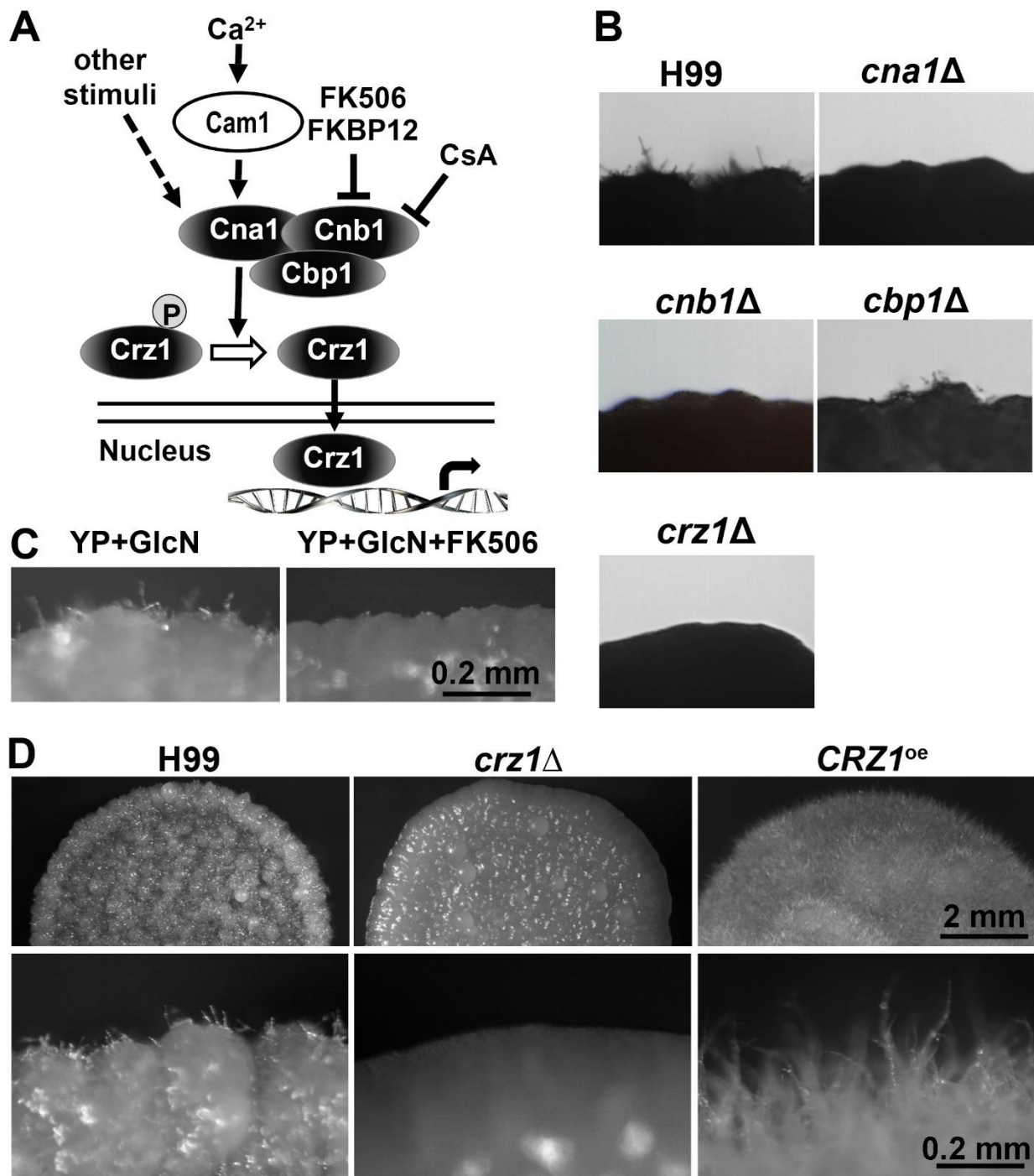


**Figure 3.4. The calcineurin pathway is required for glucosamine-induced self-filamentation.** (A) A diagram depicting the calcineurin pathway. (B) The wild-type H99, the *cna1Δ* mutant, the *cnb1Δ* mutant, the *cbp1Δ* mutant, and two independent *crz1Δ* mutants were cultured on glucosamine medium for 7 days. (C) The wild-type H99 was cultured on

glucosamine medium with or without the calcineurin inhibitor FK506. **(D)** The wild-type H99, the *crz1* $\Delta$  mutant, and the *CRZ1<sup>oe</sup>* strain (*P<sub>GPD1</sub>-CRZ1*) were cultured on glucosamine medium for 7 days.

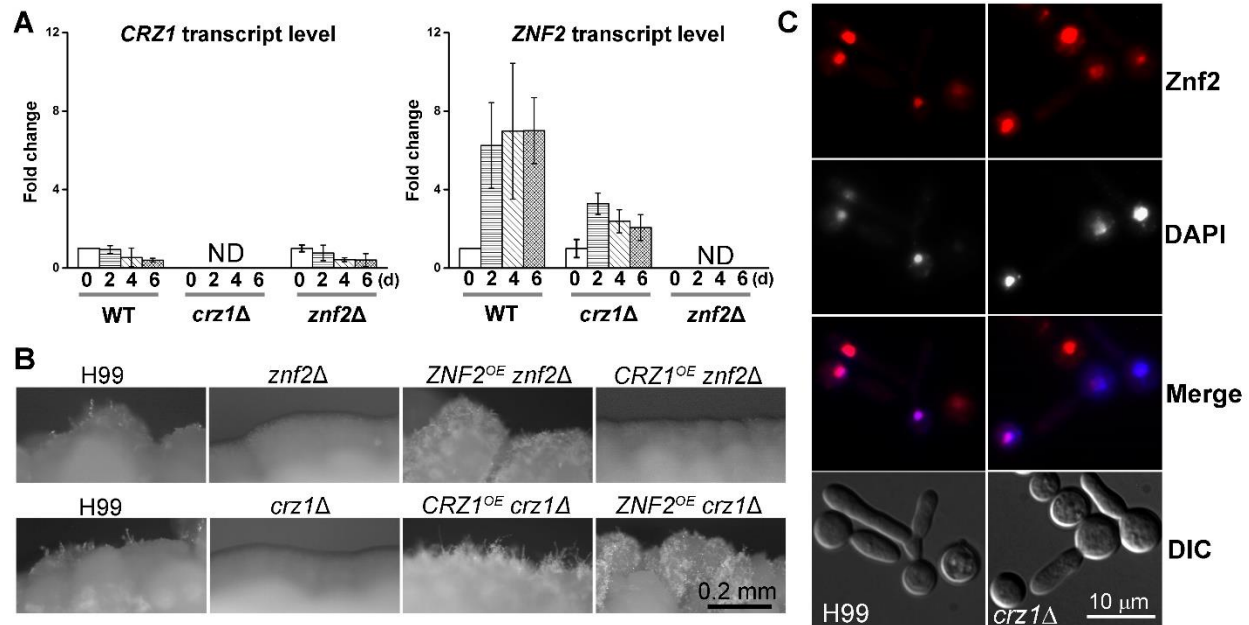


**Figure 3.5. Crz1 acts upstream of Znf2 in regulating filamentation induced by glucosamine.**

(A) Transcript levels of *CRZ1* and *ZNF2* in the wild-type H99, the *crz1Δ* mutant, and the *znf2Δ* mutant cultured on glucosamine medium for 2 days, 4 days, and 6 days compared to the control of 0 days. (B) The wild-type H99, the *znf2Δ* mutant, the *ZNF2<sup>oe</sup> znf2Δ* strain, the *CRZ1<sup>oe</sup> znf2Δ* strain, the *crz1Δ* mutant, the *ZNF2<sup>oe</sup> crz1Δ* strain, and the *CRZ1<sup>oe</sup> crz1Δ* strain were cultured on glucosamine medium for 7 days. The overexpression of both *CRZ1* and *ZNF2* was driven by the constitutively active *GPD1* promoter and the inducible *CTR4* promoter respectively. (C) The subcellular localization of mCherry-Znf2 in the *crz1Δ* mutant and in the wild-type strain H99 on glucosamine medium. DAPI was used to indicate nuclear localization.

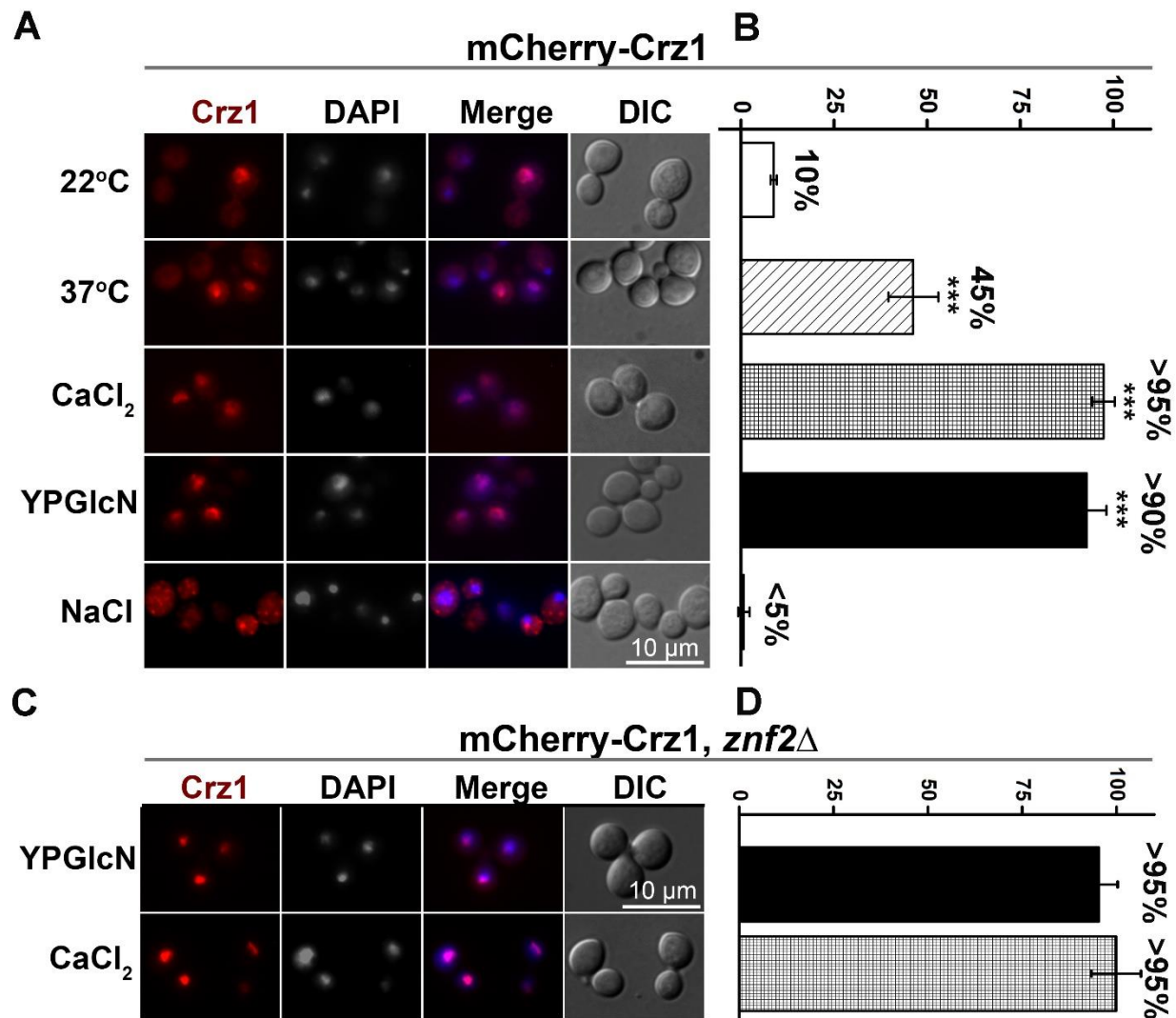
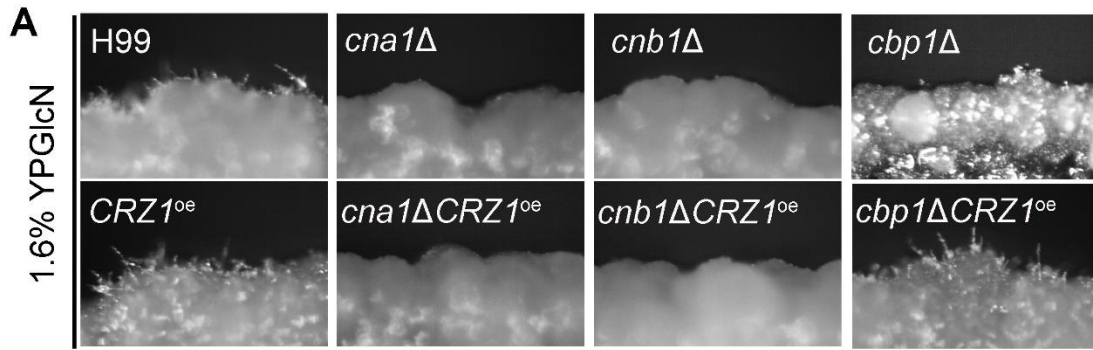
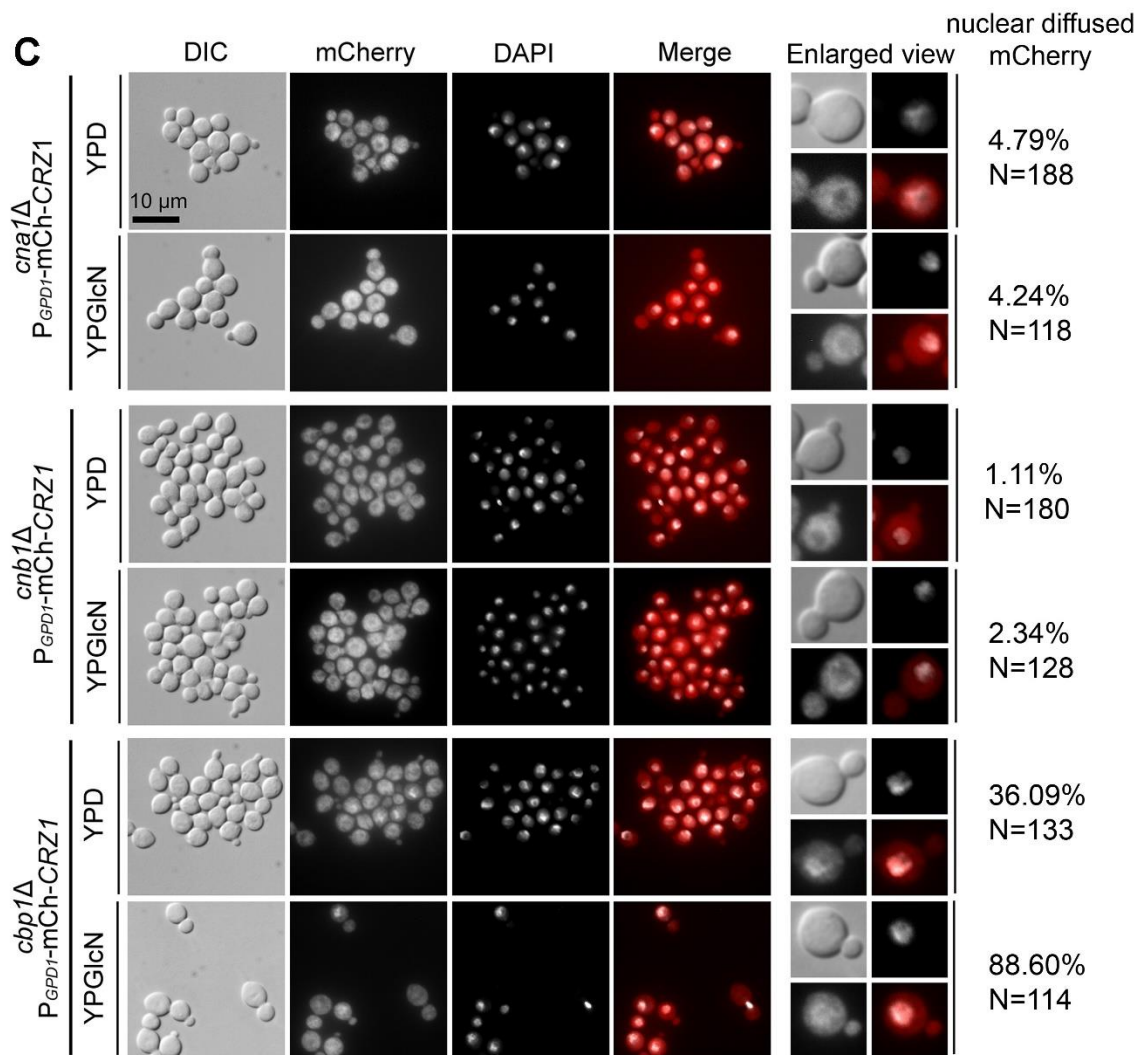
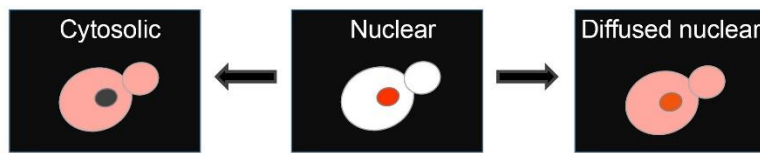


**Figure 3.6. Glucosamine stimulates Crz1 translocation to the nucleus.** (A) Localization of mCherry-Crz1 under different the indicated conditions. To test temperature's effect on the subcellular localization of mCrz1, the strain  $P_{GPD1}$ -mCherry-*CRZ1* was cultured in YPD liquid at 22°C (first row, or 37°C (2<sup>nd</sup> row) with shaking overnight. To test the effect of calcium or NaCl on the subcellular localization of mCrz1, cells of the strain  $P_{GPD1}$ -mCherry-*CRZ1* were collected from an overnight culture in liquid YPD at 22°C and then suspended in 100 mM CaCl<sub>2</sub> or 1.5 M NaCl solution for 10-20 min (3<sup>rd</sup> and 5<sup>th</sup> rows). To test the effect of glucosamine on mCrz1's localization, the strain  $P_{GPD1}$ -mCherry-*CRZ1* was cultured in YPGlcN liquid medium for 12

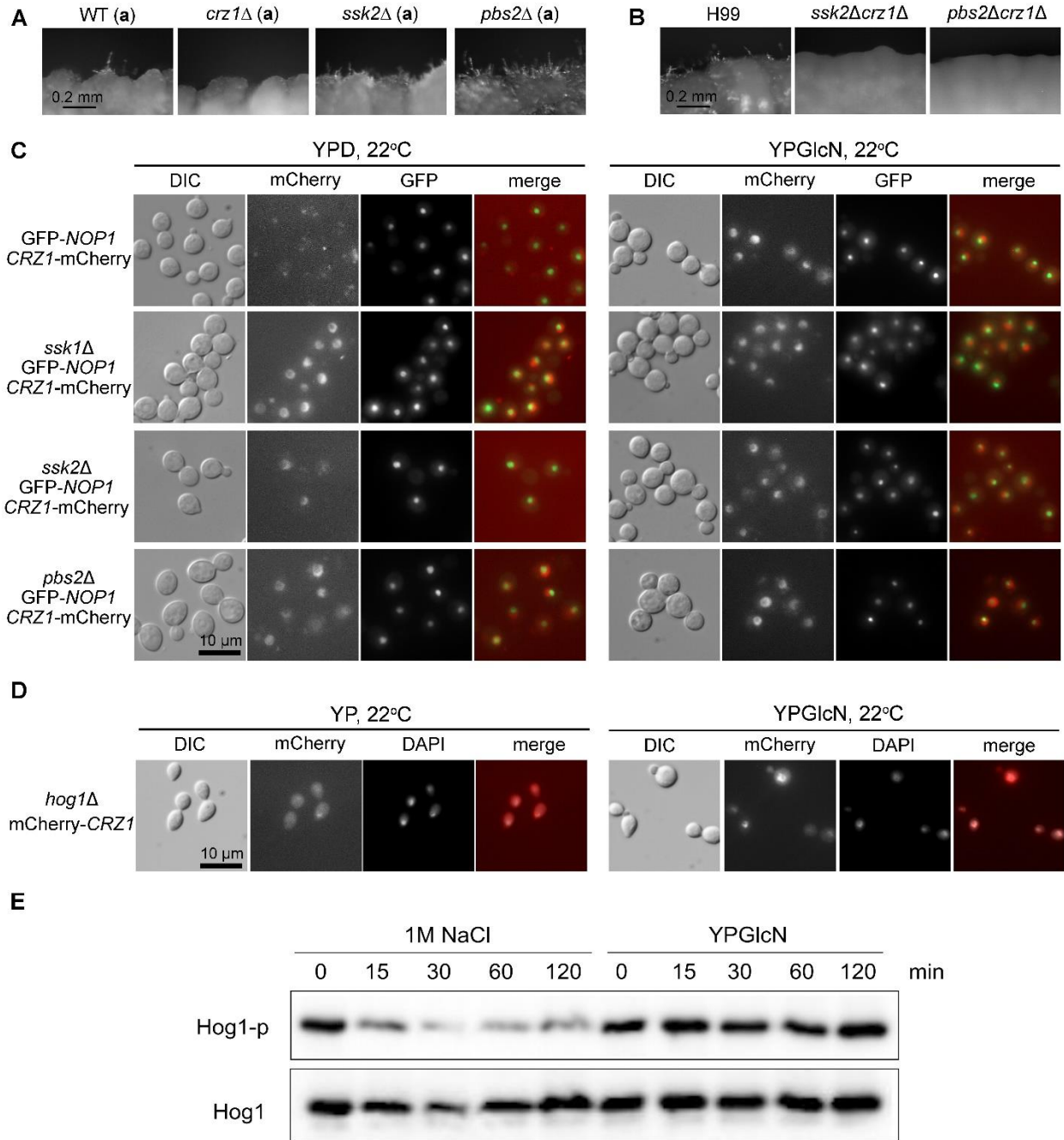
hours at 22°C (4<sup>th</sup> row). **(B)** Quantification of the percent of cells with mCherry-Crz1 located to the nucleus under the conditions used in panel A. (n≥60) (\*\*\*) p<0.001). **(C)** Cells of the strain mCherry-*CRZ1/znf2Δ* were tested for the effect of glucosamine and CaCl<sub>2</sub> on the localization of mCherry-Crz1 as described in panel A. **(D)** Quantification of the percentage of cells with mCherry-Crz1 located to the nucleus under the same conditions used in panel C.



**B** Crz1 localization patterns (mCherry)

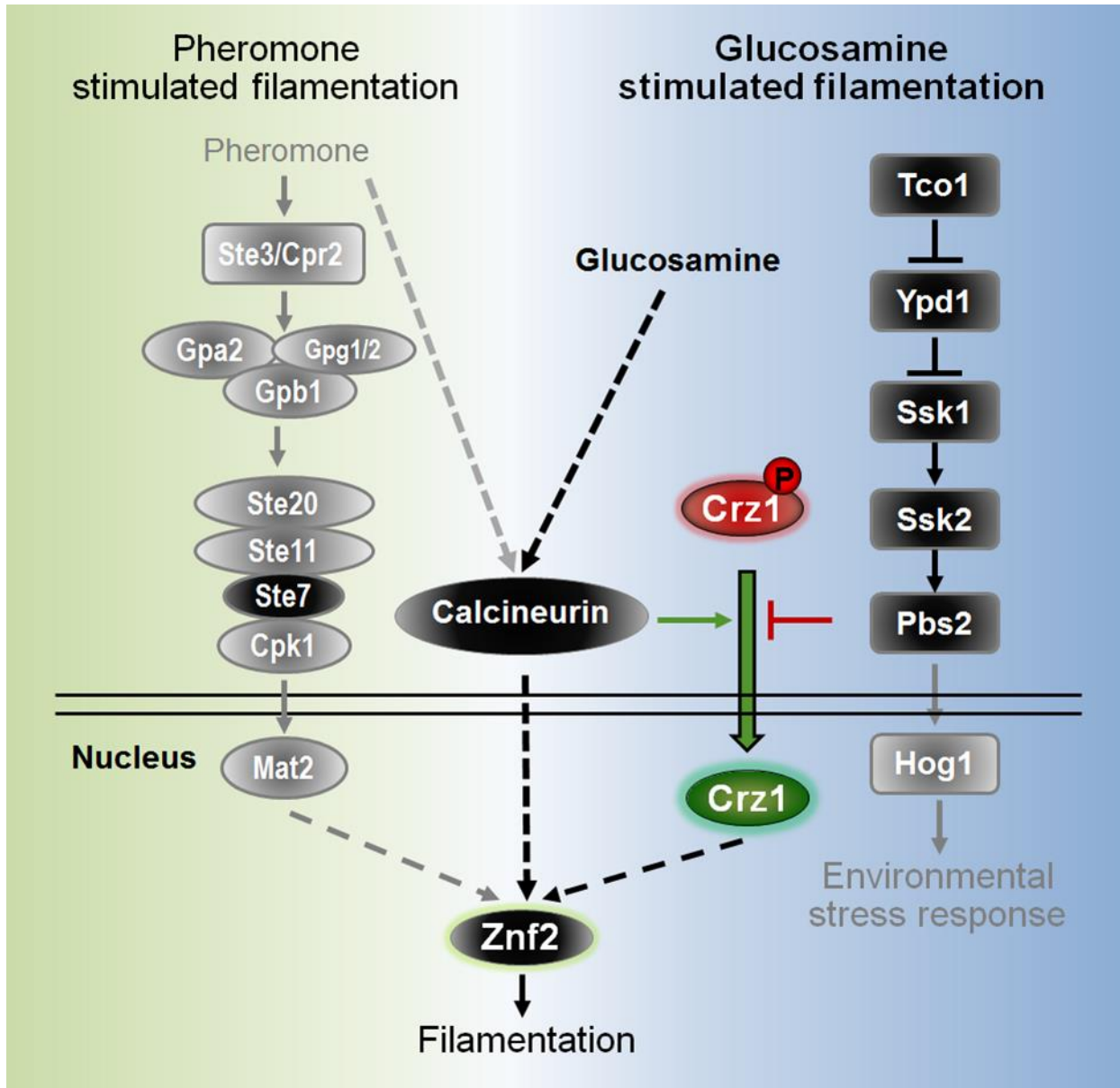


**Figure 3.7. Crz1 depends on calcineurin for its nuclear localization and its regulation of filamentation on glucosamine medium.** (A) Strains *cna1Δ*, *cna1ΔP<sub>GPD1</sub>-mCherry-Crz1*, *cnb1Δ*, *cnb1ΔP<sub>GPD1</sub>-mCherry-Crz1*, *cbp1Δ*, and *cbp1ΔP<sub>GPD1</sub>-mCherry-Crz1* were cultured on YP+GlcN medium for 7 days. (B) a diagram depicting the different localization patterns of Crz1: diffused in the cytosol with nuclear exclusion (left); localized to the nucleus (middle); localized to both cytoplasm and the nucleus but more concentrated in the nucleus (right), (C) Strains *cna1ΔP<sub>GPD1</sub>-mCherry-Crz1*, *cnb1ΔP<sub>GPD1</sub>-mCherry-Crz1*, and *cbp1ΔP<sub>GPD1</sub>-mCherry-Crz1* were cultured either in YPD medium or in YP+GlcN medium overnight. The mCherry-Crz1 signal showed diffused cytoplasmic localization in the *cna1Δ* and *cnb1Δ* mutants under both conditions. The mCherry-Crz1 signal showed diffused cytoplasmic localization but with more concentrated signals in the nucleus in the *cbp1Δ* mutant.

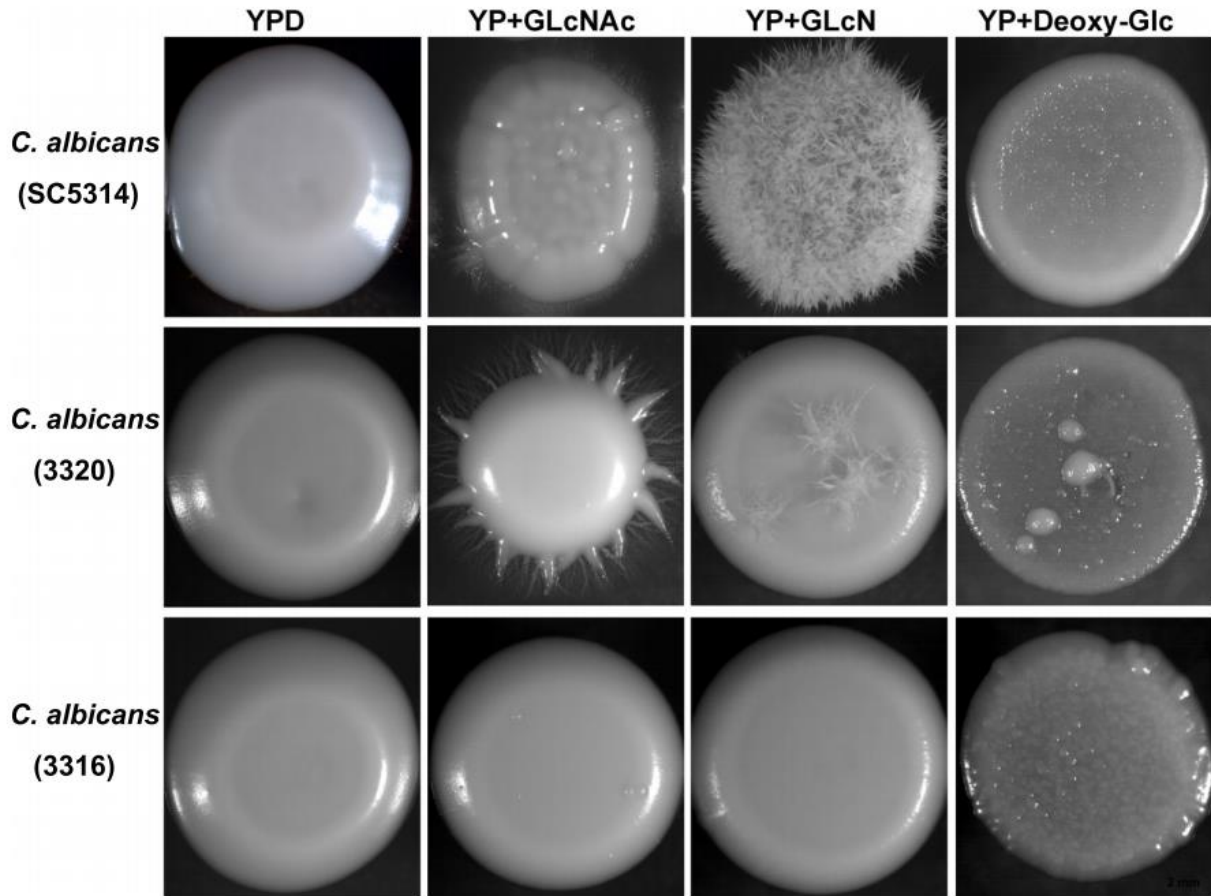


**Figure 3.8. The HOG components function upstream of Crz1 and suppress Crz1's nuclear localization.** (A) Cells of the wild-type KN99a, *crz1Δ* (a), *ssk2Δ* (a), and *pbs2Δ* (a) were cultured on YP+GlcN (0.5%) medium for 7 days. (B) Cells of the wild-type H99, the *ssk2Δcrz1Δ* double mutant, and the *pbs2Δcrz1Δ* double mutant were cultured on YP+GlcN medium for 7

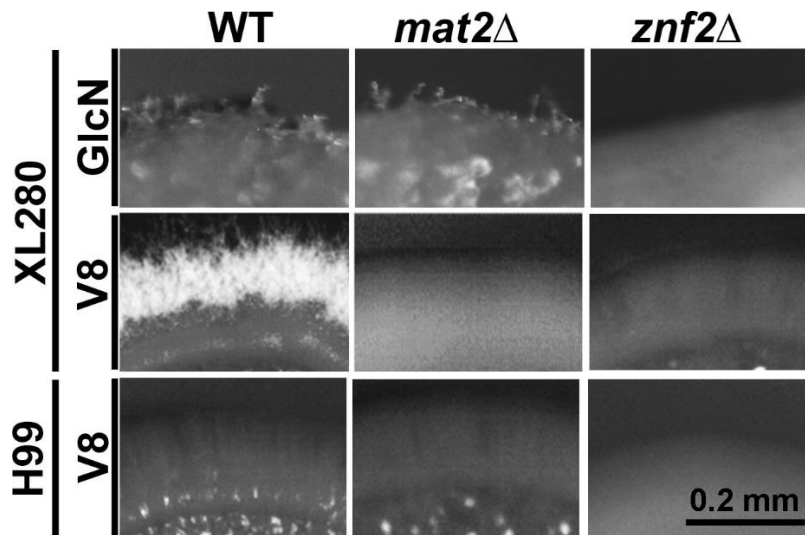
days. **(C)** The control strain XW252 (GFP-Nop1,  $P_{CRZ1}$ -Crz1-mCherry) [156] and the corresponding *ssk1* $\Delta$ , *ssk2* $\Delta$ , and *pbs2* $\Delta$  mutants in the XW252 background were cultured in YPD or YP+GlcN medium overnight at 22°C. GFP-Nop1 labels the nucleolus within the nucleus [156]. **(D)** The strain JL408 ( $MAT\alpha$ , *hog1* $\Delta$ ;  $P_{GPD1}$ -mCherry-*CRZ1*) was generated from a cross between the *hog1* $\Delta$  mutant in the mating type **a** background and the strain JL410 ( $MAT\alpha$ ,  $P_{GPD1}$ -mCherry-*CRZ1*). JL408 was cultured in YP or YP+GlcN medium overnight at 22°C. **(E)** The wild-type strain H99 was grown to mid-logarithmic phase and then exposed to 1 M NaCl or 2% glucosamine (YPGlcN) for the indicated time points. Hog1 phosphorylation levels were monitored using anti-P-p38 antibody. The blot was stripped and then used for detection of Hog1 protein level with a polyclonal anti-Hog1 antibody as a loading control.



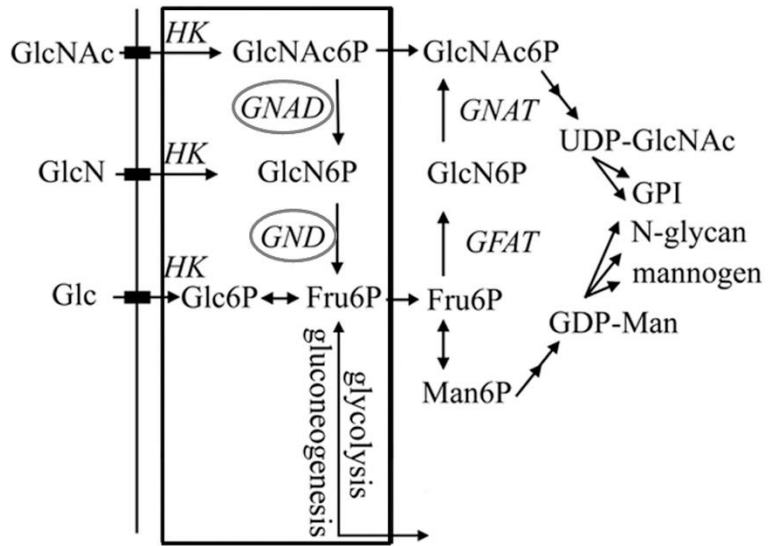
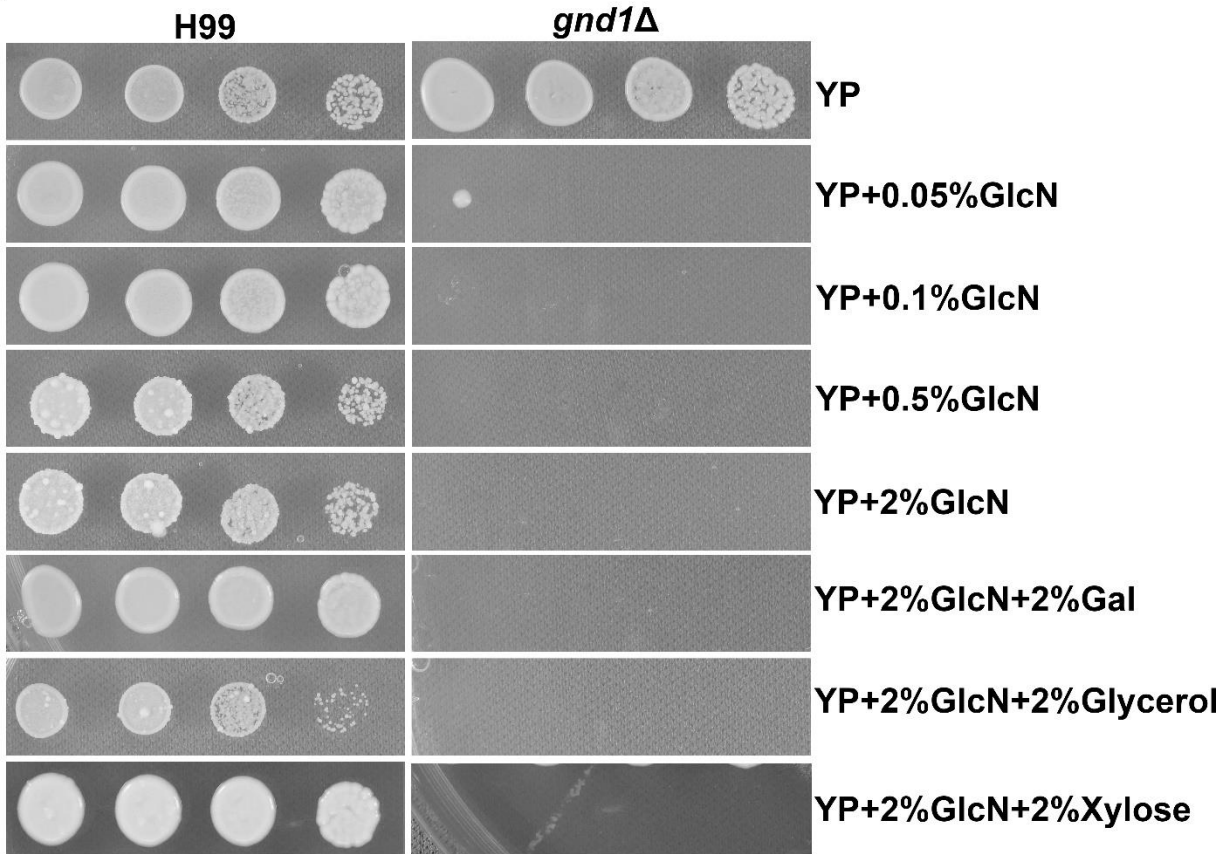
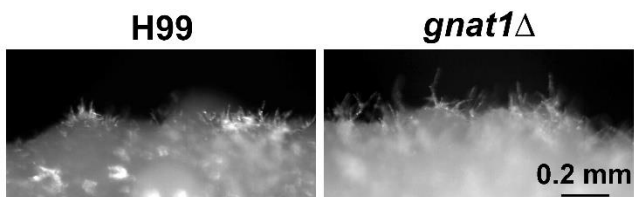
**Figure 3.9. Proposed model of genetic regulation of glucosamine-stimulated filamentation in *Cryptococcus neoformans*.**



**Figure S3.1.** Phenotypes of *Candida albicans* strains on YPD, YP+GlcNAc, YP+GlcN, and YP+Deoxyl-Glc. Cells (optical density of  $OD_{600}=1.0$ ) were dropped onto the indicated medium and cultured at 30°C for 2 days followed by additional incubation at 22°C for 4 days.



**Figure S3.2.** Znf2, but not Mat2, is required for filamentation of the serotype D strain XL280 on glucosamine medium. The wild-type serotype D strain XL280 and the corresponding *mat2* $\Delta$  and *znf2* $\Delta$  mutants were cultured on V8 juice agar medium for 6 days at 22°C or on glucosamine medium for 2 days at 30°C followed by additional 4 days of incubation at 22°C. (upper two panels). The wild-type serotype A strain H99 and the corresponding *mat2* $\Delta$  and *znf2* $\Delta$  mutants were cultured on V8 juice agar medium at 22°C for 4 days.

**A****B****C**

**Figure S3.3.** Phenotypes of the hexamine metabolism mutants *gnd1Δ* and *gnat1Δ*. **(A)** A diagram of the hexamine metabolism pathway. HK: Hexose Kinase, GNAD: Glucosamine Deacetylase, GND: Glucosamine Deaminase, GNAT: Glucosamine N-acetyl transferase. **(B)** The growth of the *gnd1Δ* mutant is hypersensitive to glucosamine. Wild-type H99 and the *gnd1Δ* mutant were cultured at 30°C for 2 days on YP medium containing glucosamine of different concentrations with or without the addition of other carbon sources (galactose, glycerol, or xylose). **(C)** The *gnd1Δ* mutant filamented similarly as the wild-type strain H99. The wild-type H99 and the *gnd1Δ* mutant was cultured on glucosamine medium for 2 days at 30°C followed by additional 4 days of incubation at 22°C.

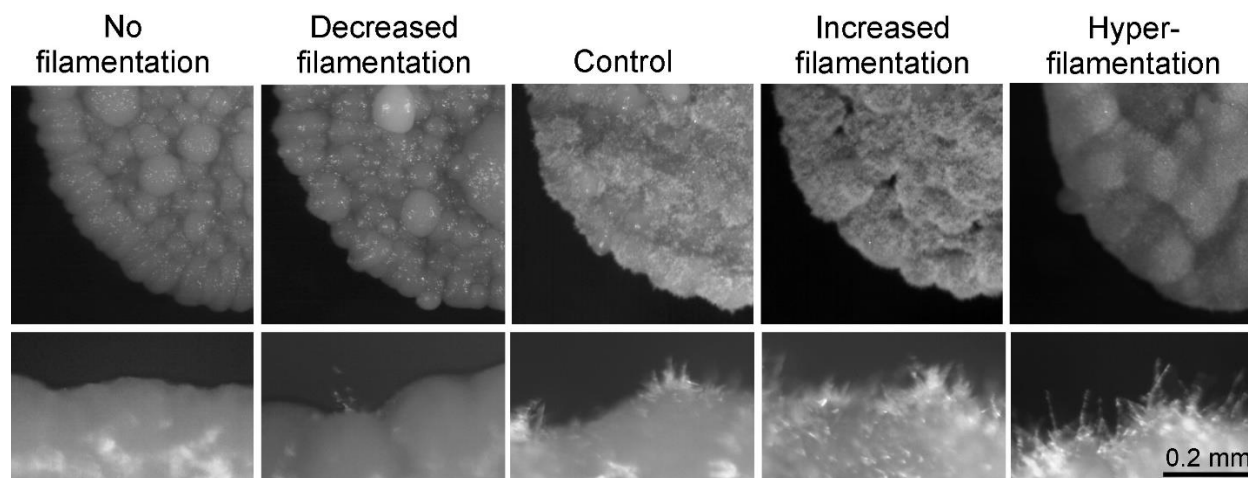


**Figure S3.4.** Colony images of represented strains of the four classified groups based on the robustness of filamentation on glucosamine medium compared to the control.

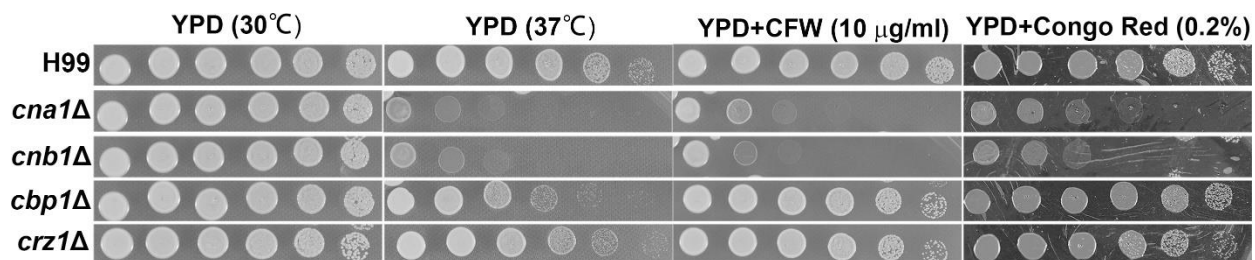
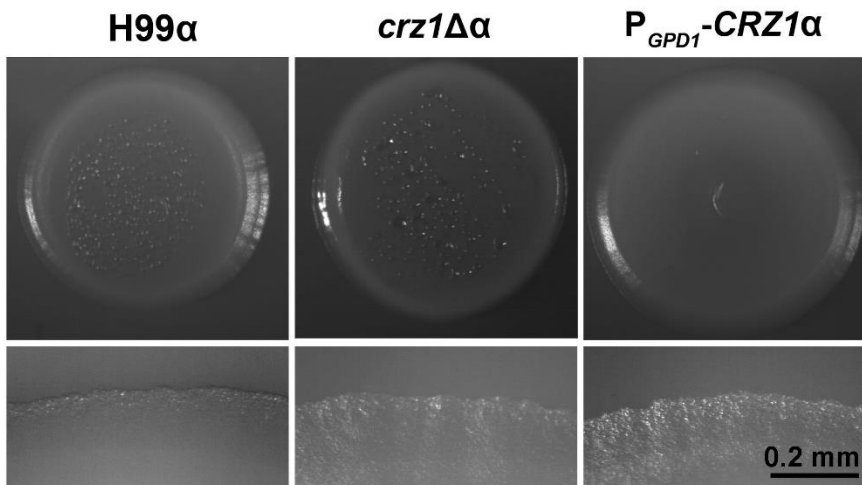


**Figure S3.5.** Mutants in the calcineurin pathway showed different susceptibility towards various stresses. Cells from the wild-type H99, the *cna1Δ* mutant, the *cnb1Δ* mutant, the *cbp1Δ* mutant, and the *crz1Δ* mutant were serial diluted (5x) and spotted onto YPD medium or YPD medium with Calcofluor white/CFW (10  $\mu\text{g/ml}$ ) or Congo Red (0.2%). The cells on YPD medium were incubated at 30°C or 37°C as indicated. Cells on medium with Calcofluor white or Congo red were cultured at 30°C.

## **A** $\alpha$ alone on V8



## **B** $\alpha$ and a coculture on V8

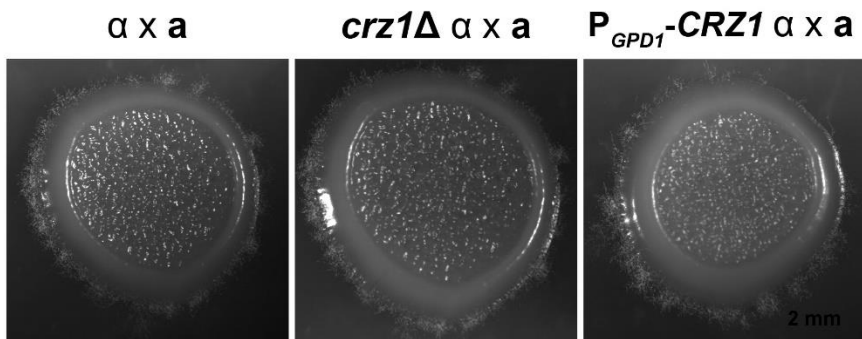


**Figure S3.6.** Crz1 does not regulate pheromone-induced filamentation. (A) The wild-type H99, the *crz1* $\Delta$  mutant, and the *CRZ1*<sup>oe</sup> strain all in the mating type  $\alpha$  were cultured alone on V8 juice agar medium at 22°C for 9 days. 3  $\mu$ l of cells at the density of OD<sub>600</sub> = 3 were used to inoculate. (B) The wild-type H99 $\alpha$ , the *crz1* $\Delta$   $\alpha$  mutant, and the *CRZ1*<sup>oe</sup>  $\alpha$  strain were mixed with the mating partner KN99a of the opposite mating type. The mixed co-cultures were inoculated and cultured on V8 medium at 22°C in the dark for 9 days.

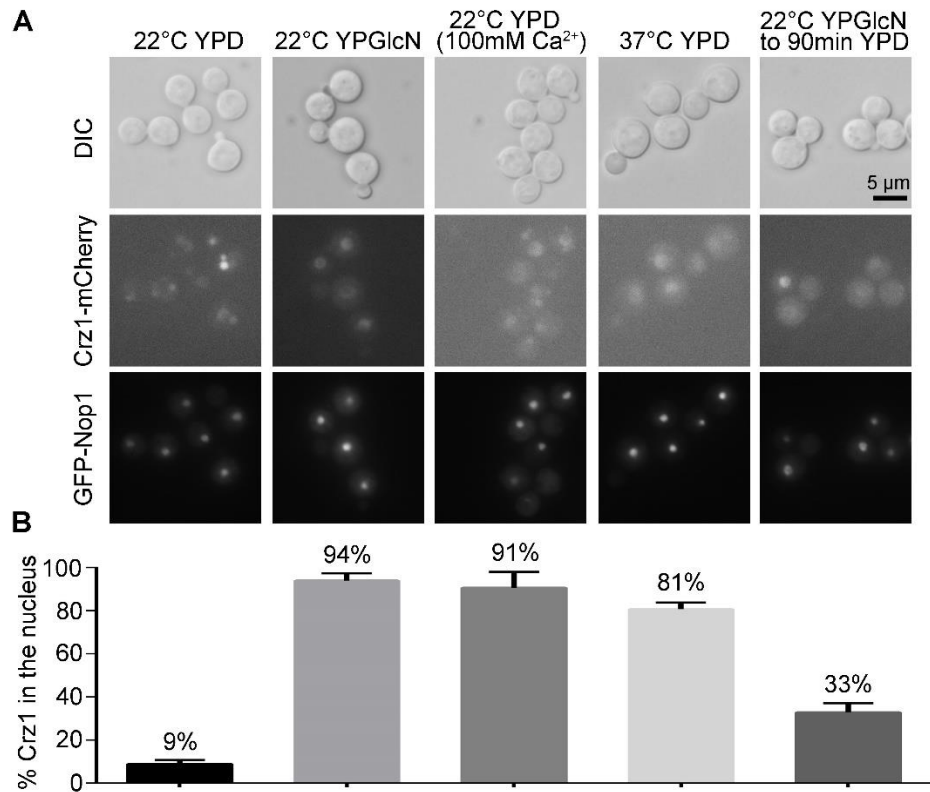


**Figure S3.7.** Calcium, high temperature, and glucosamine induce the nuclear translocation of Crz1-mCherry expressed under its native promoter. To test temperature's effect on the subcellular localization of Crz1-mCherry, the strain XW252 ( $P_{CRZI}$ - $CRZI$ -mCherry, GFP-Nop1) was cultured in YPD liquid at 37°C with shaking for 9 hours. To test the effect of calcium, cells of the strain  $P_{CRZI}$ -mCherry- $CRZI$  were first collected from the culture in liquid YPD at 22°C for 9 hours and then suspended in YPD with 100 mM of CaCl<sub>2</sub> for 10-20 min. To test the effect of glucosamine, the strain  $P_{CRZI}$ -mCherry- $CRZI$  was cultured in YP-glucosamine liquid medium at 22°C for 9 hours. For the examination of a shift in carbon-source, cells were incubated in YP-glucosamine liquid medium at 22°C for 9 hours and then shifted to glucose medium at 22°C for 90 minutes. **(A)** Images of the cells under the conditions tested. **(B)** Quantification of cells with nuclear localization of Crz1.

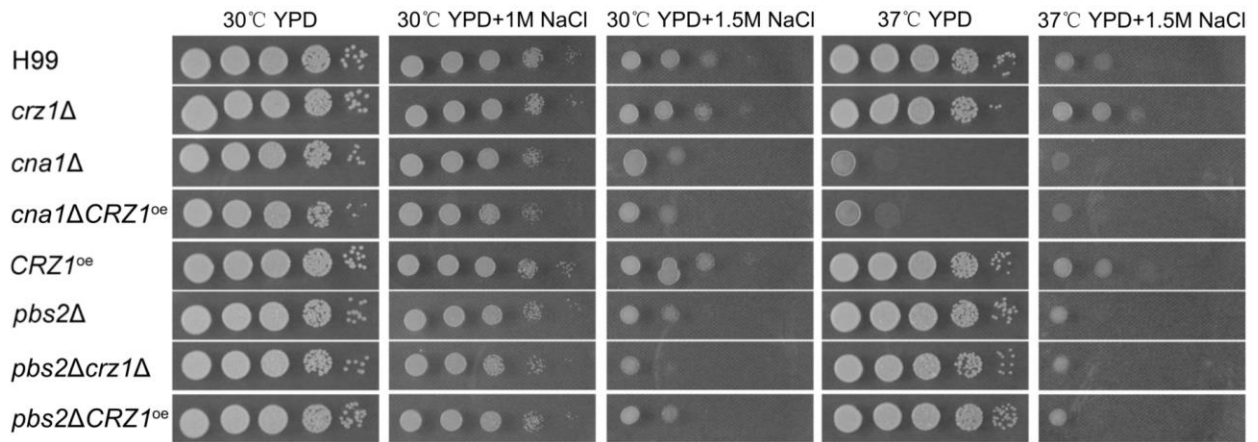


**Figure S3.8.** Crz1 is not important for osmotic stress response. Cells of the following strains (wild-type H99, *crz1*Δ, *cna1*Δ, *cna1*Δ*CRZ1*<sup>oe</sup>, *CRZ1*<sup>oe</sup>, *pbs2*Δ, *pbs2*Δ*crz1*Δ, and *pbs2*Δ*CRZ1*<sup>oe</sup>) were serially diluted and spotted onto YPD medium with or without the addition of NaCl at 1M, or 1.5M. Cells were then incubated at 30°C or 37°C for 3 days before images were taken.

## Supplemental Tables

The tables can be found on the website of *PLoS Genetics* journal at

<https://journals.plos.org/plosgenetics/article?id=10.1371/journal.pgen.1006982#sec023>

**Table S3.1:** The screening results from forward genetic screening.

**Table S3.2:** The strains used in this research

**Table S3.3:** The primers used in this research

CHAPTER 4

TRANSCRIPTION FACTOR ZNF2 COORDINATES WITH CHROMATIN REMODELING

SNF/SWI COMPLEX TO REGULATE DIFFERENTIATION IN *CRYPTOCOCCUS*

*NEOFORMANS*<sup>3</sup>

---

<sup>3</sup> Jianfeng Lin, Youbao Zhao, Aileen R Ferraro, Ence Yang, Zachary A Lewis, and Xiaorong Lin, 2019. *Submitted to Nature Communications*

## **Abstract**

Cellular differentiation is instructed by development regulators in coordination with chromatin remodeling complexes. Much information about their coordination comes from studies in the model ascomycetous yeasts. It is not clear, however, of the kind of information that can be extrapolated to species of other phyla in Kingdom Fungi. In the basidiomycete *Cryptococcus neoformans*, the transcription factor Znf2 controls yeast-to-hypha differentiation. Through a forward genetic screen, we identified the basidiomycete-specific factor Brf1 and discovered that it works together with the core subunit Snf5 in the SWI/SNF chromatin remodeling complex in concert with existent Znf2 to execute cellular differentiation. We further demonstrated that the SWI/SNF complex assists Znf2 opening up the promoter regions of hyphal specific genes, including the *ZNF2* gene itself. In addition, this complex supports Znf2 to fully associate with its target regions. Importantly, our findings revealed key differences in composition and biological function of the SWI/SNF complex in the two major phyla of Kingdom Fungi.

## **Introduction**

Cellular differentiation allows genetically identical cells to exhibit distinct phenotypes and carry out distinct cellular functions. Human cells, for example, can differentiate into more than 120 cell types. Although functional and morphological differences are most pronounced in higher eukaryotes, cellular differentiation is a universal phenomenon often directed by differential gene expression. In eukaryotes, nucleosomes serve as a general barrier preventing gene transcription because eukaryotic genomic DNA is packed into chromatin. Hence, chromatin regulation is a necessity for transcription in eukaryotes, brought about by specific positive regulatory mechanisms that make certain genomic DNA regions accessible to transcription

factors and RNA polymerase II. The ATP-dependent switch/sucrose non-fermentable (SWI/SNF) chromatin remodeling family mainly facilitates *in cis* sliding and/or *in trans* ejecting of nucleosomes on DNA <sup>1</sup>, allowing activation or repression of gene transcription. Through modulating gene expression, the SWI/SNF family of complexes are critical to a variety of cellular processes including stemness, differentiation, and development. Remarkably, about 20% of cancer types bare mutations in SWI/SNF subunits in humans <sup>2</sup>.

The SWI/SNF complex is the first ATP-dependent chromatin remodeling complex of the SWI/SNF family to be identified. To avoid confusion, we use the term “family” when we discuss the SWI/SNF family of complexes. The SWI/SNF complex is composed of 12 subunits in *Saccharomyces cerevisiae* and 11-15 subunits in humans <sup>3,4</sup>. However, most human SWI/SNF subunits have several isoforms, permitting dozens of combinatorial assemblies and a spectrum of related complexes <sup>5</sup>. It is therefore challenging to attribute observed phenotypes based on a mutation of a particular subunit to the function of a specific complex. In *S. cerevisiae* and *Schizosaccharomyces pombe*, there are only two complexes in the SWI/SNF family: the SWI/SNF complex and the RSC (remodeling structure of chromatin) complex. These two complexes have their distinct catalytic and accessory subunits while sharing a small set of common subunits <sup>6,7</sup>. The relative simplicity in these model ascomycete yeasts has facilitated the investigation into the molecular functions of the SWI/SNF complexes and their individual subunits. It is unclear, however, what functions and features of the SWI/SNF complexes established in these two model yeast species can be extrapolated to other eukaryotic species, including other distantly related fungal species.

In contrast to these model yeasts, the human fungal pathogen *Cryptococcus neoformans* belongs to a different phylum in Kingdom Fungi: Basidiomycota. Basidiomycetes diverged from

ascomycetes about 1 billion years ago and share key features with higher eukaryotes that are absent from the model ascomyceteous yeasts. For instance, >90% of the protein-coding genes in *C. neoformans* contain multiple introns and epigenetic regulation like RNAi and DNA methylation that play important roles in its biology<sup>8, 9, 10, 11, 12</sup>. *C. neoformans* can exist in multiple morphotypes, including basidiospore, blastospore, chlamydospores, yeast, titan cell, pseudohypha, hypha, clamp, and basidium. Cellular differentiation in *C. neoformans* is an area of great interest as morphological changes are associated with its pathogenicity<sup>13</sup>. For instance, yeasts and spores are infectious and virulent<sup>14, 15</sup>; titan cells are proposed to be dormant and stress-resistant in hosts<sup>16, 17</sup>; pseudohyphae and hyphae are attenuated in virulence in mammalian hosts<sup>18, 19</sup>. In the environment, however, hyphae are an integral part of its life cycle and the filamentous forms (pseudohyphae and hyphae) confer cryptococcal resistance to its natural predators (e.g. soil amoeba)<sup>20</sup>.

The yeast-to-hypha transition is the most understood cellular differentiation pathway in *C. neoformans*. During bisexual reproduction, compatible **a** and  $\alpha$  yeast partners conjugate after activating their pheromone sensing cascade, and the resulting **a**- $\alpha$  dikaryotic zygote differentiates to hyphae. Some aerial hyphae eventually develop into fruiting bodies and generate infectious meiotic basidiospores. We previously discovered that *C. neoformans*, in the absence of a compatible mating partner, can undergo similar cellular differentiation events (self-fruiting or unisexual reproduction)<sup>21</sup>, with the exception that the non-self-recognition system (the pheromone sensing cascade) is dispensable<sup>22, 23</sup>. A zinc-finger transcription factor, Znf2, is an absolutely required master regulator for hyphal growth<sup>19, 22, 23, 24</sup>. Deletion of *ZNF2* confines *C. neoformans* cells to the yeast form and overexpression of *ZNF2* drives filamentation regardless

of growth conditions<sup>19, 24</sup>. Whether chromatin remodeling factors coordinate with Znf2 to control the yeast-hypha differentiation in this basidiomycete remains unknown.

The *SWI* (switch) and *SNF* (sucrose nonfermenting) genes were initially discovered in *S. cerevisiae* genetic screens aimed towards identifying factors that control the induction of the endonuclease HO required for mating type switching or the induction of the invertase Suc2 required for sucrose metabolism<sup>25, 26</sup>. It later became apparent that these genes encode subunits of two large protein complexes (SWI/SNF and RSC) which are global regulators of transcription through ATP-dependent chromatin remodeling.

Here, we identified two genes, *SNF5* and *BRF1*, that are essential for hyphal differentiation even when Znf2 protein is produced via a forward genetic screen in a *ZNF2* overexpression strain of *C. neoformans*. Snf5 is a conserved core subunit in the SWI/SNF complex, while *BRF1* encodes a novel basidiomycete-specific protein with an AT-rich interacting domain (ARID). Excitingly, we discovered that Brf1 works together with Snf5 within the SWI/SNF complex to regulate hyphal differentiation. We demonstrated that Brf1 is essential for transcriptional induction of *ZNF2* and is required for Znf2's full association to the promoter regions of its downstream target genes, including the *ZNF2* gene itself. Furthermore, the promoter region of *ZNF2* and its downstream targets become transcriptionally inaccessible in the absence of *BRF1* or *SNF5*. This is the first identification and functional characterization of a phylum-specific subunit in the SWI/SNF complex in basidiomycetes. Our findings also reveal major and intriguing differences in composition and biological functions of both the SWI/SNF and RSC complex between the two major phyla in the Kingdom Fungi.

## Results

### **Insertional mutagenesis screen identified mutants that fail to filament when Znf2 protein is produced and localized to the nucleus**

Here we sought to identify factors that work in concert with Znf2 or downstream in controlling yeast-to-hypha morphological differentiation through a forward genetic approach. We employed a reporter strain where the native *ZNF2* gene is deleted and an ectopic copy of mCherry-fused *ZNF2* is expressed under the control of an inducible promoter of a copper transporter *CTR4* (XL280 $\alpha$ , *znf2::NAT/ P<sub>CTR4</sub>-2mCherryZNF2-NEO*). This reporter strain switched from yeasts to hyphae when *ZNF2* was induced in response to copper limitation in the presence of the copper chelator bathocuproinedisulfonic acid (BCS) (Figure 4.1A), as expected based on our previous studies<sup>24,27</sup>. The production of Znf2 can be monitored through the nuclear localized mCherry fluorescence signal (Figure 4.1A). Here we used insertional mutagenesis through *Agrobacterium*-mediated transformation (AMT) and generated 88,000 T-DNA insertional mutants in this reporter strain. We screened these mutants visually for smooth yeast colonies on filamentation-inducing V8 agar medium containing BCS (Figure 4.1B). 84 filamentation-defective mutants were isolated (strains AMT001-AMT084, Table S4.1).

We next examined the cellular morphology, and the expression and localization of mCherry-tagged Znf2 protein upon induction of these 84 isolated mutants. 58 of these mutants showed nuclear mCherry-Znf2 localization while 26 had altered subcellular distribution of the fluorescence signal. Among these 58 mutants, 25 candidate mutants showed only yeast cellular morphology in the population and nuclear mCherry-Znf2 signal when cultured in YPD+BCS inducing condition (Table S4.1). These 25 mutants were then chosen for further analysis.

Multiple T-DNA insertions and cryptic mutations could occur during *Agrobacterium*-mediated transformation<sup>28,29</sup>. To determine if the T-DNA insertion is genetically linked to the non-filamentous phenotype in these 25 mutants, we backcrossed these 25 mutants (in the  $\alpha$  mating type) to the wild-type congenic mating partner XL280a, micro-dissected the meiotic basidiospores, and analyzed the phenotypes of the progeny. If the genome of the insertional mutant harbors only one copy of the T-DNA, which carries the hygromycin selection marker *HYG*, then we would expect a 1:1 ratio of hygromycin sensitive ( $HYG^S$ ) and hygromycin resistant ( $HYG^R$ ) progeny. If that single T-DNA insertion caused the non-filamentous phenotype, then all  $HYG^R$  progeny would be non-filamentous while all  $HYG^S$  progeny would be filamentous under a *Znf2*-inducing condition. In comparison, when multiple T-DNAs inserted in the genome, the ratio between  $HYG^S$  and  $HYG^R$  meiotic progeny would be 1:3 (two unlinked insertions) or smaller ( $>2$  unlinked T-DNA insertions). Based on our genetic linkage analyses of the meiotic progeny dissected from the 25 crosses, 8 out of the 25 mutants likely harbor a sole T-DNA insertion that is genetically linked to their non-filamentous phenotype on media containing BCS (Figure 4.1C).

### **Two candidate genes, *SNF5* and *BRF1*, were identified as critical filamentation activators**

To identify the genes affected by the T-DNA insertions in the selected 8 mutants, we used genome sequencing approach developed by Dr. Alspaugh's group<sup>29</sup>. The 8 mutants carry not only the T-DNA insertion ( $HYG^R$  marker), but also the *znf2* $\Delta$  construct ( $NAT^R$  marker) and the  $P_{CTR4-2}mCherryZNF2$  construct ( $NEO^R$  marker). Because all three drug selection markers share the same promoter and terminator sequences, we decided to sequence their meiotic progeny derived from the backcrosses that have only the T-DNA insertion ( $HYG^R$ ). From the

genome sequences of the 8 “clean” insertional mutants, we identified 8 insertion sites (Table S4.2), including two singleton and six paired insertions. Singleton insertions could be the result of big chromosomal fragment deletion or chromosomal rearrangement<sup>29</sup>, and so we did not pursue them further. The remaining six paired insertions revealed four possible disrupted genetic loci (Figure 4.1D), with two loci being inserted twice independently in different isolates. *CND05760* encodes the Ste11 $\alpha$  MAP kinase, which is known to be involved in the pheromone sensing cascade but not essential for filamentation<sup>23</sup>. To verify the role of the other three identified genes *CNK02410*, *CNA02310*, and *CNA07190* in filamentation, we carried out independent targeted gene deletion in the wild-type XL280 $\alpha$  background. *CNK02410* encodes Ssn6, a general transcriptional co-repressor<sup>30</sup>. Deletion of *SSN6* reduced filamentation in the wild type background (Figure 4.1E). *CNA02310* and *CNA07190* were recovered twice from independent insertions (Figure 4.1D). Independent targeted deletion of these two genes in the wild type background nearly abolished filamentation, similar to the corresponding insertional mutants (Figure 4.1C, E). Thus, *CNA02310* and *CNA07190* are critical for yeast-hypha transition in *C. neoformans*.

*CNA07190* encodes Snf5 (1784 aa, 195kDa), a core subunit of the conserved SWI/SNF chromatin remodeling complex. Snf5 is critical for cellular differentiation in all organisms tested, including ascomycetous and basidiomycetous fungi<sup>31, 32, 33, 34, 35, 36</sup>. For instance, deletion of *SNF5* in the basidiomycete *Coprinopsis cinerea*, commonly known as the gray shag mushroom, results in severe defects in dikaryon development and fruiting<sup>34, 35</sup>. In *C. neoformans*, *SNF5* was shown to be critical for bisexual reproduction in the serotype A H99 strain background, as a *snf5* $\Delta\alpha$  x *snf5* $\Delta\mathbf{a}$  cross yielded no mating hyphae or fruiting body<sup>28</sup>. Consistently, we found that a cross between *snf5* $\Delta\alpha$  and *snf5* $\Delta\mathbf{a}$  mutants in XL280 background yielded no mating hyphae

(Figure 4.2A). This indicates that the function of Snf5 is conserved in both serotypes of *C. neoformans*. Besides Snf5, no other subunits in the SWI/SNF complex have been identified or characterized in *C. neoformans*.

*CNA02310* encodes an uncharacterized novel protein (1033 aa, 112kDa). The predicted protein has an AT-rich interacting domain (ARID) but no other recognizable domains. Because it is basidiomycete specific (Figure S4.1), we named this gene *BRF1* (basidiomycete-specific regulator of filamentation 1).

### **Brf1 functions in the same biological processes as Snf5, a known core component of the SWI/SNF complex**

Brf1 and Snf5 share a similar function in filamentation. As mentioned earlier, independent deletion of *SNF5* or *BRF1*, or their disruption by T-DNA insertion abolished or nearly abolished self-filamentation (Figure 4.1E). Unilateral crosses between the *snf5* $\Delta$  or the *brf1* $\Delta$  mutant in the  $\alpha$  mating type with a non-self-filamentous reference **a** strain (*snf5* $\Delta$  $\alpha$  x **a** or *brf1* $\Delta$  $\alpha$  x **a**) on V8 medium produced fewer mating hyphae (Figure S4.2A), likely due to their reduced cell fusion efficiency (Figure S4.2B). Bilateral crosses between the mutant partners (*snf5* $\Delta$  $\alpha$  x *snf5* $\Delta$ **a** or *brf1* $\Delta$  $\alpha$  x *brf1* $\Delta$ **a**) did not produce any aerial mating hyphae or sexual spores (Figure 4.2A). As bisexual mating or self-filamentation on V8 medium is mostly driven by the pheromone signaling cascade, we decided to examine the impact of these mutations on filamentation independent of the pheromone cascade on V8 medium supplemented with a high concentration of copper (500 $\mu$ M CuSO<sub>4</sub>). We previously showed that self-filamentation under this condition is independent of the nonself-recognition system<sup>22</sup>. Neither the *brf1* $\Delta$  mutant nor

the *snf5* $\Delta$  mutant filamented under this condition (Figure 4.2A), confirming the similarly critical role of Brf1 and Snf5 in filamentation.

Brf1 and Snf5 also share similar function in other assays. Here we examined the *brf1* $\Delta$  mutant and the *snf5* $\Delta$  mutant for their susceptibility to heat stress (37°C), osmotic stress (1M NaCl or KCl), or cell wall stress (0.5% Congo Red). The *brf1* $\Delta$  and *snf5* $\Delta$  mutants showed slightly increased sensitivity to osmotic stress and both mutants grew similarly in other conditions tested (Figure 4.2B). *SNF5* is known to be required for normal growth on media with disaccharide sucrose or trisaccharide raffinose as the sole carbon source<sup>28</sup>. Here we found that the *brf1* $\Delta$  mutant showed a similar defect in growth on the raffinose medium as the *snf5* $\Delta$  mutant (Figure 4.2C-D). Neither the *brf1* $\Delta$  mutant nor the *snf5* $\Delta$  mutant showed any significant defect in growth when glucose was used as the sole carbon source (Figure 4.2C-D).

Given the striking resemblance of the *brf1* $\Delta$  mutant and the *snf5* $\Delta$  mutant, we postulate that Brf1 functions in the same biological pathway as Snf5. To test this hypothesis, we constructed the *brf1* $\Delta$ *snf5* $\Delta$  double mutant. If *BRF1* and *SNF5* work in the same pathway, we expect that the double deletion mutant would show similar phenotypes as the single gene deletion mutants. Indeed, the *brf1* $\Delta$ *snf5* $\Delta$  double mutant behaved similarly as the *brf1* $\Delta$  or the *snf5* $\Delta$  single mutant in all assays (stress tolerance, filamentation, and growth on the raffinose medium) (Figure 4.2B-D). When we tagged Brf1 with tdTomato controlled by a constitutively active promoter ( $P_{TEF1}$ -*BRF1*-tdTomato), it restored the filamentation defect of the *brf1* $\Delta$  mutant (Figure S4.4A), indicating functionality of the tagged Brf1. The tagged Brf1 localized to the nucleus (Figure S4.4A), as is Snf5<sup>37</sup>. Taken together, we propose that Brf1 functions together with Snf5.

As Snf5 is a conserved and core subunit of the SWI/SNF complex, we postulate that this novel protein Brf1 may also function in this chromatin remodeling complex. Every known SWI/SNF complex incorporates a subunit with an ARID domain<sup>38,39,40</sup>, which can bind to DNA<sup>39</sup>. In the ascomycete fungal pathogen *Candida albicans*, Swi1, the ARID-containing subunit in the SWI/SNF complex, is critical for filamentation and virulence<sup>31,32,33</sup>. The *C. neoformans* genome carries three genes encoding ARID-containing proteins: *RUM1α* (CND05870), *AVC1* (CNK00710), and *BRF1*. None of these three cryptococcal genes showed high sequence homology to *SWI1* or *SOL1*, the ARID containing subunit in the SWI/SNF complex in *S. cerevisiae* or *S. pombe*. However, in terms of domain architecture, Brf1 is more similar to ScSwi1 or SpSol1 than Avc1 or Rum1α (Figure 4.3A). Consistent with our idea that Brf1, but not Avc1 or Rum1α, works in the same complex as Snf5, deletion of *BRF1*, but not *AVC1* or *RUM1α*, caused defects in filamentation (Figure 4.3B) and slowed growth on raffinose medium (Figure S4.3).

### **Brf1 is a subunit of the SWI/SNF complex**

If Brf1 and Snf5 work together in the SWI/SNF complex, we expect that Brf1 and Snf5 interact with each other, either directly or indirectly through other subunits of the SWI/SNF complex. To test the hypothesis, we performed co-immunoprecipitation assays using the FLAG-tagged Brf1 as the bait. As *BRF1* is a lowly expressed gene based on our and others' transcriptome data<sup>41</sup>, we used the constitutively active *TEF1* promoter to drive the expression of FLAG-tagged Brf1 protein and it restored the *brf1Δ*'s mating deficiency (Figure S4.4B). We then carried out Co-IP in two independent isolates and the wild-type H99 strain without any tag was used as the negative control. We applied the following criteria to exclude nonspecific

proteins: (i) proteins shared among the samples and the negative control, (ii) proteins not shared between samples of the two  $P_{TEF1}$ -*BRF1*-CBP-2xFLAG strains, and (iii) non-nuclear localized proteins as Brf1 localizes to the nucleus. Accordingly, we identified many putative SWI/SNF components that are homologous to the SWI/SNF complex subunits in *S. cerevisiae* and/or *S. pombe*, including Snf5, Snf2, Arp4, Arp9, Rsc6, and Rsc8 (Table 4.1).

The SWI/SNF complex and the RSC complex of the SWI/SNF family are assembled modularly, with some subunits/modules shared by both complexes<sup>5, 42, 43</sup>. In *S. cerevisiae* and *S. pombe*, homologues of Arp4, Arp9, Rsc6, and Rsc8 participate in both the SWI/SNF complex and the RSC complex. Since Brf1 pulled down subunits unique to the SWI/SNF complex and the ones shared by both complexes, we speculate that Brf1 is SWI/SNF-specific in *C. neoformans*. In most fungal species examined, the SWI/SNF complex and the RSC complex each harbors a Snf5 domain-containing subunit, with Snf5 in the SWI/SNF complex and Sfh1 in the RSC complex (Figure 4.3C). When we used the mNeonGreen-tagged RSC-specific protein Sfh1 (CNC06140) to perform co-immunoprecipitation in *C. neoformans*, the Sfh1 pulled down RSC-specific subunits including Rsc1, Rsc7, and Rsc9. In addition, tagged Sfh1 pulled down the shared subunits including Snf2, Arp4, Arp9, Rsc6, and Rsc8 (Table S4.3). However, Sfh1 did not pull down Brf1 or the SWI/SNF-specific subunit Snf5. Taken together, these lines of evidence support that Brf1 is a subunit specific to the SWI/SNF complex in *C. neoformans*.

Based on the Co-IP data and the homology of the SWI/SNF and RSC subunits among *S. cerevisiae*, *S. pombe* and *C. neoformans*, we inferred that Brf1 and Snf5 are subunits specific to the SWI/SNF complex (brownish yellow) while Sfh1, Rsc1, Rsc4, Rsc7, and Rsc9 are subunits specific to the RSC complex (blue in Table 4.2). Snf2, Arp4, Arp9, Rsc6 and Rsc8 are the shared subunits between the SWI/SNF and the RSC complexes in *C. neoformans* (green in Table 4.2,

Figure S4.5A). Consistent with the idea that these two complexes have overlapping and distinct subunits, the transcript levels of the shared components are generally higher (green) than the complex-specific subunits (yellow or blue) based on a cell-cycle-regulated transcriptome data<sup>41</sup> (Figure 4.3D). In *S. cerevisiae*, the RSC complex is approximately 10 times more abundant at the protein level than the SWI/SNF complex<sup>44</sup>. Consistently, the genes encoding for the RSC subunits are expressed at higher levels than those encoding the SWI/SNF subunits in *S. cerevisiae* (Figure 4.3D). In both *S. cerevisiae* and *S. pombe*, many subunits in the RSC complex are essential for growth, including Sfh1 and Rsc9 (Table 4.2)<sup>6, 44, 45</sup>. By contrast, the RSC-specific *SFH1* and *RSC9* genes are not essential for growth in *C. neoformans* as the gene deletion mutants are viable, albeit with slower growth on either nutrient rich media or minimum media (Figure 4.3F-G). Surprisingly, deletion of the SNF/SWI complex specific *BRF1* or *SNF5* did not cause any gross defects in growth under the same conditions (Figure 4.3F-G). Remarkably, the *snf5Δsfh1Δ* double mutant, where both the SWI/SNF-specific subunit Snf5 and the RSC-specific subunit Sfh1 were knocked out, was still viable despite a much more pronounced growth defect (Figure 4.3G). Thus, the SWI/SNF complex functionally differ from the RSC complex in *C. neoformans*. Neither the RSC complex nor both RSC and SWI/SNF complexes together are essential in this basidiomycetous fungus, in contrast to what is known in ascomycetes.

Given that the two SWI/SNF complex specific subunits Brf1 and Snf5, and none of the RSC complex specific subunits were identified from our genetic screen, we predicate that the SWI/SNF complex, but not the RSC complex, specifically regulates the yeast-hypha differentiation in *C. neoformans*. To test this hypothesis, we examined the impact of the disruption of the SWI/SNF complex (*brf1Δ* and *snf5Δ*) or the RSC complex (*sfh1Δ* and *rsc9Δ*) on filamentation. Indeed, the RSC complex mutants, *sfh1Δ* and *rsc9Δ*, were still filamentous on

V8 medium, in contrast to the yeast growth of the SWI/SNF complex mutants *brf1* $\Delta$  and *snf5* $\Delta$  (Figure 4.3E). The findings support the view that the SWI/SNF complex, but not the RSC complex, is critical for yeast-to-hyphal differentiation in *C. neoformans*.

### ***BRF1* is required for the induction *ZNF2* transcript level**

The evidence presented so far supports the idea that Brf1 and Snf5 work together in the SWI/SNF complex. Here we used Brf1 to dissect the relationship between the SWI/SNF complex and Znf2 in controlling morphogenesis in *C. neoformans*. To study the genetic relationship between Brf1 and Znf2, we set up a cross between a *brf1* $\Delta$ /*BRF1*<sup>oe</sup>  $\alpha$  strain and a *znf2* $\Delta$ /*ZNF2*<sup>oe</sup> **a** strain. We micro-dissected meiotic progeny from the cross and confirmed the genotypes of the progeny by diagnostic PCRs (Figure 4.4A). As expected, progeny of the wild-type genotype were self-filamentous, while progeny of the *znf2* $\Delta$  or the *brf1* $\Delta$  genotype were non-filamentous. *ZNF2*<sup>oe</sup>*znf2* $\Delta$  strains were filamentous, but not *ZNF2*<sup>oe</sup>*brf1* $\Delta$  (Figure 4.4B). This result is consistent with our earlier observation that overexpression of *ZNF2* did not restore filamentation in the *brf1*<sup>Tn</sup> insertional mutant (Figure 4.1C). Likewise, *BRF1*<sup>oe</sup>*brf1* $\Delta$  strains were filamentous, but not *BRF1*<sup>oe</sup>*znf2* $\Delta$  (Figure 4.4B). These results indicate that overexpression of *BRF1* restored filamentation in the *brf1* $\Delta$  mutant, but it could not bypass the requirement of Znf2. Taken together, overexpression of either *BRF1* or *ZNF2* cannot override the absence of the other, and both are essential for yeast-hypha differentiation in *C. neoformans*.

We next analyzed the transcriptomes of wild type, *brf1* $\Delta$ , *brf1* $\Delta$ /*BRF1*<sup>oe</sup>, and *ZNF2*<sup>oe</sup> strains cultured under filamentation-repressing YPD medium and filamentation-inducing V8 medium. More than 60% of the differentially expressed genes in the *brf1* $\Delta$  and the *znf2* $\Delta$  mutants under filamentation-inducing condition were shared (Figure 4.4C). Remarkably, more than 98%

(101/103) of the overlapping genes were down-regulated upon deletion of *BRF1* or *ZNF2*, suggesting that Brf1 and Znf2 activate these genes during hyphal differentiation. As *ZNF2*/filamentation is primarily induced by the pheromone pathway when cells are cultured on V8 medium<sup>22</sup>, it is not surprising that deletion of either *BRF1* or *ZNF2* dampened the induction of the pheromone sensing pathway genes, including *MF1 $\alpha$*  (pheromone gene, 345 fold reduction), *STE3 $\alpha$*  (pheromone receptor gene, 14 fold reduction), *STE6* (pheromone exporter gene, 7 fold reduction), *CPK1* (pheromone MAPK gene, 5.2 fold reduction), and *MAT2* (pheromone transcription factor gene, 9 fold reduction) (Figure 4.4C). The reduced activation of the pheromone sensing pathway in the *brf1 $\Delta$*  mutant likely caused reduced cell fusion which we observed earlier (Figure S4.2B).

The transcript level of *ZNF2* in the wild type increased 32-fold under filamentation-inducing condition compare to filamentation suppressing condition. In the absence of *BRF1*, however, the *ZNF2* transcript level remained extremely low, similar to the basal level when cells were cultured under filamentation-suppressing condition (Figure 4.4D). Ectopic expression of *BRF1* under the control of *TEF1* constitutive promoter in the *brf1 $\Delta$*  strain restored the dramatic induction of the *ZNF2* transcript level under filamentation-inducing condition (Figure 4.4D). By contrast, constitutive expression of *ZNF2* (54.75 fold increase) had minimal impact on the transcript level of *BRF1* (1.27 fold increase). The transcript of *BRF1* remained at a low and steady level when cells were cultured either in YPD or on V8 medium. The steady level of *BRF1* transcripts was also observed at different stages of the cell cycle (Figure 4.3D)<sup>41</sup>. The results indicate that *BRF1* itself is expressed at a low but constant level and is not influenced by Znf2. The induction of *ZNF2*, however, requires Brf1.

## **Brf1 and Znf2 work in concert in controlling genetic loci critical for cellular differentiation**

The SWI/SNF chromatin-remodeling complex is known to evict or slide nucleosomes to open up chromatin for transcription. As Brf1 is required for *ZNF2* induction, we postulate that deletion of *BRF1* impairs chromatin remodeling at the *ZNF2* promoter region, which consequently diminishes transcription induction of *ZNF2*. Moreover, we showed earlier that when the Znf2 protein was produced due to ectopic expression controlled by a non-native promoter, it still failed to drive filamentation in the absence of Brf1 (Figure 4.1C and 4.4B). Say, Brf1 also functions beyond transcription activation of *ZNF2* as Brf1 is critical for existent Znf2 protein to execute its function. We thus hypothesize that Brf1 is required for chromatin remodeling not only at the promoter region of *ZNF2*, but also those of Znf2's targets.

To test our hypothesis, we employed the assay for transposase-accessible chromatin followed by next generation sequencing (ATAC-seq)<sup>46,47</sup> and compared genetic regions with open chromatin structures in wild type, grown on V8 or YPD, as well as in the *znf2Δ*, *snf5Δ*, and *brf1Δ* strains. As an additional control, we analyzed accessible chromatin regions in the *brf1Δ/BRF1<sup>oe</sup>* strain. As expected, accessible chromatin fell in gene promoter regions, with expressed genes having a higher level of accessibility based on the relative enrichment of ATAC-seq reads (Figure 4.5A). Globally, chromatin accessibility was similar in all strains tested (Figure 4.5B). We identified 39 regions that displayed reduced accessibility in the *brf1Δ* strain (Figure 4.5C). A subset of regions that lose accessibility in *brf1Δ* are also inaccessible in WT growing under yeast-promoting condition (Figure 4.5C). Ten of the Brf1-dependent ATAC-seq peaks overlapped with genes that are up-regulated in hyphal-promoting growth conditions. A genome browser image illustrating RNA-seq and ATAC-seq reads for three of these genes is shown in Figure 4.5D, along with a control gene that does not require Brf1 for open chromatin.

Of particular interest is the hypha marker gene *CFL1* (Figure 4.5D). The promoter region of *CFL1* is the most significantly differentially accessible region ( $\log_{10}[\text{likelihood}] = 29.678$ ), and *CFL1* is also one of the highest induced genes controlled by Znf2<sup>24</sup>. Notably, Brf1, Snf5, and Znf2 are each required for accessible chromatin in the *CFL1* promoter, whereas overexpression of *BRF1* in *brf1* $\Delta$  restored chromatin accessibility (Figure 4.5D). Collectively, these data suggest interdependence between the transcription factor Znf2 and the SWI/SNF complex in opening up chromatin to facilitate transcription of filamentation genes.

To determine if the ability of Znf2 to bind to its downstream targets is affected by the SWI/SNF complex, we conducted chromatin-immunoprecipitation (ChIP) experiments using 3xFLAG-tagged Znf2 as the bait. The FLAG tagged Znf2 was expressed under the control of the inducible *CTR4* promoter in the wild type or in the *brf1* $\Delta$  mutant background. We compared the relative abundance of precipitated genetic loci pulled down by the tagged Znf2 using qPCR. Here we chose the locus of the filamentation marker gene *CFL1* as a proxy for Znf2 downstream targets<sup>23, 27, 48, 49</sup>. We included six regions upstream of the transcription start site (TSS) of *CFL1*, one region spanning the TSS, one region shortly downstream of the TSS, and one region within the ORF (Figure S4.6A). As expected for a transcription factor, the signal at the ORF region was low irrespective of the presence or the absence of Brf1 (Figure S4.6A). The signal became stronger around the -750 position and peaked near the -150 position from the TSS in the Znf2 tagged strain (Figure S4.6A). The results indicate that Znf2 strongly binds to the *CFL1* promoter. Interestingly, when we tested the *ZNF2* locus by ChIP-qPCR, we also found higher abundance of the promoter region than its ORF region (Figure S4.6B). The data indicate that Znf2 associates with its own promoter and it likely autoregulates itself. Autoregulation is not uncommon for transcription factors. Interestingly, the association of Znf2 to the promoter regions of *CFL1* and

*ZNF2* decreased 2-3 folds in the absence of Brf1 (Figure 4.5E, S4.6). The result supports the idea that the SWI/SNF complex helps Znf2 associate with its downstream targets, including *ZNF2* itself. The finding is consistent with our earlier transcriptome data showing that *BRF1* is required for *ZNF2* transcription induction (Figure 4.4D). Thus, Brf1, a subunit of the chromatin-remodeling SWI/SNF complex, is required for full association of the transcription factor Znf2 with its downstream targets.

## Discussion

Chromatin remodeling plays critical roles in cellular differentiation in eukaryotes. The model ascomycetous yeast species *S. cerevisiae* and *S. pombe* have offered a relatively simple system for mechanistic studies in this research area. Basidiomycetous fungi resemble more of the higher eukaryotes in terms of genome structures, epigenetic regulation, and transcriptome complexity, but research on chromatin remodeling in this major phylum of the fungal kingdom is spotty.

In this study, we identified and characterized, for the first time, a basidiomycete specific factor Brf1 that serves as a critical subunit in the SWI/SNF complex. We demonstrated that Brf1, as well as the conserved and previously known subunit Snf5 of the SWI/SNF complex, are essential for hyphal growth and sexual development in the basidiomycete *C. neoformans*. This complex opens the chromatin structure of the promoter regions of filamentation genes to render them accessible for transcription (Figure 4.5F). Brf1 is vital not only for transcriptional induction of *ZNF2*, but also full association of Znf2 protein to the promoters of its downstream targets like *CFL1*. Our findings are consistent with published literature in other organisms, in which the SWI/SNF complex contributes to the DNA binding of the transcription factor<sup>50, 51</sup>. The

SWI/SNF complex has been shown being targeted to specific genetic loci by sequence-specific transcription factors and acetylation of histone tails<sup>50, 52, 53</sup>. In the ascomycetous fungus *C. albicans*, the transcription factor Efg1 recruits the histone acetyltransferase complex NuA4 to the promoters of hypha-associated genes, allowing in turn the recruitment of the SWI/SNF complex to activate their transcription to drive morphological transition<sup>54</sup>. We reason that Znf2 may recruit the SWI/SNF complex to its target sites given that deletion of *ZNF2* caused the loss of open chromatin at the *CFL1* promoter region (Figure 4.5D-F). That said, we could not establish direct physical interaction between Znf2 and the SWI/SNF complex via Co-IP experiment after multiple attempts. It is possible the interaction is too weak or transient to be captured by our assay. Alternatively, histone modifications or the modification enzymes could be involved in bringing the SWI/SNF complex to the target loci. Several subunits in the SWI/SNF complex possess domains that recognize histone modifications, such as bromodomains for histone acetylation<sup>55</sup>. How exactly the SWI/SNF complex works with Znf2 in *C. neoformans* to control differentiation warrants further investigation.

Our findings revealed striking differences in the two complexes (SWI/SNF and RSC) within the SWI/SNF family in Ascomycota and Basidiomycota. In *Saccharomyces* and *Schizosaccharomyces* species, most subunits in the RSC complex are essential for growth, including the catalytic ATPase subunit Snf2 (or SpSnf22), Sfh1, and Rsc9<sup>44, 45, 56</sup> (Table 4.2). By contrast, deletion of the shared ATPase catalytic subunit Snf2 is not lethal in *C. neoformans*. Consistently, deletion of both *SNF5* (SWI/SNF-specific) and *SFHI* (RSC-specific) together slowed growth but did not cause lethality (Figure 4.3G). Thus, either the SWI/SNF complex, the RSC complexes, or both combined, are likely not essential for growth in this basidiomycete. Hence, despite conserved compositions among different lineages of eukaryotes, the biological

function of the RSC complex differs substantially in different species. Comparative functional analyses of the RSC complex among evolutionarily diverse species, therefore, provides a unique vantage point to understand its biology.

All SWI/SNF complexes, either in yeasts or humans, have a subunit with a conserved Snf5 domain. The majority of fungal species examined carry two proteins bearing a Snf5 domain (Pfam domain ID PF04855), presumably one acting as the Snf5 subunit in the SWI/SNF complex and one acting as the Sfh1 subunit in the RSC complex (Figure 4.3C, Table S4.4). Based on primary protein sequences, Snf5 proteins in Ascomycota separate clearly into two clades: Snf5 and Sfh1 (Figure 4.3C). *C. neoformans* genome also encodes two proteins with a Snf5 domain: *SNF5* and *SFH1* (Figure 4.3C). Surprisingly, both Snf5-containing proteins in *C. neoformans* and those in other basidiomycetes cluster closely with the Sfh1 clade in ascomycetes (Figure 4.3C).

The SWI/SNF complex assemble in an ordered modular fashion and Snf5 acts as a scaffold protein<sup>5, 42, 43</sup>. In *S. cerevisiae*, Snf5 and Swi1 (the ARID containing protein) are likely in two different modules of the complex<sup>5, 42, 43</sup> given the phenotypical differences of the *snf5* and *swi1* mutants<sup>57</sup>. In *C. neoformans*, however, *snf5* and *brf1* mutants have nearly identical phenotypes. It is unclear if the difference, or the lack thereof, between mutations in Snf5 and the ARID domain protein in different organisms reflects the difference in their modular assembly. Interestingly, Snf5 proteins in basidiomycetes are much larger in size comparing to the Snf5 proteins in ascomycetes or Snf5 in humans (e.g. *C. neoformans*: 1784 aa, *U. maydis*: 2080 aa, *S. cerevisiae*: 905 aa, *S. pombe*: 632aa, or humans: 385aa) (Figure 4.3C). The much larger Snf5 proteins in basidiomycetes with two internal repeats near the N-terminus (Figure S4.5B) could

potentially increase binding surface area and consequently help recruit and assemble the SWI/SNF complex.

The SWI/SNF family employs Snf2 as the ATPase catalytic subunit. In the ascomycetous fungi like *S. cerevisiae* and *S. pombe*, the ATPase subunit is complex-specific: the SWI/SNF and the RSC complexes use different ATPase subunits. In comparison, we showed here that the ATPase subunit Snf2 was shared between the SWI/SNF and the RSC complexes in *C. neoformans*. Snf2 proteins in SWI/SNF family complexes are characterized by the presence of a HSA domain and a BROMO domain flanking the ATPase domain (the DEXDc and HELICc regions) (Figure S4.5C)<sup>4</sup>. However, a search for the HSA domain (PF07529) and the BROMO domain (PF00439) among dozens of fungal species belonging to three different major phyla in the fungal kingdom revealed that some fungi, including ascomycete *S. cerevisiae* and zygomycete *Mucor circinelloides*, have two distinct Snf2 family ATPases, presumably one for the SWI/SNF complex and one for the RSC complex. Some other fungi, including ascomycete *Aspergillus nidulans* and basidiomycete *C. neoformans*, however, have only one Snf2 ATPase, presumably shared by both the SWI/SNF complex and the RSC complex (Table 4.2 and S4.5). Intriguingly, in *Drosophila melanogaster*, the BAP (SNF/SWI) complex and the PBAP (RSC) complex share the same catalytic ATPase subunit (BRM). Human BAF (mSNF/SWI) complex and PBAF (mRSC) complex can either share the same ATPase BRG-1 subunit or use different ATPases (hBRM and BRG-1)<sup>4</sup>. Thus, to share or not to share the ATPase by the SWI/SNF and the RSC complexes is species-specific. The copy number variation of Snf2 in different organisms might have driven such divergence independent of the evolutionary distance of the species.

In conclusion, here we identified and characterized the first basidiomycete-specific subunit of the SWI/SNF chromatin remodeling complex and revealed the major differences in composition and biology of this complex between ascomycetes and basidiomycetes. The universal importance of the SWI/SNF family in eukaryotes, and the phylum-specific or even species-specific features of this complex that we reported here, highlight the value and power of comparative analyses among evolutionarily diverse species.

## **Methods and Materials**

### **Strains and growth conditions**

Strains used in this study were listed in Table S4.6. All strains were stored in 15% glycerol at -80°C and were freshly streaked out onto YPD media (2% peptone, 1% yeast extract, 2% glucose, 2% agar, gram/liter) for each experiment. *C. neoformans* cells were cultured in YPD medium unless stated otherwise. For some assays, the defined minimal YNB medium (6.7 gram/liter nitrogen base w/o amino acids, 2% agar, 2% glucose) was used as specified in the figure legends. For mating or filamentation assays, V8 juice agar medium (1 liter medium, 50mL V8 original juice, 0.5g KH<sub>2</sub>PO<sub>4</sub>, 4% agar, pH 5.0 or 7.0) was used.

### ***Agrobacterium*-mediated T-DNA insertional mutagenesis**

The *Agrobacterium*-mediated cryptococcal transformation was carried out as described previously<sup>58</sup>. Briefly, engineered *Agrobacterium* cells that carry a Ti plasmid with the hygromycin resistant marker were co-incubated with the recipient *Cryptococcus* cells (P<sub>CTR4</sub>-*mCherryZNF2-NEO*, *znf2::NAT*) on the induction medium at 22°C for 2 days. The *Cryptococcus*-*Agrobacterium* cocultures were collected, diluted, and transferred onto the selection medium (with 50μM of BCS) that would induce *ZNF2* expression. Cryptococcal

transformants were cultured on this selective medium for 3-5 days at 22°C in dark.

Approximately 500 colonies grew on each selective plate and about 88,000 transformants were screened for smooth yeast colonies.

### **Insertion site identification in the selected AMT mutants**

Genomic DNA of the selected mutants was prepared with the CTAB DNA extraction protocol as described previously<sup>59</sup>. The genomic DNA for each individual strain was then pooled together with equal-molar concentration and the pooled DNA was sent for sequencing (Illumina MiSeq, 175bp x175bp, paired end reads, BioProject accession number: PRJNA534125, SRA: SRR8943502). The insertion sites in the mutants were identified via the AIMHII program developed by Esher et.al with default parameters<sup>29</sup>.

### **Gene deletion, gene overexpression, and protein tagging**

The gene knockout constructs were constructed by fusing 5' and 3' homologous arms (each about 1kb) with dominant drug marker via overlap PCRs as previously described<sup>60</sup>. The constructs were introduced into cryptococcal cells by biolistic transformation or by TRACE (Transient CRISPR-Cas9 Coupled with Electroporation) as described previously<sup>61,62</sup>. Single guide RNAs were designed with Eukaryotic Pathogen CRISPR guide RNA/DNA Design Tool (<http://grna.ctegd.uga.edu/>) for TRACE.

To generate gene overexpression strains, the ORF amplicon with added *FseI* and *AsiSI* cutting sites was digested and ligated into the vectors where the ORF was placed downstream of the *GPD1*, the *TEF1*, or the *CTR4-2* promoter, as we described previously<sup>48</sup>. A fluorescent tag (tdTomato or mNeonGreen) or a CBP-2xFLAG tag was placed immediately in frame downstream of the *AsiSI* cutting site, which allows in frame tagging of the protein at the C-terminus. *ZNF2* ORF was ligated into a vector where a 3xFLAG tag was downstream of the

*CTR4* promoter to allow tagging at the N-terminus. The functionality of the tagged proteins was confirmed by their ability to rescue/restore the phenotypes in the corresponding gene deletion strains. All constructed plasmids used in this study are listed in Table S4.7. All the primers used for constructing or confirming gene deletion, gene overexpression, or protein tagging are listed in Table S4.8.

### **Phenotypic assays**

For phenotypic analyses, cells of the tested strains were cultured in YPD broth overnight at 30°C with shaking at 230rpm. Cells were collected by centrifugation, washed twice with sterile water, and then suspended with water to the same optical density at 600nm ( $OD_{600}=3$ ). Three microliters of cell suspension and 10x serial dilutions were spotted onto YPD agar medium or YPD with the supplement of Congo Red (0.3-0.5%) and were incubated at 30°C or 37°C for 1-2 days. To test carbon source utilization, glucose in the YNB medium was replaced by either sucrose or raffinose (final concentration: 2%).

To test the ability of these strains to undergo self-filamentation, 3 $\mu$ L of cells with  $OD_{600}=3$  were spotted onto V8 or V8+500 $\mu$ M  $Cu^{2+}$  medium and incubated at 22°C in dark for 2-10 days. To examine filamentation during bisexual mating, equal number of cells of compatible mating types were mixed, spotted onto V8 agar medium (pH 5 for mating assay of serotype A strains, and pH 7 for mating assay of serotype D strains) and incubated at 22°C in dark for 1-7 days.

For strains that use the *CTR4-2* inducible promoter to drive the expression of the examined genes, cells were maintained on YPD medium with 50 $\mu$ M  $CuSO_4$  to suppress the gene expression. To induce the gene expression, the copper chelator BCS was supplemented to the medium with the final concentration of 200 $\mu$ M in YPD and 50 $\mu$ M in V8.

## Cell growth assay

Cryptococcal cells from overnight culture in YPD broth were centrifuged, washed twice with water, and resuspended in water. The cell concentration was normalized to the optical density of  $OD_{600}=1$ . Fifty microliters of each strain were added to 950 $\mu$ L of the indicated liquid medium in 24 well plate (#353047, Falcon). The growth of the cryptococcal strains (each with 2 replicates) were monitored at  $OD_{600}$  hourly in the Cytation 5 multi-mode reader (BioTek Instrument) with double orbit shaking (at 365 cpm) at 30°C. The reads for each well were fitted to a preloaded logistic model ( $y = \frac{A1-A2}{1+(\frac{x}{x_0})^p} + A2$ ) in Origin software and the curated reads were simulated and graphed in the GraphPad Prism software.

## Mating, genetic crosses, and cell fusion assays

Strains of  $\alpha$  and **a** mating partners were crossed on V8 juice agar medium (pH 5 or 7) and incubated at 22°C in dark for 2-3 weeks until adequate spores were produced. Spores were micro-manipulated using a dissecting microscope. The mating type of the germinated spores was determined by successful mating with either JEC20**a** or JEC21 $\alpha$  reference strain. Genetic linkage between the presence of the drug marker and the observed mutant phenotype was established by analyzing the dissected spores as we described previously<sup>63</sup>. For each genetic linkage assay, approximately 32 viable spores were analyzed, which gave a 97% confidence level of our analysis (confidence = 100% -  $(\frac{1}{2})^{\log_2 \#of\ spores}$ ).

To analyze the genetic relationship between Znf2 and Brf1, we crossed *brf1::NAT/ P<sub>TEF1</sub>BRF1-CBP-2xFLAG-NEO* ( $\alpha$ ) with *znf2::NAT/ P<sub>CTR4-2</sub>3xFLAG-ZNF2-NEO* (**a**) and examined the segregation of the genotypes (by diagnostic PCRs) and phenotypes in the progeny (Figure 4A).

To determine the cell-cell fusion efficiency, mutants of the mating type  $\alpha$  (*znf2::NAT*; *mat2::NAT*; *brf1::NAT*; and *snf5::NAT*) and the control strain (*prf1::NAT*) were collected and suspended in water to the same optical density (the calculated  $OD_{600}=0.3 \times 10$ ). Each mutant with  $NAT^R$  was mixed with the mating type **a** tester strain with  $NEO^R$  marker (strain YSB133) with equal volume<sup>64</sup>. Three microliters of cell mixture were spotted onto V8 medium and incubated at 22°C in dark for 24 hours before they were collected, plated (in serial dilution) onto YPD+NEO+NAT agar medium, and incubated at 30°C for 3-5 days to select for fusion products.

### Databases and online tools

We used FungiDB (<http://fungidb.org/fungidb/>) to acquire the gene/protein sequences or the normalized FPKM data of *C. neoformans* H99 genes, *S. cerevisiae* genes and genes in other fungi. Clustal Omega (<https://www.ebi.ac.uk/Tools/msa/clustalo/>) was used for protein multiple sequence alignment and phylogenetic tree analysis. The gene tree of *BRF1* (*CNA02310*) was retrieved from the Ensembl Fungi database (<https://fungi.ensembl.org/index.html>). Simple modular architecture research tool (SMART, <http://smart.embl-heidelberg.de/>) online server was used to analyze the domain layouts for proteins. IBS online illustrator tool (<http://ibs.biocuckoo.org/online.php>) was used to illustrate all the protein domain layouts<sup>65</sup>.

### RNA extraction and RNA-seq

RNAs were extracted from cells cultured on V8 medium at 22°C in dark for 24 hours and prepared for sequencing as previously described<sup>22, 23, 66</sup>. HiSeq Rapid 175bp pair-end RNA sequencing was performed at the Georgia genome sequencing facility. The low-quality bases of the raw reads were trimmed with a custom perl script as published before<sup>66</sup>. Tophat2 was used to map the processed reads to the reference genome. The program HTSeq-count and DESeq2 were used to count the reads and identify the differentially expressed genes. The raw sequencing reads

were deposited at NCBI with the BioProject accession number PRJNA534125, and SRA file numbers from SRR8947060 to SRR8947075.

### **Co-Immunoprecipitation**

Strains with tagged proteins were cultured in 15mL YPD media overnight, washed twice with cold water, flash frozen in liquid nitrogen, and lyophilized. Lyophilized cells were broken into fine powder with silica beads in a Bullet Blender Blue<sup>®</sup> (Next Advance) without buffer for 5 cycles (60s maximum blending followed by 90s chilling on ice) and then with 1mL of lysis buffer (50mM Tris HCl pH 8.0, 150 mM NaCl, 1mM EDTA, 5mM MgCl<sub>2</sub>, 1mM DTT, 10% glycerol, 0.5mM PMSF and cocktail protease inhibitors (#A32963, ThermoFisher)) for another 5 cycles. Cell lysates were centrifuged at x500g at 4°C for 5mins. The supernatant was collected and centrifuged again at x10000g at 4°C for 20 minutes. The supernatant was then incubated with pre-washed anti-FLAG M2 agarose beads (#F2426, Sigma) at 4°C on rotator overnight. For immunoprecipitation with mCherry or mNeonGreen tagged proteins, RFP-Trap<sup>®</sup>\_MA or mNeonGreen-Trap\_MA beads from Chromotek (Germany) were used following the manufacturer's instructions.

After washing, immunoprecipitated protein samples were released from beads in the 2xSDS loading buffer (120mM Tris-HCl pH6.8, 20% Glycerol, 4% SDS, 0.04% bromophenol blue, and 10% β-mercaptoethanol) by boiling for 10 minutes. Co-IP protein samples were then loaded into pre-casted 4-12% SurePAGE<sup>™</sup> Bis-Tris Gel (GeneScript), ran for 5minutes and visualized by Coomassie Blue staining. The total pulled down protein samples were excised from the gel and sent to the proteomics and mass spectrometry facility (<https://pams.uga.edu/>) at the University of Georgia for identification.

## Chromatin immunoprecipitation and qPCR

FLAG tagged Znf2 strains (strain JL653 and JL665) (initial OD<sub>600</sub>=0.2) were incubated in 50mL YPD+BCS broth at 30°C until the optical density reached OD<sub>600</sub>=1. Cells were then fixed in the medium with formaldehyde at 1% final concentration at 22°C for 15 minutes with occasional swirling. Glycine with the final concentration of 0.125M was added to quench the crosslinking at 22°C for 5 minutes. The cells were then washed twice with cold sterile water and lyophilized. Lyophilized cells were broken as described above for Co-IP experiment with a different lysis buffer (50mM HEPES-KOH pH 7.5, 140mM NaCl, 1mM EDTA, 1% Triton X-100, 0.1% NaDOC, 1mM of PMSF and proteinase inhibitor cocktail). The following steps were similar to what has been described previously<sup>49, 67, 68, 69</sup> and Briefly, the cell lysates were centrifuged at 8000 rpm at 4°C for 10 mins to enrich nuclei. The released nuclei were resuspended in 350uL of lysis buffer. The nuclear suspensions were sheared by sonication in a Diagenode Bioruptor™ for 25 cycles at 4°C (30s on, 30s off; cycle numbers varied). Protein-chromatin complex were recovered from the supernatant after centrifugation at 14000 rpm at 4°C for 10 mins and the volume was brought to 1mL. 50uL of each protein-chromatin suspension was saved as “Input DNA”. The rest of the sample was added to 30uL anti-FLAG M2 monoclonal antibodies on magnetic beads (#M8823, Sigma) to precipitate the FLAG tagged protein. After incubation with antibodies at 4°C overnight, the beads were washed twice with 1mL ChIP lysis buffer, once in 1mL ChIP lysis buffer containing 0.5M NaCl, once in 1mL ChIP wash buffer (10mM Tris-HCl, pH 8.0; 0.25M LiCl; 0.5% NP-40; 0.5% NaDOC; 1mM EDTA), and once in 1mL TE (10mM Tris-HCl, pH 8.0; 1mM EDTA), all at 4°C. The immunoprecipitated Znf2-3xFLAG was eluted twice by adding 200 μL of TES buffer (10mM Tris-HCl, pH 8.0; 10mM EDTA; 1% SDS) and incubated at 75°C for 15 min before the

supernatant was transferred to a new tube. 20 $\mu$ L of 5M NaCl was added to each sample to de-crosslink at 65°C for 4 hours. 350 $\mu$ L of TES was added to each “Input DNA” sample before adding 20 $\mu$ L of 5M NaCl to reverse formaldehyde crosslinks. 1 $\mu$ L of RNAse A (10 $\mu$ g/ $\mu$ L) was added and the sample was incubated at 37°C for 30 minutes. 4 $\mu$ L of Proteinase K (20 $\mu$ g/ $\mu$ L) was then added to each sample and incubated at 45°C for at least one hour to digest all the proteins. Eventually, 2 $\mu$ L of glycogen (molecular level, 20mg/mL) was added to chromatin DNA samples. Ethanol of 2.5 volumes was added to each sample to precipitate the glycogen tangled DNA. Precipitated DNA sample was then suspended in 80 $\mu$ L of nuclease free water.

For ChIP-qPCR, 3 $\mu$ L of 5 times diluted DNA sample and 1 $\mu$ L each from two primers (50 $\mu$ M) were added to 5 $\mu$ L of SYBR Green 2x qPCR premix reagents (Invitrogen). The qPCR was carried out in a Realplex system (Eppendorf). The % Input is calculated as  $2^{-\Delta C_t [\text{normalized ChIP}]}$  where  $\Delta C_t [\text{normalized ChIP}] = C_t [\text{ChIP}] - (C_t [\text{Input}] - \log_2^{\text{(Input Dilution Factor)}})$  as described previously<sup>69</sup>.

### **ATAC-seq and data analysis**

*C. neoformans* cells were cultured in 15mL YPD liquid media at 30°C overnight or on V8 medium (pH 7) at 22°C in dark for 24 hours. Cells were collected and washed 2 times with cold sterile water. 500 $\mu$ L of cold lysis buffer (15mM Tris pH 7.5; 2mM EDTA; 0.5mM spermine; 80mM KCl; 20mM NaCl; 15mM (or 0.1% v/v)  $\beta$ -me; 0.3% TritonX-100) and 200 $\mu$ L (~1 PCR tube) of acid washed glass beads (0.5mm, #9831 RPI) were added to the cell pellet of about 10<sup>8</sup> cells in 1.7mL Eppendorf tubes. Cells were broken in a cell disruptor (Scientific Industries, Inc., SI-D238) at 4°C with maximum speed for 2 minutes and then spun down at x50g at 4°C for 2 minutes to remove the glass beads. Supernatant was transferred into a new Eppendorf tube and spun at x200g for another 2 minutes to remove most of the broken cells and

debris. The enrichment of nuclei in the supernatant was verified by microscopic observation and the nuclei was collected for making the ATAC-seq library.

ATAC-seq libraries were generated as described previously<sup>70</sup>. Briefly, about 0.2 million nuclei were incubated with Tn5 transposase pre-loaded with Illumina sequencing adapters at 37°C for 30 minutes followed by purification of the DNA fragments by a reaction cleanup kit (Qiagen, # 28204). Libraries were PCR amplified for 10 cycles with Phusion polymerase (ThermoFisher Scientific, # F530L). Sequencing libraries were then cleaned with magnetic beads to remove free adapters and primer dimers (Beckman Coulter, #A63880). Libraries were mixed in equimolar ratios and pair-end sequenced by the Georgia Genomics Facility (UGA) on an Illumina NextSeq500 platform.

ATAC-seq reads were filtered for low-quality and short reads with Trim Galore (<https://github.com/FelixKrueger/TrimGalore>). Duplicate reads were removed using Picard MarkDuplicates tool (<http://broadinstitute.github.io/picard/>). Reads were aligned to the XL280 reference genome with HISAT2 using non-spliced alignment and a maximum fragment length of 2000 bp. Peak calling was performed with MACS2 using a q-value of 0.01, extension size of 73, and shifting reads by 37 bp to center on the insertion site. MACS2 was also used to call differential peaks<sup>71</sup>. Differential peak files were first sorted by log<sub>10</sub> likelihood and then combined into a single file. Heatmaps were generated using deepTools with the differential peaks<sup>72</sup>. Heatmap matrices were scaled appropriately to WT cells on V8 medium to bring all samples to a comparable scale for analysis. Differential peaks from ATAC-seq were compared to genes identified as being up-regulated in WT V8 from RNA-seq analysis using BEDTools<sup>73</sup> intersect to isolate these genes from the XL280 annotation file for determining genes associated with differential peaks. The BioProject accession number PRJNA534125.

## **Data Accessibility**

All data supporting the findings of the current study are available within the article and its Supplementary Information files or from the corresponding author upon request. All RNA-seq, ATAC-seq and DNA-seq data has been deposited in NCBI under the BioProject accession number PRJNA534125.

## **Funding**

This work was supported by National Institutes of Health (R01AI140719 to XL and R01GM132644 to ZL), the American Cancer Society (RSG-14-184-01-DMC to ZL), NSF GRFP (NSF# 1443117 to AF), and the University of Georgia (startup fund to XL). Dr. Lin holds an Investigator Award in the Pathogenesis of Infectious Disease from the Burroughs Wellcome Fund (1012445). The funders had no role in study design, data collection and interpretation, or the decision to submit the work for publication.

## **Acknowledgement**

We thank Dr. Karl Lehtreck from Department of Cellular Biology at UGA for the kind gift of the mNeonGreen plasmid, Dr. Chau-wen Chou at the UGA proteomics and mass spectrometry facility (<https://pams.uga.edu/>) for the mass spectrometry analysis of our Co-IP samples, Brigitte Hofmeister and Dr. Bob Schmitz in Department of Genetics of UGA for the generous help on ATAC-seq experiments, and Lin lab members for their helpful comments.

## References

1. Clapier CR, Iwasa J, Cairns BR, Peterson CL. Mechanisms of action and regulation of ATP-dependent chromatin-remodelling complexes. *Nat Rev Mol Cell Bio* **18**, 407-422 (2017).
2. Kadoch C, *et al.* Proteomic and bioinformatic analysis of mammalian SWI/SNF complexes identifies extensive roles in human malignancy. *Nat Genet* **45**, 592-601 (2013).
3. Mohrmann L, Verrijzer CP. Composition and functional specificity of SWI2/SNF2 class chromatin remodeling complexes. *Biochim Biophys Acta* **1681**, 59-73 (2005).
4. Tang L, Nogales E, Ciferri C. Structure and function of SWI/SNF chromatin remodeling complexes and mechanistic implications for transcription. *Prog Biophys Mol Biol* **102**, 122-128 (2010).
5. Mashtalir N, *et al.* Modular Organization and Assembly of SWI/SNF Family Chromatin Remodeling Complexes. *Cell* **175**, 1272-1288 e1220 (2018).
6. Monahan BJ, Villen J, Marguerat S, Bahler J, Gygi SP, Winston F. Fission yeast SWI/SNF and RSC complexes show compositional and functional differences from budding yeast. *Nature Structural & Molecular Biology* **15**, 873-880 (2008).
7. Vignali M, Hassan AH, Neely KE, Workman JL. ATP-dependent chromatin-remodeling complexes. *Molecular and cellular biology* **20**, 1899-1910 (2000).
8. Wang X, Hsueh YP, Li W, Floyd A, Skalsky R, Heitman J. Sex-induced silencing defends the genome of *Cryptococcus neoformans* via RNAi. *Genes Dev* **24**, 2566-2582 (2010).
9. Feretzaki M, Billmyre RB, Clancey SA, Wang X, Heitman J. Gene Network Polymorphism Illuminates Loss and Retention of Novel RNAi Silencing Components in the *Cryptococcus* Pathogenic Species Complex. *PLoS genetics* **12**, e1005868 (2016).

10. Loftus BJ, *et al.* The genome of the basidiomycetous yeast and human pathogen *Cryptococcus neoformans*. *Science* **307**, 1321-1324 (2005).
11. Janbon G, *et al.* Analysis of the genome and transcriptome of *Cryptococcus neoformans* var. *grubii* reveals complex RNA expression and microevolution leading to virulence attenuation. *PLoS genetics* **10**, e1004261 (2014).
12. Catania S, *et al.* Epigenetic maintenance of DNA methylation after evolutionary loss of the *de novo* methyltransferase. *bioRxiv*, 149385 (2017).
13. Zhao Y, Lin J, Fan Y, Lin X. Life Cycle of *Cryptococcus neoformans*. *Annual review of microbiology* **73**, (2019).
14. Velagapudi R, Hsueh YP, Geunes-Boyer S, Wright JR, Heitman J. Spores as infectious propagules of *Cryptococcus neoformans*. *Infection and immunity* **77**, 4345-4355 (2009).
15. Giles SS, Dagenais TR, Botts MR, Keller NP, Hull CM. Elucidating the pathogenesis of spores from the human fungal pathogen *Cryptococcus neoformans*. *Infection and immunity* **77**, 3491-3500 (2009).
16. Okagaki LH, Nielsen K. Titan cells confer protection from phagocytosis in *Cryptococcus neoformans* infections. *Eukaryotic cell* **11**, 820-826 (2012).
17. Zaragoza O, Nielsen K. Titan cells in *Cryptococcus neoformans*: cells with a giant impact. *Current opinion in microbiology* **16**, 409-413 (2013).
18. Goldman DL, Fries BC, Franzot SP, Montella L, Casadevall A. Phenotypic switching in the human pathogenic fungus *Cryptococcus neoformans* is associated with changes in virulence and pulmonary inflammatory response in rodents. *Proceedings of the National Academy of Sciences of the United States of America* **95**, 14967-14972 (1998).
19. Lin X, Jackson JC, Feretzaki M, Xue C, Heitman J. Transcription factors Mat2 and Znf2

- operate cellular circuits orchestrating opposite- and same-sex mating in *Cryptococcus neoformans*. *PLoS genetics* **6**, e1000953 (2010).
20. Lin J, Idnurm A, Lin X. Morphology and its underlying genetic regulation impact the interaction between *Cryptococcus neoformans* and its hosts. *Med Mycol* **53**, 493-504 (2015).
  21. Lin XR, Hull CM, Heitman J. Sexual reproduction between partners of the same mating type in *Cryptococcus neoformans*. *Nature* **434**, 1017-1021 (2005).
  22. Gyawali R, *et al.* Pheromone independent unisexual development in *Cryptococcus neoformans*. *PLoS genetics* **13**, e1006772 (2017).
  23. Xu X, *et al.* Glucosamine stimulates pheromone-independent dimorphic transition in *Cryptococcus neoformans* by promoting Crz1 nuclear translocation. *PLoS genetics* **13**, e1006982 (2017).
  24. Wang L, Zhai B, Lin X. The link between morphotype transition and virulence in *Cryptococcus neoformans*. *PLoS pathogens* **8**, e1002765 (2012).
  25. Neigeborn L, Carlson M. Genes affecting the regulation of *SUC2* gene expression by glucose repression in *Saccharomyces cerevisiae*. *Genetics* **108**, 845-858 (1984).
  26. Stern M, Jensen R, Herskowitz I. Five SWI genes are required for expression of the *HO* gene in yeast. *J Mol Biol* **178**, 853-868 (1984).
  27. Chacko N, Zhao Y, Yang E, Wang L, Cai JJ, Lin X. The lncRNA *RZE1* Controls Cryptococcal Morphological Transition. *PLoS genetics* **11**, e1005692 (2015).
  28. Walton FJ, Idnurm A, Heitman J. Novel gene functions required for melanization of the human pathogen *Cryptococcus neoformans*. *Molecular microbiology* **57**, 1381-1396 (2005).

29. Esher SK, Granek JA, Alspaugh JA. Rapid mapping of insertional mutations to probe cell wall regulation in *Cryptococcus neoformans*. *Fungal genetics and biology : FG & B* **82**, 9-21 (2015).
30. Smith RL, Johnson AD. Turning genes off by Ssn6-Tup1: a conserved system of transcriptional repression in eukaryotes. *Trends Biochem Sci* **25**, 325-330 (2000).
31. Mao XM, Cao F, Nie XY, Liu HP, Chen JY. The Swi/Snf chromatin remodeling complex is essential for hyphal development in *Candida albicans*. *Febs Lett* **580**, 2615-2622 (2006).
32. Mao X, Li Y, Wang H, Cao F, Chen J. Antagonistic interplay of Swi1 and Tup1 on filamentous growth of *Candida albicans*. *FEMS microbiology letters* **285**, 233-241 (2008).
33. Mao X, Nie X, Cao F, Chen J. Functional analysis of ScSwi1 and CaSwi1 in invasive and pseudohyphal growth of *Saccharomyces cerevisiae*. *Acta Biochim Biophys Sin (Shanghai)* **41**, 594-602 (2009).
34. Ando Y, Nakazawa T, Oka K, Nakahori K, Kamada T. *Cc.snf5*, a gene encoding a putative component of the SWI/SNF chromatin remodeling complex, is essential for sexual development in the agaricomycete *Coprinopsis cinerea*. *Fungal genetics and biology : FG & B* **50**, 82-89 (2013).
35. Nakazawa T, Ando Y, Hata T, Nakahori K. A mutation in the *Cc.arp9* gene encoding a putative actin-related protein causes defects in fruiting initiation and asexual development in the agaricomycete *Coprinopsis cinerea*. *Current genetics* **62**, 565-574 (2016).
36. Venkataramanan S, Douglass S, Galivanche AR, Johnson TL. The chromatin remodeling complex Swi/Snf regulates splicing of meiotic transcripts in *Saccharomyces cerevisiae*.

- Nucleic Acids Res* **45**, 7708-7721 (2017).
37. Breker M, Gymrek M, Schuldiner M. A novel single-cell screening platform reveals proteome plasticity during yeast stress responses. *J Cell Biol* **200**, 839-850 (2013).
  38. Dallas PB, Pacchione S, Wilsker D, Bowrin V, Kobayashi R, Moran E. The human SWI-SNF complex protein p270 is an ARID family member with non-sequence-specific DNA binding activity. *Molecular and cellular biology* **20**, 3137-3146 (2000).
  39. Chandler RL, Brennan J, Schisler JC, Serber D, Patterson C, Magnuson T. ARID1a-DNA interactions are required for promoter occupancy by SWI/SNF. *Molecular and cellular biology* **33**, 265-280 (2013).
  40. Wilsker D, *et al.* The DNA-binding properties of the ARID-containing subunits of yeast and mammalian SWI/SNF complexes. *Nucleic Acids Res* **32**, 1345-1353 (2004).
  41. Kelliher CM, Leman AR, Sierra CS, Haase SB. Investigating Conservation of the Cell-Cycle-Regulated Transcriptional Program in the Fungal Pathogen, *Cryptococcus neoformans*. *PLoS genetics* **12**, e1006453 (2016).
  42. Dutta A, *et al.* Composition and Function of Mutant Swi/Snf Complexes. *Cell Rep* **18**, 2124-2134 (2017).
  43. Sen P, *et al.* Loss of Snf5 Induces Formation of an Aberrant SWI/SNF Complex. *Cell Rep* **18**, 2135-2147 (2017).
  44. Cairns BR, *et al.* RSC, an essential, abundant chromatin-remodeling complex. *Cell* **87**, 1249-1260 (1996).
  45. Cao YX, Cairns BR, Kornberg RD, Laurent BC. Sfh1p, a component of a novel chromatin-remodeling complex, is required for cell cycle progression. *Molecular and cellular biology* **17**, 3323-3334 (1997).

46. Buenrostro JD, Wu B, Chang HY, Greenleaf WJ. ATAC-seq: A Method for Assaying Chromatin Accessibility Genome-Wide. *Curr Protoc Mol Biol* **109**, 21 29 21-29 (2015).
47. Buenrostro JD, Giresi PG, Zaba LC, Chang HY, Greenleaf WJ. Transposition of native chromatin for fast and sensitive epigenomic profiling of open chromatin, DNA-binding proteins and nucleosome position. *Nat Methods* **10**, 1213-1218 (2013).
48. Wang L, *et al.* Morphotype transition and sexual reproduction are genetically associated in a ubiquitous environmental pathogen. *PLoS pathogens* **10**, e1004185 (2014).
49. Tian XY, *et al.* *Cryptococcus neoformans* sexual reproduction is controlled by a quorum sensing peptide. *Nat Microbiol* **3**, 698-707 (2018).
50. Burns LG, Peterson CL. The yeast SWI-SNF complex facilitates binding of a transcriptional activator to nucleosomal sites *in vivo*. *Molecular and cellular biology* **17**, 4811-4819 (1997).
51. Wallberg AE, Neely KE, Hassan AH, Gustafsson JA, Workman JL, Wright APH. Recruitment of the SWI-SNF chromatin remodeling complex as a mechanism of gene activation by the glucocorticoid receptor tau 1 activation domain. *Molecular and cellular biology* **20**, 2004-2013 (2000).
52. Kim JH, Saraf A, Florens L, Washburn M, Workman JL. Gcn5 regulates the dissociation of SWI/SNF from chromatin by acetylation of Swi2/Snf2. *Genes Dev* **24**, 2766-2771 (2010).
53. Neely KE, Hassan AH, Brown CE, Howe L, Workman JL. Transcription activator interactions with multiple SWI/SNF subunits. *Molecular and cellular biology* **22**, 1615-1625 (2002).
54. Lu Y, Su C, Mao X, Raniga PP, Liu H, Chen J. Efg1-mediated recruitment of NuA4 to

- promoters is required for hypha-specific Swi/Snf binding and activation in *Candida albicans*. *Molecular biology of the cell* **19**, 4260-4272 (2008).
55. Yun M, Wu J, Workman JL, Li B. Readers of histone modifications. *Cell Res* **21**, 564-578 (2011).
  56. Monahan BJ, Villen J, Marguerat S, Bahler J, Gygi SP, Winston F. Fission yeast SWI/SNF and RSC complexes show compositional and functional differences from budding yeast. *Nat Struct Mol Biol* **15**, 873-880 (2008).
  57. Giaever G, *et al.* Functional profiling of the *Saccharomyces cerevisiae* genome. *Nature* **418**, 387-391 (2002).
  58. Idnurm A, Reedy JL, Nussbaum JC, Heitman J. *Cryptococcus neoformans* virulence gene discovery through insertional mutagenesis. *Eukaryotic cell* **3**, 420-429 (2004).
  59. Mondon P, *et al.* Heteroresistance to fluconazole and voriconazole in *Cryptococcus neoformans*. *Antimicrobial agents and chemotherapy* **43**, 1856-1861 (1999).
  60. Lin X, Chacko N, Wang L, Pavuluri Y. Generation of stable mutants and targeted gene deletion strains in *Cryptococcus neoformans* through electroporation. *Med Mycol* **53**, 225-234 (2015).
  61. Toffaletti DL, Rude TH, Johnston SA, Durack DT, Perfect JR. Gene transfer in *Cryptococcus neoformans* by use of biolistic delivery of DNA. *Journal of bacteriology* **175**, 1405-1411 (1993).
  62. Fan Y, Lin X. Multiple Applications of a Transient CRISPR-Cas9 Coupled with Electroporation (TRACE) System in the *Cryptococcus neoformans* Species Complex. *Genetics* **208**, 1357-1372 (2018).
  63. Zhai B, Zhu P, Foyle D, Upadhyay S, Idnurm A, Lin X. Congenic strains of the

- filamentous form of *Cryptococcus neoformans* for studies of fungal morphogenesis and virulence. *Infection and immunity* **81**, 2626-2637 (2013).
64. Bahn YS, Cox GM, Perfect JR, Heitman J. Carbonic anhydrase and CO<sub>2</sub> sensing during *Cryptococcus neoformans* growth, differentiation, and virulence. *Curr Biol* **15**, 2013-2020 (2005).
  65. Liu W, *et al.* IBS: an illustrator for the presentation and visualization of biological sequences. *Bioinformatics* **31**, 3359-3361 (2015).
  66. Zhao Y, Upadhyay S, Lin X. PAS Domain Protein Pas3 Interacts with the Chromatin Modifier Bre1 in Regulating Cryptococcal Morphogenesis. *MBio* **9**, (2018).
  67. Dumesic PA, *et al.* Product binding enforces the genomic specificity of a yeast polycomb repressive complex. *Cell* **160**, 204-218 (2015).
  68. Garcia-Santamarina S, *et al.* Genome-wide analysis of the regulation of Cu metabolism in *Cryptococcus neoformans*. *Molecular microbiology* **108**, 473-494 (2018).
  69. Kim TH, Dekker J. ChIP-Quantitative Polymerase Chain Reaction (ChIP-qPCR). *Cold Spring Harb Protoc* **2018**, pdb prot082628 (2018).
  70. Lu Z, Hofmeister BT, Vollmers C, DuBois RM, Schmitz RJ. Combining ATAC-seq with nuclei sorting for discovery of cis-regulatory regions in plant genomes. *Nucleic Acids Res* **45**, e41 (2017).
  71. Zhang Y, *et al.* Model-based analysis of ChIP-Seq (MACS). *Genome Biol* **9**, R137 (2008).
  72. Ramirez F, *et al.* deepTools2: a next generation web server for deep-sequencing data analysis. *Nucleic Acids Res* **44**, W160-165 (2016).
  73. Quinlan AR, Hall IM. BEDTools: a flexible suite of utilities for comparing genomic features. *Bioinformatics* **26**, 841-842 (2010).

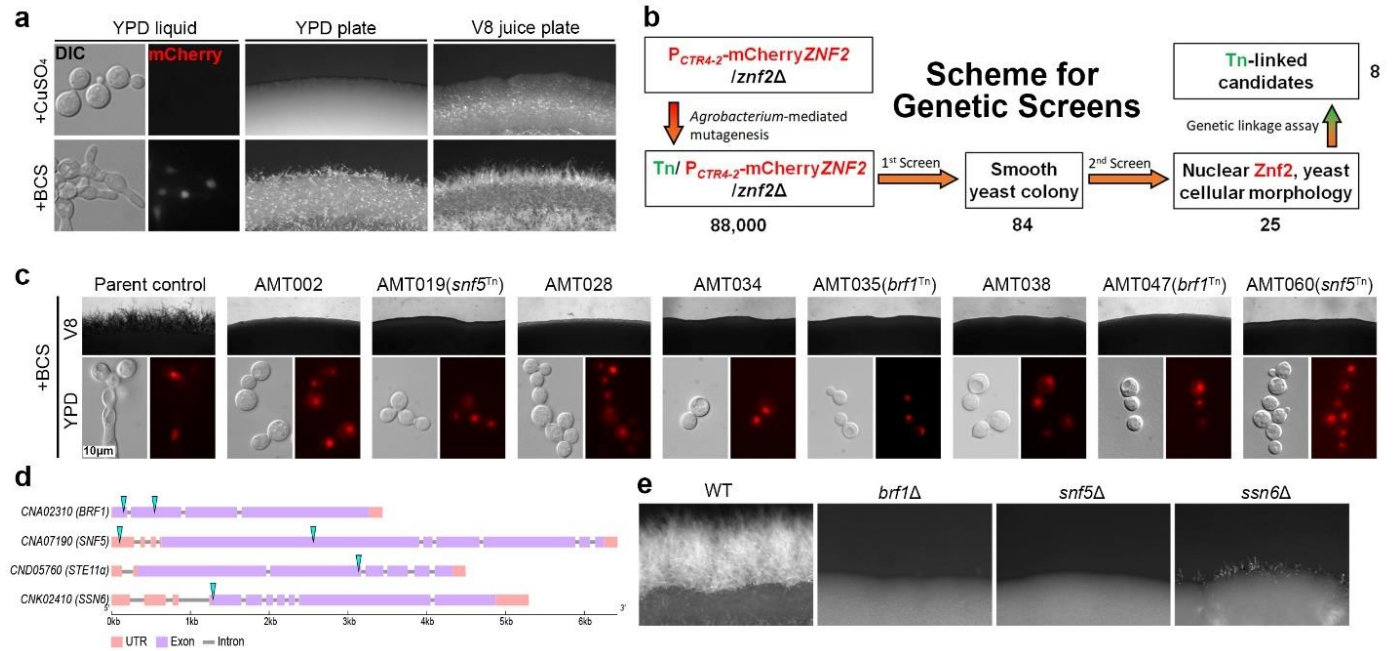


**Figure 4.1. *BRF1* and *SNF5* are essential factors for filamentation.** (a). Phenotypes of the parental reporter strain  $P_{CTR4-2}$ -mCherry-*ZNF2*/*znf2*Δ used in the forward genetic screen. The reporter strain was cultured under *Znf2*-inducing conditions (YPD+BCS liquid overnight, YPD+BCS and V8+BCS agar medium for 2 days) or *Znf2*-suppressing conditions (YPD+CuSO<sub>4</sub>, V8+CuSO<sub>4</sub>). The fluorescence signal of mCherry-*Znf2* was detected in the nucleus under inducing conditions. A fluffy colony edge reflects filamentous growth while a smooth edge reflects yeast growth. (b). The scheme for the genetic screens to identify factors important for filamentation when *Znf2* is produced and localized in the nucleus. (c). The eight selected insertional mutants were cultured on V8+BCS medium for 2 days or in YPD+BCS medium overnight. (d). The genetic loci disrupted by the T-DNA insertions with paired sequences. The cyan triangles indicate the T-DNA insertion sites. (e). WT XL280 and the independent targeted gene deletion mutants *brf1*Δ, *snf5*Δ, and *ssn6*Δ were cultured on V8 medium for 7 days.

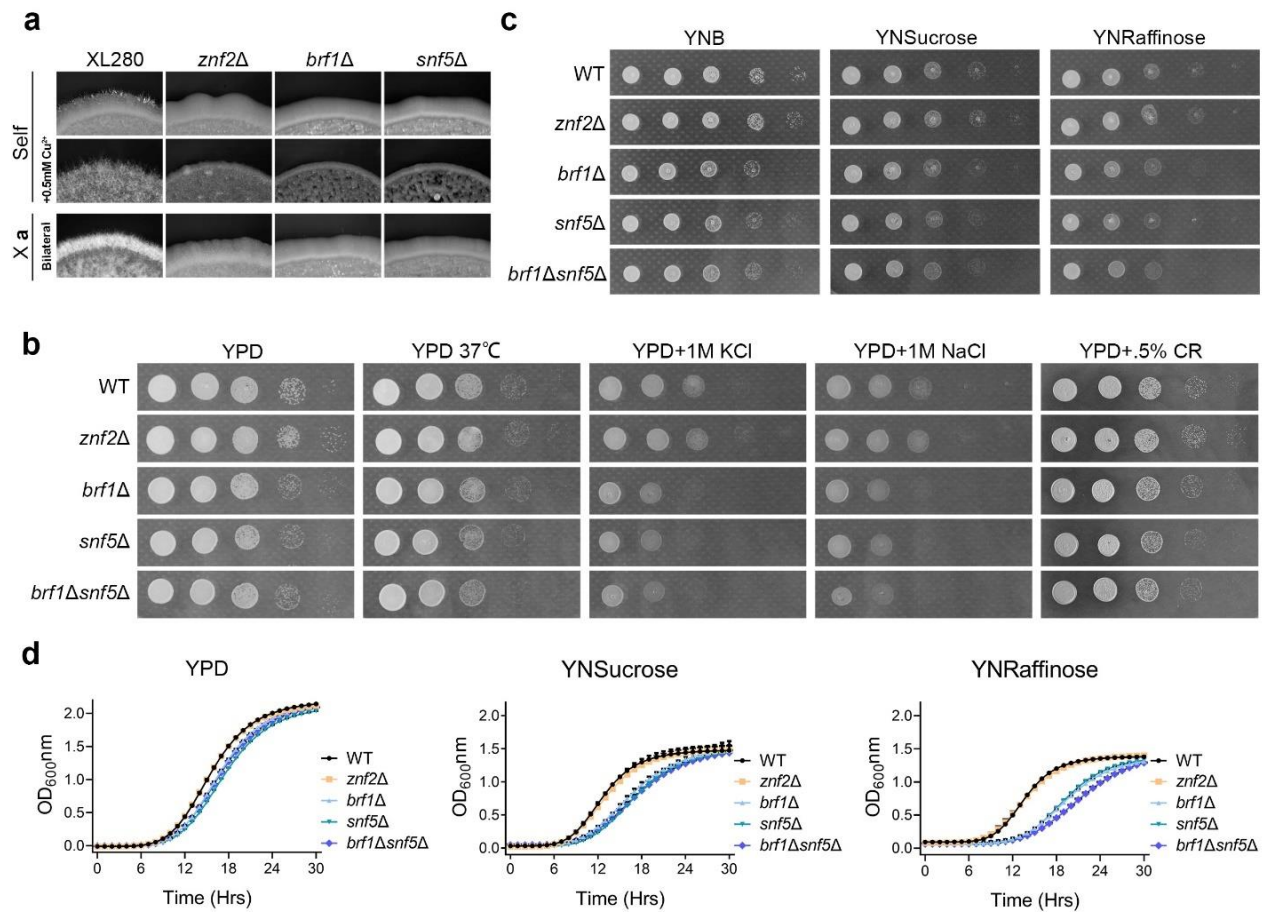


**Figure 4.2. The *brf1Δ*, *snf5Δ*, and *brf1Δsnf5Δ* mutants are phenotypically identical.** (a). WT XL280, *znf2Δ*, *brf1Δ*, and *snf5Δ* in the  $\alpha$  background were cultured on V8 or V8+500 $\mu$ M Cu<sup>2+</sup> medium (self-filamentation, upper images), or crossed with the corresponding **a** mating partners (bilateral bisexual mating, bottom images) on V8 medium in dark for 4 days. (b). WT XL280, *znf2Δ*, *brf1Δ*, *snf5Δ*, and *brf1Δsnf5Δ* strains were cultured on YPD medium at 30°C or 37°C, or with the addition of KCl, NaCl, or Congo Red. (c). WT XL280, *znf2Δ*, *brf1Δ*, *snf5Δ* and *brf1Δsnf5Δ* strains were cultured on minimal nitrogen base agar media with glucose, sucrose, or raffinose as the sole carbon source. (d). WT XL280, *znf2Δ*, *brf1Δ*, *snf5Δ*, and *brf1Δsnf5Δ* strains were cultured in YPD, YNSucrose, or YNRaffinose broth at 30°C. The optical density at 600nm was plotted against the time after inoculation.

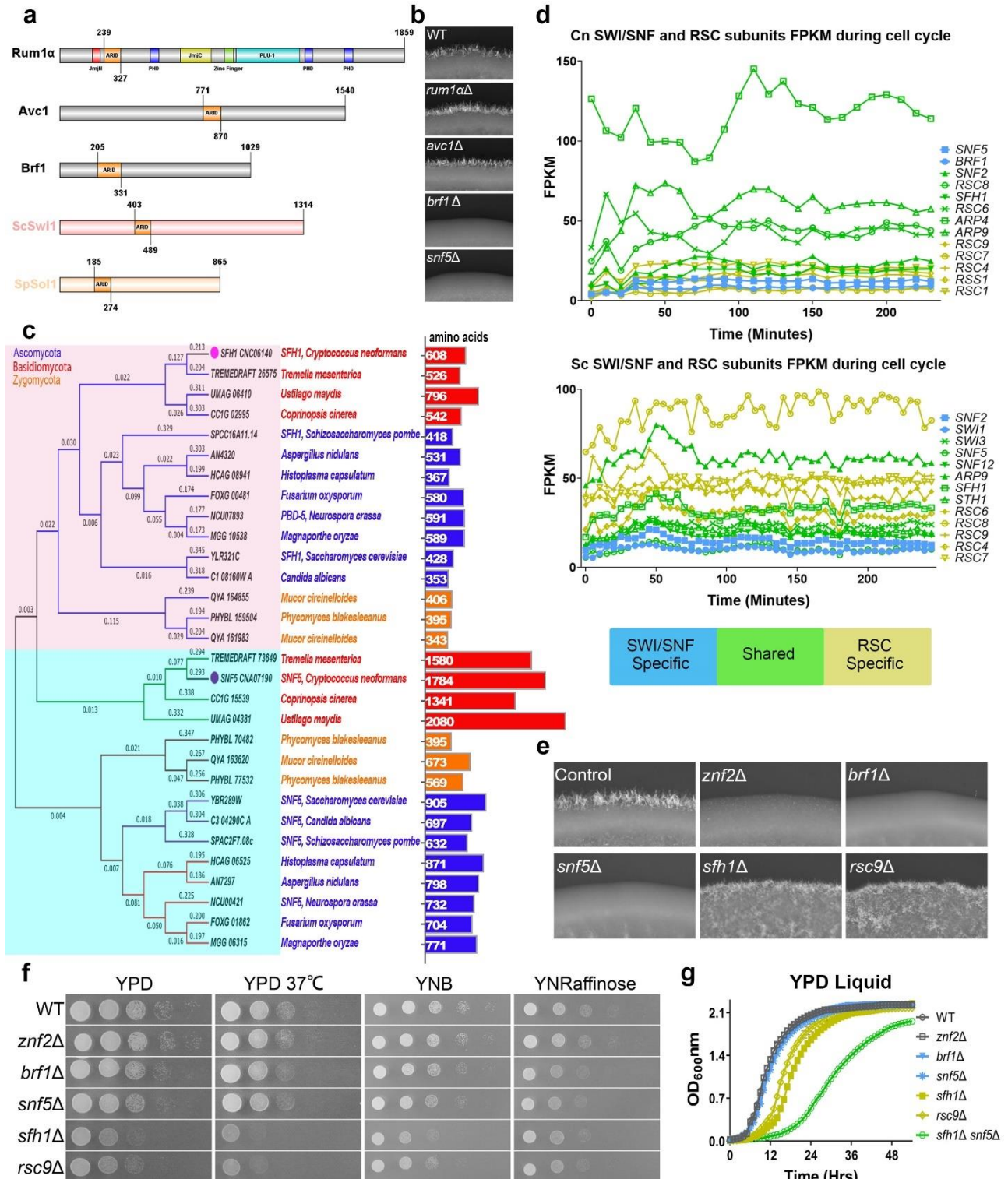


**Figure 4.3. Brf1 and Snf5 are both subunits specific to the SWI/SNF complex. (a).** Diagrams of domain organization of the three ARID-containing proteins in *C. neoformans* (Rum1 $\alpha$ , Avc1, and Brf1), and the SWI/SNF ARID-containing subunit Swi1 in *S. cerevisiae* and Sol1 in *S.*

*pombe*. **(b)**. WT XL280, *snf5* $\Delta$ , *rum1a* $\Delta$ , *avc1* $\Delta$ , and *brf1* $\Delta$  strains were cultured on V8 agar medium at 22°C in dark for 2 days. **(c)**. A phylogenetic tree of Snf5-domain containing proteins in the selected ascomycetes, basidiomycetes and zygomycetes. The number of amino acids for each protein was indicated on the right. **(d)**. The FPKM values for genes encoding the selected SWI/SNF and RSC subunits in *C. neoformans* and *S. cerevisiae* were plotted against the time across the cell cycle. The SWI/SNF-specific subunits are in blue, the RSC-specific subunits are in yellow, and the shared subunits are in green. **(e)**. WT XL280, *znf2* $\Delta$ , *brf1* $\Delta$ , *snf5* $\Delta$ , *sfh1* $\Delta$ , and *rsc9* $\Delta$  strains were cultured on V8 agar medium at 22°C in dark for 2 days. **(f)**. WT XL280, *znf2* $\Delta$ , *brf1* $\Delta$ , *snf5* $\Delta$ , *sfh1* $\Delta$ , and *rsc9* $\Delta$  strains were cultured on YPD agar medium at 30°C or at 37°C, YNB or YNRaffinose agar medium at 30°C. **(g)**. WT XL280, *znf2* $\Delta$ , *brf1* $\Delta$ , *snf5* $\Delta$ , *sfh1* $\Delta$ , *rsc9* $\Delta$ , and *snf5* $\Delta*sfh1* $\Delta$  strains were cultured in YPD broth. The optical density at OD<sub>600nm</sub> was plotted against the time after inoculation. The SWI/SNF-specific subunits are in blue and the RSC-specific subunits are in yellow.$

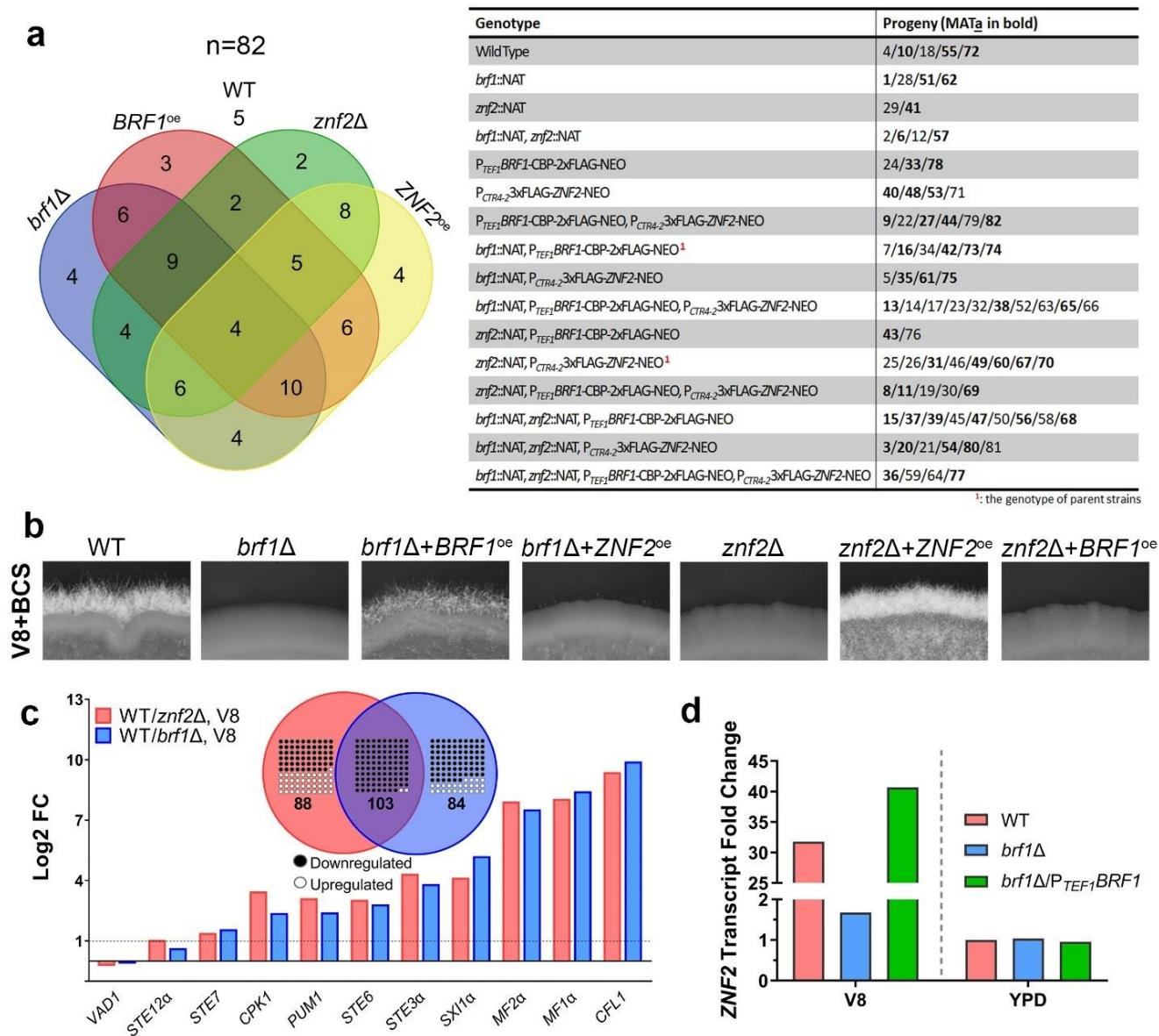


**Figure 4.4. *BRF1* is required for *ZNF2* transcription induction during hyphal differentiation.** (a). The list of the genotypes of the 82 meiotic progeny dissected from a cross between *znf2Δ/ZNF2<sup>oe</sup>* and *brf1Δ/BRF1<sup>oe</sup>* and the Venn diagram showing the number of progeny for each genotype (progeny in the mating type **a** are bolded). (b). WT XL280 and selected progeny of the following genotypes (*brf1Δ*, *brf1Δ+BRF1<sup>oe</sup>*, *brf1Δ+ZNF2<sup>oe</sup>*, *znf2Δ*, *znf2Δ+ZNF2<sup>oe</sup>*, and *znf2Δ+BRF1<sup>oe</sup>*) were cultured on V8+BCS medium (to induce *ZNF2*) at 22°C in dark for 5 days. (c). Relative transcript levels of the selected genes in the *znf2Δ* and the *brf1Δ* mutants compared to wild type cultured on V8 agar medium for 24 hours. The Venn diagram shows the number of differentially expressed genes in the *znf2Δ* and the *brf1Δ* strains with  $|\log_2^{FC}| \geq 2$ . Dots in the Venn diagram indicate the percentage of genes that were upregulated (white) or downregulated (black) in the *znf2Δ* and *brf1Δ* mutants comparing to WT. (d). The relative transcript levels of *ZNF2* in WT, *brf1Δ*, and *brf1Δ/BRF1<sup>oe</sup>* cultured on V8 agar and YPD

medium. The *ZNF2* transcript level in WT cultured on YPD medium was used for normalization and was set as 1.

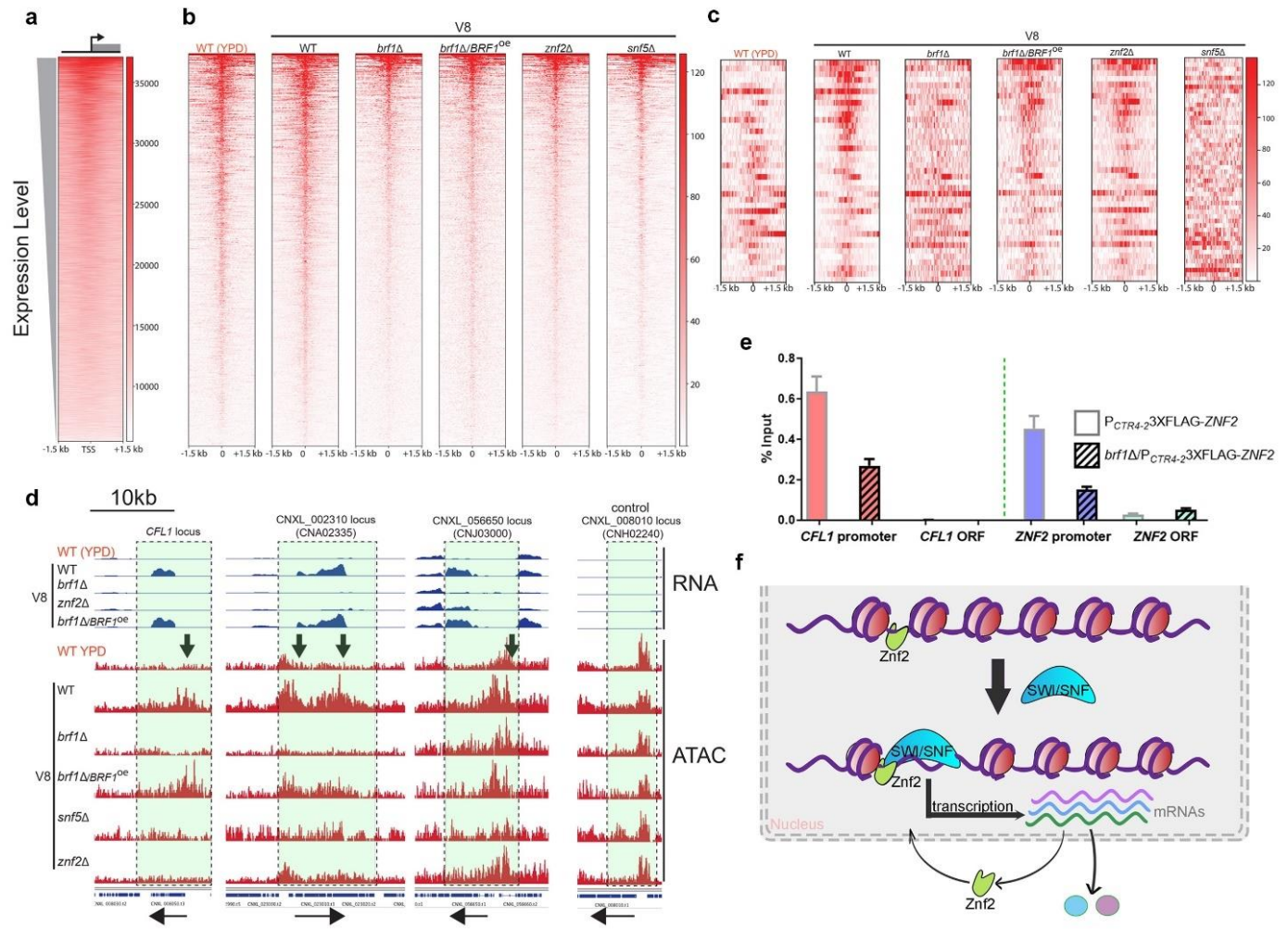


**Figure 4.5. Znf2 and the SWI/SNF complex coordinate in transcription activation of filamentation genes.** (a). The heatmap depicts relative enrichment of ATAC-seq reads from a wild type strain grown on V8 medium. It is centered on the transcription start sites (TSS) for all genes arranged from highest expression level (top) to lowest expression level (bottom). (b). Global chromatin accessibility in the tested mutants. For each indicated strain, the relative enrichment of ATAC-seq reads are shown for all ATAC-seq peaks from the wild type strain grown on V8 medium. (c). Relative enrichment of ATAC-seq reads is shown for the indicated strains across the 39 ATAC-seq peaks that exhibit differential accessibility in WT and *brf1Δ*. Peaks are ordered by the differential enrichment likelihood value generated by MACS2. (d). Genome browser images depict relative transcript levels (blue) and ATAC-seq enrichment (red) for the indicated strains (left). Images depicting three representative ATAC-seq peaks that display reduced ATAC-seq enrichment in *brf1Δ* as well as one control gene (right) that does not exhibit altered accessibility. WT grown in YPD is used as a negative control for filamentation, whereas WT grown on V8 medium is used as a positive control for filamentation. The arrows above the ATAC-seq plot indicate the location of differential accessible regions. The arrows at the bottom of the plot indicate the transcription direction. (e). ChIP-qPCR analysis of the relative

abundance of DNAs associated with Znf2 in designated strains. Cells were grown in YPD+BCS media to induce the expression of Znf2. The left panel shows the %input values with or without Brf1 at the *CFL1* promoter and the ORF region; the right panel shows the %input values at the *ZNF2* promoter and the ORF region. (f). A diagram of the working model depicting the coordination between Znf2 and the SWI/SNF complex in regulating gene transcription. Znf2 binds to its target sites at a low basal level. Upon culturing under filamentation-inducing condition, Znf2 recruits the SWI/SNF complex to its target sites to open chromatin and activate gene transcription.

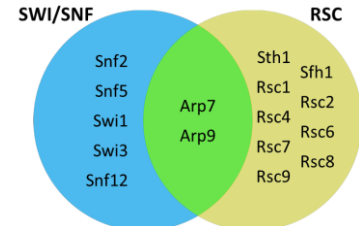
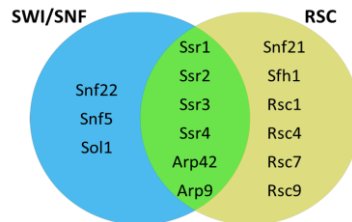
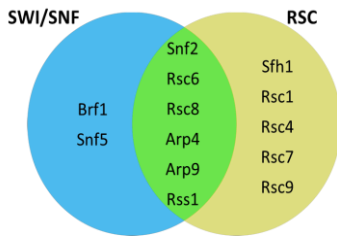
**Table 4.1.** The list of proteins identified from Co-IP/MS by Brf1-CBP-2xFLAG as bait.

Coding locus(D)	Coding locus(A)	Protein name	JL401 (strain 1)	JL402 (strain 2)
			# peptide spectrum matches	
CNE04020	CNAG_02134	Rsc8	12	20
CNK02030	CNAG_01863	Snf2	10	23
CNI00980	CNAG_04460	Arp9	8	9
CNA07190	CNAG_00740	Snf5	4	5
CND01230	CNAG_00995	Msc1	4	3
CNG02900	CNAG_03285	Rsc6	3	10
CNB05320	CNAG_04048	Arp4	3	4
CNE02000	CNAG_02350	Rss1	3	3
CNA02310	CNAG_00240	Brf1	2	6
CNA00820	CNAG_00091	N/A	2	2
CNK02620	CNAG_01920	Ubi4	2	2

**Table 4.2.** The BLAST analysis of the SWI/SNF and RSC subunits in *C. neoformans*, *S. cerevisiae* (selected subunits) and *S. pombe* (selected subunits).

<i>C. neoformans</i>		<i>S. pombe</i>		<i>S. cerevisiae</i>	
Subunit	Deletion phenotype	Subunit	Deletion phenotype	Subunit	Deletion phenotype
Snf5	viable, nonfilamentous	Snf5	viable	Snf5	viable
		Sol1	viable	Swi1	lethal/ viable *
Brf1	viable, nonfilamentous				
Snf2	viable, reduced filament	Snf22	viable	Snf2	viable
Rsc8		Ssr1	lethal	Swi3	viable
		Ssr2	lethal		
Rsc6		Ssr3	lethal/ viable *	Snf12	viable
		Ssr4	lethal/ viable *		
Arp9		Arp9	viable	Arp9	lethal or sick
				Arp7	lethal or sick
Arp4		Arp42	viable		
Rss1					
				Rsc8	lethal
				Rsc6	lethal
Snf2	viable, reduced filament	Snf21	lethal	Sth1	lethal
Sfh1	viable, filamentous	Sfh1	lethal	Sfh1	lethal
Rsc9	viable, filamentous	Rsc9	lethal	Rsc9	lethal
Rsc7		Rsc7	lethal	Rsc7	viable
Rsc1		Rsc1	viable	Rsc1	double mutant lethal
				Rsc2	
Rsc4		Rsc4	viable	Rsc4	lethal

\* the phenotype depends on strain backgrounds.



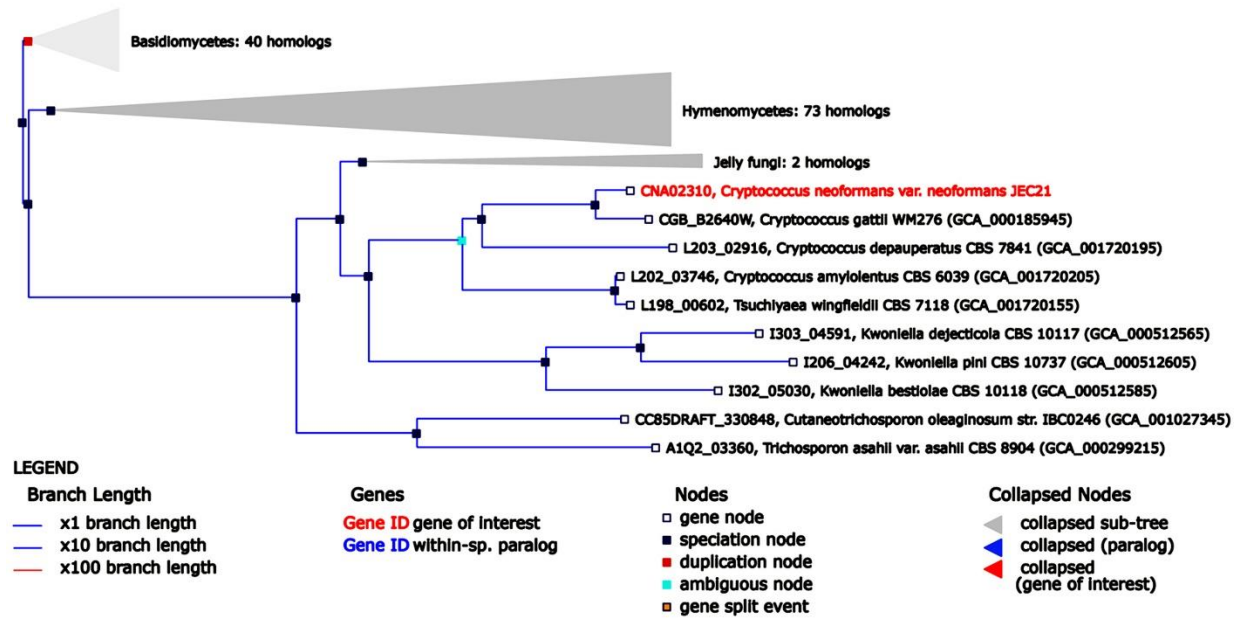


**Figure S4.1. A *BRF1* gene tree.** The gene tree was constructed on EnsemblFungi with the *BRF1* gene (gene ID *CNA02310*) as input. The gene tree was generated by the Gene Orthology/Paralogy prediction pipeline where the maximum likelihood phylogenetic gene trees (generated by TreeBeST<sup>5</sup>) play a central role.

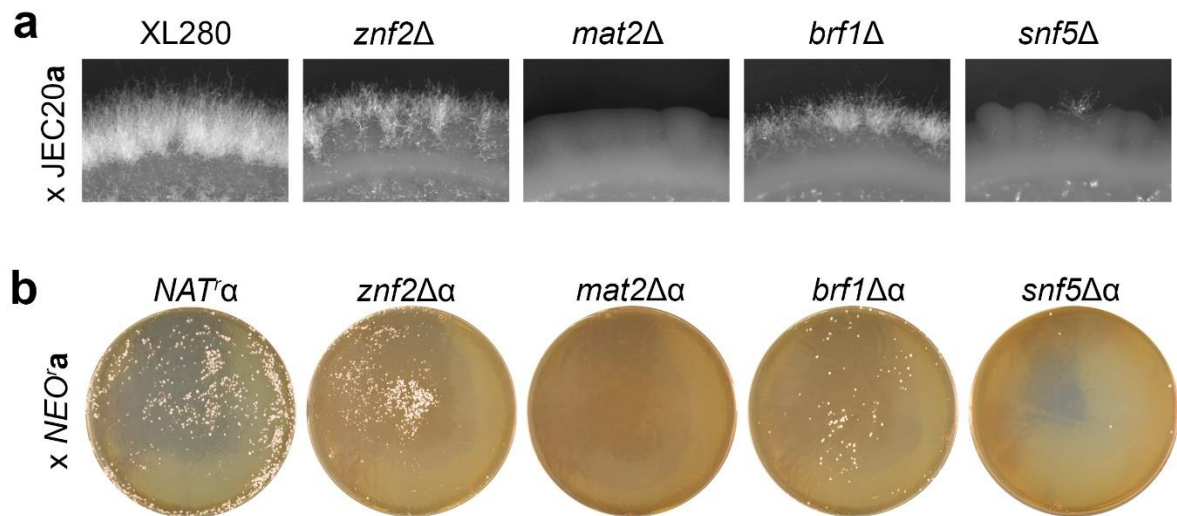


**Figure S4.2. The *brf1Δ* and *snf5Δ* strains are defective in cell fusion. (a).** WT, *znf2Δ*, *mat2Δ*, *brf1Δ*, and *snf5Δ*  $\alpha$  strains were crossed to the wild type JEC20a reference strain on V8 medium at 22°C in dark for 4 days. JEC20a is non-filamentous by itself on V8 medium. **(b).** The  $\alpha$  strains including the control XL1319, *znf2Δ*, *mat2Δ*, *brf1Δ*, and *snf5Δ* mutants with NAT<sup>R</sup> were crossed with the mating type **a** strain YSB133 with G418<sup>R</sup>. After 24 hours, the co-cultures were collected, and fusion products were selected on media supplemented with NAT and G418 drugs.

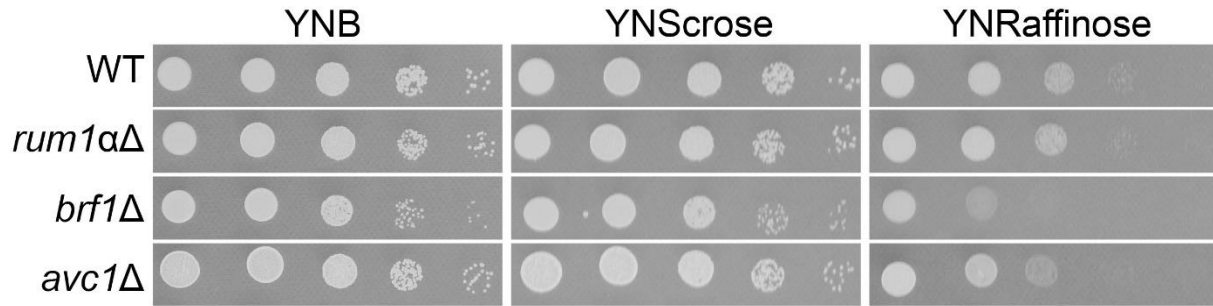


**Figure S4.3. *BRF1* is the only ARID containing gene involved in growth on raffinose medium.** The ARID containing gene deletion mutants *rum1αΔ*, *avc1Δ* and *brf1Δ* along with the WT XL280 were serial diluted and spotted onto YNB, YNSucose, and YNRaffinose media and cultured at 30°C for 1 day.

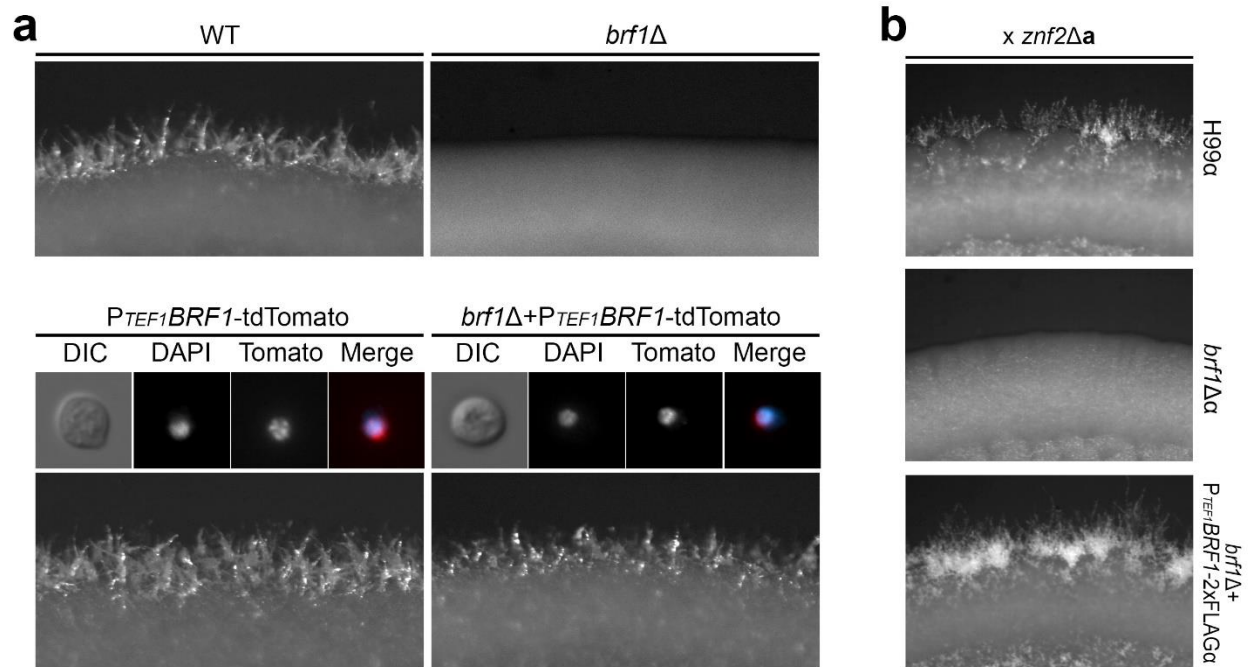


**Figure S4.4. The *BRF1* overexpression restored the defects in *brf1*Δ. (a).** WT, *brf1*Δ, *brf1*Δ+*P<sub>TEF1</sub>BRF1*-tdTomato strains was cultured on V8 medium for 2 days. The fluorescence images were from the *P<sub>TEF1</sub>BRF1*-tdTomato cells cultured overnight in YPD liquid. **(b).** WT H99, *brf1*Δ (JL131, MATα), and *brf1*Δ+*P<sub>TEF1</sub>BRF1*-CBP-2xFLAG strains were crossed with a *znf2*Δ strain (strain XT110, MATa). The crosses were cultured on V8 medium for 3 days.

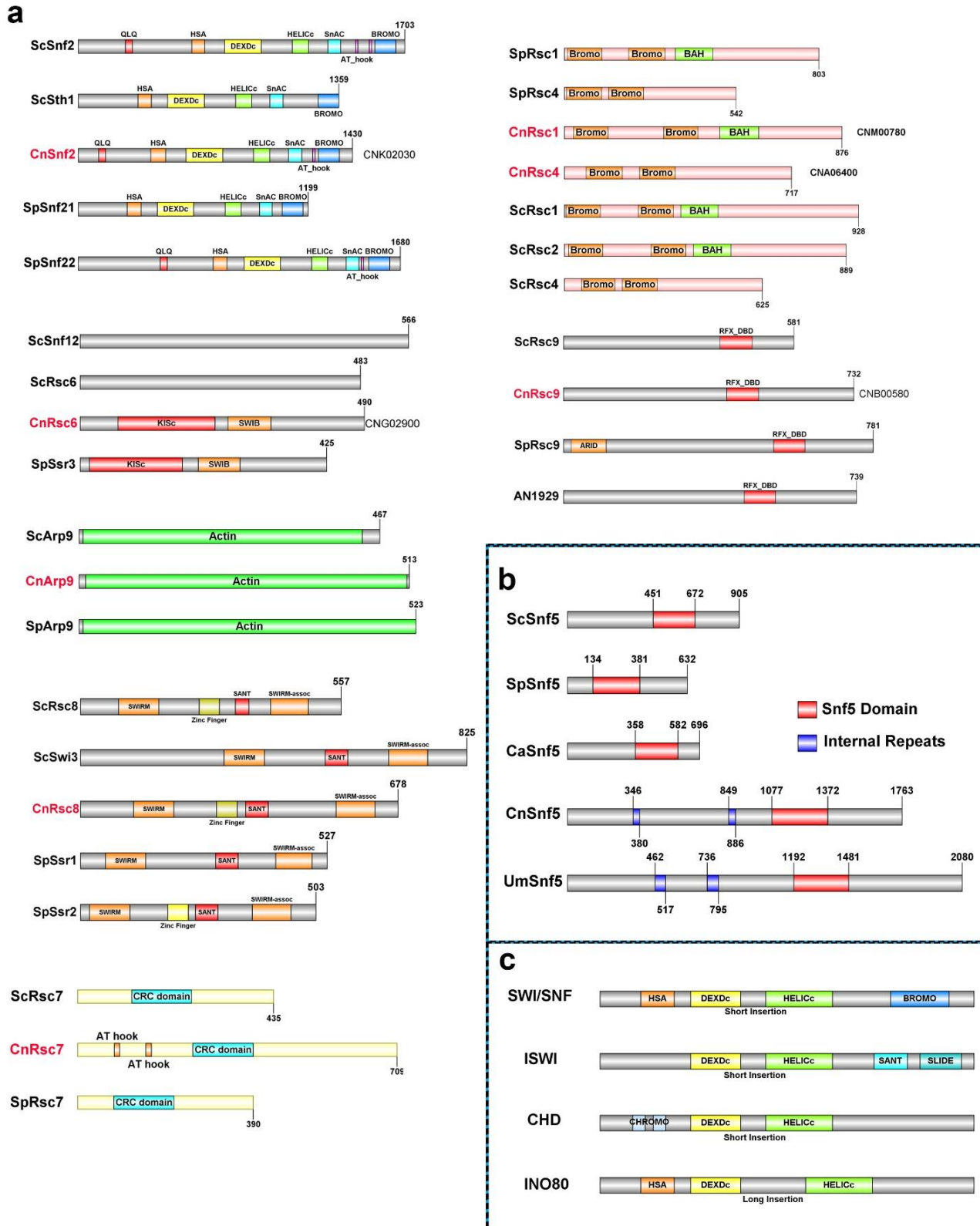


**Figure S4.5.** Diagrams of domain layout of the subunits in the SWI/SNF and RSC complex in *C. neoformans*. (a). The domain layouts for Snf2, Rsc6, Arp9, Rsc8, Rsc7, Rsc1, Rsc4 and Rsc9

subunits in the RSC complex in *C. neoformans*, together with their homologs in *S. cerevisiae* and *S. pombe*. **(b)**. The domain layouts for Snf5 proteins in ascomycetes (*S. cerevisiae*, *S. pombe*, and *C. albicans*) and basidiomycetes (*C. neoformans* and *Ustilago maydis*). **(c)**. The domain layouts for the Snf2 family ATPases in the chromatin remodeling complexes (adapted from Tang *et.al* 's review in 2010).

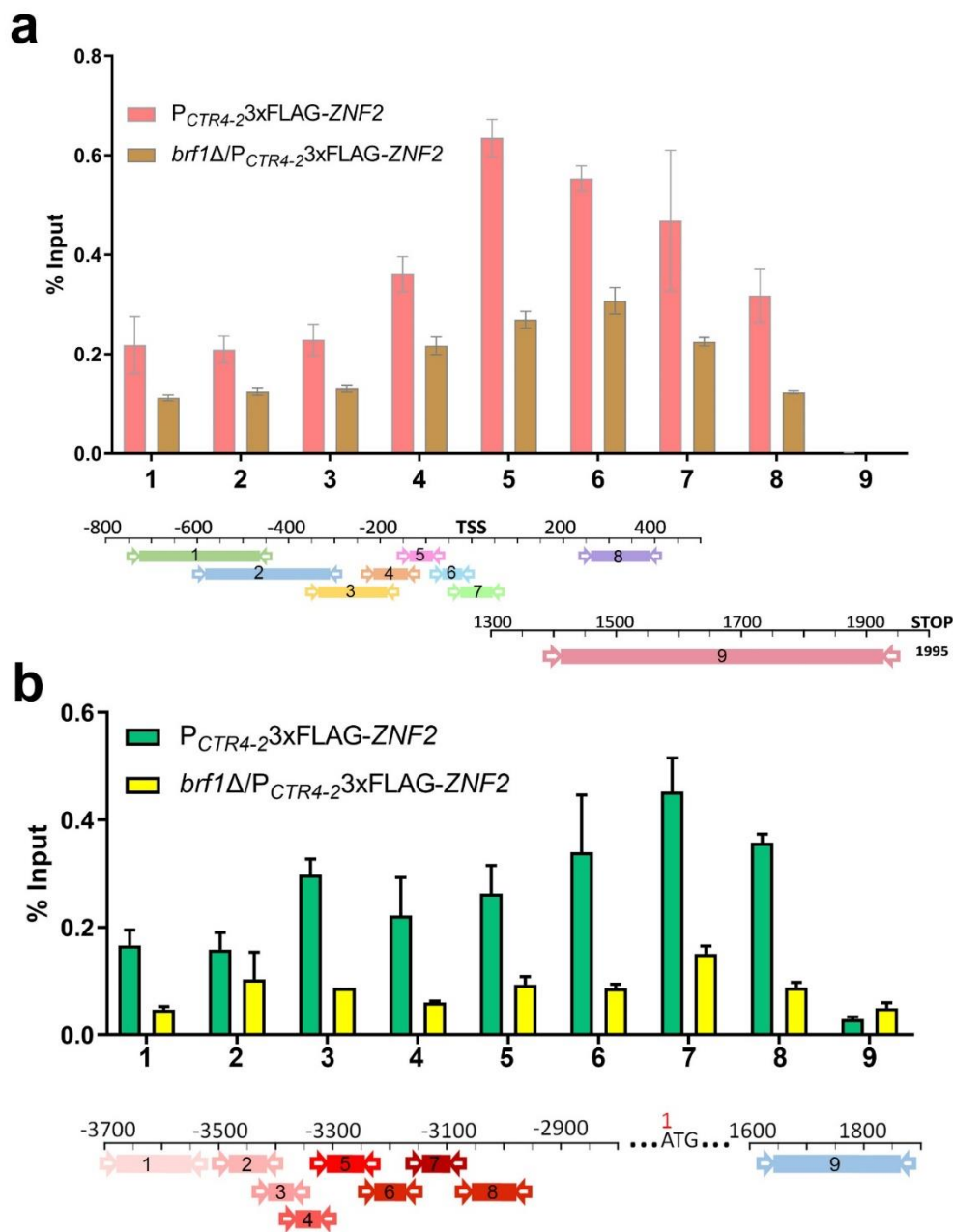


**Table S4.1.** The list of eight-four filament-defective *Agrobacterium*-mediated transformants.

**Table S4.2.** The list of insertion sites from the eight linked insertional mutants.

Type of Insertion	Insertion Site in the Genome	Potential Affected Gene(s)
Paired	169nt downstream of TSS	CNA02310
Paired	656nt downstream of TSS	CNA02310
Paired	2566nt downstream of TSS	CNA07190
Paired	126nt downstream of TSS	CNA07190
Paired	3068nt downstream of TSS	CND05760
Paired	1248nt downstream of TSS	CNK02410
Singleton	At intergenic region of CNA07150 and CNA07160	CNA07150 CNA07160
Singleton	At intergenic region of CNA07230 and CNA07240	CNA07230 CNA07240

**Table S4.3.** The list of proteins identified from Co-IP/MS by Sfh1-mNeonGreen as bait.

Coding Locus(D)	Coding Locus(A)	Protein name	# peptide spectrum matches
CNA03310	CNAG_00372	Rsc7	56
CNE04020	CNAG_02134	Rsc8	54
CNK02030	CNAG_01863	Snf2	50
CNC06140	CNAG_03003	Sfh1	35
CNG02900	CNAG_03285	Rsc6	29
CNM00780	CNAG_06068	Rsc1	22
CNE02000	CNAG_02350	Rss1	22
CNB00580	CNAG_06744	Rsc9	18
CNB05320	CNAG_04048	Arp4	15
CNI00980	CNAG_04460	Arp9	12

**Table S4.4.** The Snf5 domain search in fungi.

**Table S4.5.** The list of Snf2 proteins in fungi by RBOMO and BSA domains search.

**Table S4.6.** The strains used in this study.

**Table S4.7.** The vectors used in this study.

<b>Vector Name</b>	<b>Genotype</b>	<b>Backbone</b>	<b>Sources</b>
pXL1	P <sub>GPD1</sub> -Fse1-Pac1-T <sub>GPD1</sub> -NEO	Topo2.1	
pXC	P <sub>CTR4-2</sub> -Fse1-Pac1-T <sub>GPD1</sub> -NEO	pXL1	
pYF5	P <sub>GPD1</sub> -PHD11-mNeonGreen-NEO	pUC19	This Study
pFZ3-ZNF2(D)	P <sub>CTR4-2</sub> -3X FLAG-ZNF2(D)-NEO	pUC19	This Study
pJL1	P <sub>TEF1</sub> -Fse1-AsiS1-CBP-2X FLAG-NEO	pXC	This Study
pJL2	P <sub>TEF1</sub> -BRF1-CBP-2X FLAG-NEO	pXL1	This Study
pJL3	P <sub>TEF1</sub> -BRF1-tdTomato-NEO	pXL1	This Study
pJL4	P <sub>GPD1</sub> -SFH1-mNeonGreen-NEO	pUC19	This Study

**Table S4.8.** The primers used in this study.

## CHAPTER 5

### CONCLUSIONS

The filamentation process is inversely correlated with virulence in the human fungal pathogen *Cryptococcus neoformans*. The yeast form is pathogenic and infectious, while the filament form (hypha and pseudohypha) is virulence attenuated. Transcription factor Znf2 is the central regulator of filamentation, and it bridges filamentation and virulence in *C. neoformans*. This study was aimed to study the different interactions between *Cryptococcus* cells in various morphologies and host cells, to identify and characterize the signals and pathways that activate hyphal growth, and to investigate the mechanisms by which Znf2 regulates filamentous growth. The results advanced our understanding of the regulatory details of yeast to hyphal transition and the biology of *C. neoformans*.

*C. neoformans* cells can grow filamentously in the hypha or the pseudohyphae form. Hyphal growth typically is associated with the mating process and hyphal growth is orchestrated by the transcription factor Znf2. Pseudohyphal growth can be induced and regulated by many pathways, with the RAM pathway the most well-characterized pathway. Both hyphal and pseudohyphal cells show reduced or abolished virulence in mammalian hosts. In **Chapter 2**, we characterized the genetic relationship between RAM and Znf2 and examined the interactions between *Cryptococcus* cells in various morphologies and host cells.

Disruption of the RAM pathway (such as deletion of the RAM downstream kinase gene *CBK1*) results in pseudohyphal growth and deletion of *ZNF2* locks cells in the yeast form. *cbk1Δznf2Δ* cells grow in the pseudohyphal form and *cbk1ΔZNF2<sup>oe</sup>* cells grow in the hyphal

form, indicating that the RAM pathway and Znf2 likely work in parallel in regulating pseudohyphal and hyphal growth in *C. neoformans*. Pseudohypha are resistant to amoeba predation compared to yeast cells. In this research, we show that both pseudohypha and hypha survived amoeba predation, while yeast cells were phagocytosed and digested. Therefore, the filamentous form of *C. neoformans* (hypha and pseudohypha) provides growth advantages in response to nutrition depletion and predation stresses in the natural environment.

As a fungal pathogen, the filamentous form of *C. neoformans* is rarely observed in mammalian hosts. To successfully cause infections and diseases, evading or invading immune cells like alveolar macrophages is vital. We found that pseudohyphal and hyphal cells severely reduced cryptococcal attachment to macrophage cells compared to yeast cells. Meanwhile, the phagocytosis ratio of hypha and pseudohypha was drastically reduced compared to yeast cells due to their shape and enlarged size. We also showed that innate immune cells from insects, hemocytes, aggregate around the hypha cells in its effort to contain and constrain *C. neoformans* in the host.

Thus, for this opportunistic fungal pathogen, filamentation is a double-edged sword. The hyphal filamentous form grants *Cryptococcus* cells resistance to microbial predation in its natural habitats while attenuating cryptococcal virulence in mammalian hosts. Irrespective of the profound effect that this morphotype has on cryptococcal interactions with other organisms, hyphal growth is an integral part of its life cycle in order to complete sexual reproduction. We demonstrated that the pheromone sensing cascade is dispensable for filamentation, indicating the existence of pheromone independent pathways/factors that activate Znf2-regulated morphogenesis. In **Chapter 3**, we, for the first time, identified a signaling molecule that activates the pheromone-independent self-filamentation in *C. neoformans* serotype A H99 strain.

The molecule is glucosamine. Glucosamine stimulates pheromone independent self-filamentation in H99 cells in a dose-dependent manner. Our preliminary data suggest that glucosamine activates filamentation is not because its role in carbon repression. Our genetic screen of the transcription factor deletion mutants identified several mutants that fail to filament upon glucosamine stimulation, including *crz1*Δ and *znf2*Δ. Crz1 works upstream of Znf2 in regulating filamentation stimulated by glucosamine. Crz1 is a known downstream transcription factor of calcineurin, a phosphatase complex conserved in eukaryotes. It is shown previously that upon activation by heat-shock or calcium stress, calcineurin dephosphorylates and activates Crz1 by translocating Crz1 from the cytoplasm to the nucleus. Strikingly, we found that glucosamine stimulates Crz1 translocation to the nucleus to a similar extent as the treatment by the known calcineurin stimulus calcium. We further demonstrated that glucosamine stimulated Crz1 translocation depends on the activity of calcineurin phosphatase.

Phosphorylated Crz1 is dephosphorylated by calcineurin. To identify the kinase(s) that phosphorylate Crz1, we screened the kinase deletion mutants for an enhanced filamentation phenotype on glucosamine medium. We found that disruption of multiple components of the HOG MAPK cascade enhanced the glucosamine stimulated filamentation. Indeed, disruption of Pbs1, Ssk1 or Ssk2 resulted in constitutively elevated nuclear localization of Crz1 even in the absence of any stimuli like glucosamine. Based on the results, we conclude in **Chapter 3** that calcineurin and HOG MAPK cascade antagonize the phosphorylation status of Crz1 in regulating the glucosamine stimulated self-filamentation of *C. neoformans*. This finding opens up the opportunities of designing small molecules to activate the filamentation pathways in *C. neoformans* to combat the deadly fungal disease.

We now understand that the yeast-hypha transition can be activated/repressed by many different signaling pathways, including the pheromone sensing cascade, the HOG pathway, the calcineurin cascade etc. All these pathways converge on the same hyphal master regulator Znf2, which ultimately drives hyphal growth. However, it is not yet fully understood how Znf2 regulates its downstream targets to execute hyphal morphogenesis. In **Chapter 4**, we identified two factors, Brf1 and Snf5, that are essential for Znf2 to fulfill its genetic regulation by a forward genetics screen. As a basidiomycete-specific factor, Brf1 functions in the same genetic pathway as Snf5. We figured out later that Brf1 and Sn5 work together in the ATP-dependent chromatin remodeling complex called SWI/SNF.

SWI/SNF is a family of complexes conserved from yeast to human despite the differences in composition among various organisms. SWI/SNF uses ATP to remodel chromatin structure via sliding or evicting nucleosomes. In this study, we show that the SWI/SNF complex is required to open up the chromatin of promoter regions of Znf2 and its targets via assay for transposase-accessible chromatin using sequencing (ATAC-seq) analysis. Meanwhile, Znf2 also plays instructive roles in the chromatin structures of these regions, by recruiting SWI/SNF to its target sites. Furthermore, as a subunit in the SWI/SNF complex, Brf1 is required for transcription factor Znf2's full association to DNA as shown by chromatin-immunoprecipitation coupled with quantitative PCR (ChIP-qPCR).

In conclusion, our findings in this study advanced our understanding of the molecular mechanisms underlying hyphal morphogenesis in *Cryptococcus*, revealed the conserved and diverged features of genetic and epigenetic regulations of morphogenesis in different fungi, and raised the possibilities of combating cryptococcosis by inducing the hyphal growth to diminish the virulence of *Cryptococcus* in hosts.